Article:
Visnes, T., Cázares-Körner, A., Hao, W. et al. (37 more authors) (2018) Small-molecule inhibitor of OGG1 suppresses pro-inflammatory gene expression and inflammation. Science, 362 (6416). pp. 834-839. ISSN 0036-8075

https://doi.org/10.1126/science.aar8048

Title:

Small-molecule inhibitor of OGG1 suppresses pro-inflammatory gene expression and inflammation

Authors:

Torkild Visnes[1,2†], Armando Cázares-Körner[1†], Wenjing Hao[3†], Olov Wallner[1†], Geoffrey Masuyer[4], Olga Loseva[1], Oliver Mortusewicz[1], Elisée Wiita[1], Antonio Sarno[5,6], Aleksandr Manoilov[7], Juan Astorga-Wells[7], Ann-Sofie Jemth[1], Lang Pan[3,12], Kumar Sanjiv[1], Stella Karsten[1], Camilla Gokturk[1], Maurice Grube[1], Evert J. Homan[1], Bishoy M.F. Hanna[1], Cynthia B. J. Paulin[1], Therese Pham[1], Azita Rasti[1], Catharina von Nicolai[1], Carlos Benitez-Buelga[1], Tobias Koolmeister[1], Dag Ivanic[1], Petar Iliev[1], Martin Scobie[1], Hans E. Krokan[5,6], Pawel Baranczewski[7,8], Per Artursson[8,9], Mikael Altun[1], Annika Jenmalm Jensen[10], Christina Kalderén[1], Xueqing Ba[3,13], Roman A. Zubarev[7], Pål Stenmark[4], Istvan Boldogh[3*], Thomas Helleday[1,11*]

†, Contributed equally

*, Corresponding authors

Affiliations:

[1] Science for Life Laboratory, Department of Oncology-Pathology, Karolinska Institutet, S-171 76 Stockholm, Sweden.
[2] Department of Biotechnology and Nanomedicine, SINTEF Industry, N-7465 Trondheim, Norway.
[3] Department of Microbiology and Immunology, Sealy Center for Molecular Medicine, University of Texas Medical Branch at Galveston, Galveston, Texas 77555, USA.
[4] Department of Biochemistry and Biophysics, Stockholm University, S-106 91 Stockholm, Sweden.
[5] Department of Clinical and Molecular Medicine, Norwegian University of Science and Technology, Trondheim, Norway.
[6] The Liaison Committee for Education, Research and Innovation in Central Norway, Trondheim, Norway.
[7] Department of Medical Biochemistry and Biophysics, Karolinska Institutet, SE-17177 Stockholm, Sweden, and Science for Life Laboratory.
[8] Science for Life Laboratory Drug Discovery and Development Platform, ADME of Therapeutics facility, Department of Pharmacy, Uppsala University, Uppsala, Sweden
[9] Uppsala Drug Optimisation and Pharmaceutical Profiling Platform (UDOPP), Department of Pharmacy, Uppsala University, Uppsala, Sweden
[10] Chemical Biology Consortium Sweden, Science for Life Laboratory, Division of Translational Medicine and Chemical Biology, Department of Medical Biochemistry and Biophysics, Karolinska Institutet, S-171 21 Stockholm, Sweden.
[11] Sheffield Cancer Centre, Department of Oncology and Metabolism, University of Sheffield, Sheffield S10 2RX, UK.

[12] Permanent address: Department of Physiology, Xiangya Medicine School in Central South University, Changsha, Hunan 410078, China.
[13] Permanent address: Key Laboratory of Molecular Epigenetics of Ministry of Education, School of Life Science, Northeast Normal University, Changchun, Jilin 130024, China.

One Sentence Summary:

We developed an OGG1 inhibitor which decreases lung inflammation by a mechanism distinct from other anti-inflammatory drugs.

Abstract

The onset of inflammation is associated with reactive oxygen species and oxidative damage to macromolecules such as 8-oxoG in DNA. The OGG1 glycosylase binds 8-oxoG, and since the *Ogg1*$^{-/-}$ mice are resistant to acute and systemic inflammation, we hypothesized that OGG1 inhibition may represent a novel strategy to prevent and treat inflammation. We developed TH5487, a selective active site inhibitor of OGG1 that hampers OGG1 binding to and repair of 8-oxoG and is well tolerated by mice. TH5487 prevents TNFα-induced OGG1–DNA interactions at guanine-rich promoters of pro-inflammatory genes. This, in turn, decreases DNA occupancy of NF-κB and pro-inflammatory gene expression, resulting in decreased inflammatory cell recruitment to mouse lungs. Thus, we show in vivo proof-of-concept of targeting oxidative DNA repair to alleviate inflammatory conditions.

Main Text:

Upon exposure to pro-inflammatory agents, cells produce elevated levels of reactive oxygen species (ROS), which induce oxidative DNA damage. Guanine is particularly vulnerable because it has the lowest oxidation potential among canonical DNA bases (*1*, *2*), resulting primarily in 7,8-dihydro-8-oxoguanine (8-oxoG) particularly at guanine-rich promoter regions (*3*, *4*). 8-oxoguanine-DNA glycosylase 1 (OGG1) binds with high affinity to 8-oxoG in double-stranded DNA to initiate DNA base excision repair. In addition to this role, OGG1 has distinct signal transduction functions (*5*–*7*), interacts with 8-oxoG in gene regulatory regions, and facilitates gene expression (*3*, *7*–*12*). These observations provide a potential explanation for the decreased inflammatory responses in *Ogg1*$^{-/-}$ mice (*13*–*16*), which are otherwise viable and largely healthy (*17*). Thus, we hypothesized that small molecule OGG1 inhibitors may be clinically useful for the alleviation of inflammatory processes while still being well tolerated.

To screen for OGG1 inhibitors, we used a duplex oligonucleotide with the OGG1 substrate 8-oxo-7,8-dihydro-2'-deoxyadenosine and an excess of AP endonuclease 1 (APE1), which acts downstream of OGG1 and stimulates its activity (*18*) (Fig. 1A and 1B). We screened a compound library containing 17,940 compounds (Table S1), and identified a hit molecule with an IC_{50} of 8.6 µM. During hit expansion, we developed TH5487 as a potent OGG1 inhibitor with an IC_{50} of 342 nM, whereas structurally similar analogues TH2840 and TH5411 were inactive with IC_{50} values exceeding 100 µM (Fig. 1C, 1D, S1, S2 and S3). This compound series was selective for OGG1 and did not affect the activity of other DNA glycosylases (Fig. S5A and Table S2), various Nudix hydrolases/diphosphatases (Table S3), and did not intercalate DNA (Fig. S5B). Previously, a hydrazide-based small molecule (O8) was reported to inhibit OGG1 with similar potency as TH5487 (*19*). O8 was found to inhibit catalytic imine formation in OGG1 (*19*), and we observed an increase in the potency of O8 by omitting APE1 from the reaction, in contrast to

TH5487 (Table S4). APE1 readily released fluorescence from a natural AP-site, but only partially from an AP-site substrate pre-incubated with O8 (Fig. S5C). Thus, TH5487 primarily inhibited the DNA glycosylase activity of OGG1, whereas O8 appeared to interfere with downstream β-lyase activity. To further validate OGG1 inhibition by TH5487, we performed electrophoretic mobility shift assays (EMSAs). OGG1 bound to 8-oxoG:C-containing duplex oligonucleotide in a concentration-dependent manner (Fig. S4C). The amount of OGG1–DNA complexes decreased in a dose-dependent manner upon addition of TH5487 (Fig. 1E), demonstrating that TH5487 precludes OGG1 from binding oxidized DNA in vitro.

TH5487, but not the inactive analogs TH2840 and TH5411, increased the melting temperature for OGG1 in a concentration-dependent manner (Fig. 1F). Thus, TH5487-mediated protein destabilization did not account for the observed decrease in enzyme activity, suggesting that TH5487 binds OGG1 similarly to 8-oxoG extruded from DNA. Supporting this, treatment with TH5487 resulted in a lower deuteration for all peptides forming the active site cavity (Fig. 1G and Table S5). Thus, TH5487 is a potent and selective active site inhibitor that prevents OGG1 from recognizing its DNA substrate.

To identify the precise binding site for this class of inhibitors, we determined X-ray crystal structures of mouse OGG1 in complex with the more soluble analog TH5675 (Fig. 1H, S4 and S6A-C, Table S6). TH5675 bound the active site (Fig S6D), albeit differently from the natural substrate (Fig S6E). Notably, the iodophenyl tail of TH5675 occupied the deeper hydrophobic pocket flanked by Phe319, Cys253, and Met257 and took the place of the 8-oxoguanine base. The central piperidyl linker was stabilized by hydrogen bonds with the catalytic Lys249 and the backbone of Gly42, the residue that distinguishes 8-oxoguanine from guanine. The benzimidazolone core interacted with a lipophilic exo-site, stabilized by Ile152 and Leu323 in addition to a π-stacking interaction with His270 (*20*). Notably, the Asp322 side chain

was within hydrogen bond distance of the solvent accessible amine, which corresponds to the bromine atom in TH5487 (Fig. S6F). These interactions were the result of a local conformational change where the active site closed around the ligand (Fig. S6G, Movie S1).

For OGG1 inhibitors to be pharmacologically useful, they need to engage and inhibit OGG1 in cells. TH5487 increased the melting temperature of OGG1 in human cells (Fig. 2A), demonstrating that TH5487 engaged its intended target in living cells and protected it from thermal denaturation. Furthermore, TH5487 impaired repair of genomic 8-oxoG induced by $KBrO_3$. TH5487 caused a significant increase in genomic 8-oxoG after 2.5 h (Fig. 2B and 2C) and at 24 h, 50% ± 8% of the 8-oxoG remained in the TH5487-treated cells (Fig. 2C), without disrupting proliferation (Fig S7A). Thus, genomic 8-oxoG and TH5487 were well tolerated by cells. Furthermore, the decrease in genomic 8-oxoG was a result of repair processes and not cellular replication. To further validate target engagement, we assessed the chromatin dynamics of OGG1–GFP fusion proteins. Cells were treated with $KBrO_3$ and released into medium containing TH5487 or DMSO. Consistent with previous reports (*21*), OGG1–GFP fusion proteins were immobilized at genomic DNA lesions introduced by $KBrO_3$. Treatment with TH5487 increased the nuclear mobility of OGG1–GFP 3- and 5-h after $KBrO_3$ exposure (Fig. 2D-E, S7B-C), suggesting that TH5487 prevented OGG1 binding to its genomic substrate in living cells.

OGG1 binds 8-oxoG at gene regulatory regions to mediate transcriptional activation in response to inflammatory stimuli (*3*, *7–11*). In the absence of functional OGG1, a decreased inflammatory response is observed (*3*, *12–16*, *22*). Because TH5487 prevents OGG1 from binding 8-oxoG in DNA, we examined if TH5487 could suppress pro-inflammatory gene expression. In line with previous observations (*12*), HEK293T cells lacking OGG1 displayed a reduced induction of *CXCL1* (chemokine (C-X-C motif) ligand 1) mRNA following tumor necrosis factor (TNFα) stimulation (Fig. 2F, S7D and S7E). Treatment with 5 μM TH5487

decreased *CXCL1* expression by > 50% in wild-type but not in OGG1-knockout cells (Fig. 2F). Thus, the compound may be used to specifically inhibit OGG1-dependent pro-inflammatory gene expression. Since respiratory epithelium is a key orchestrator of pulmonary innate immune responses (*23*), we stimulated a murine airway epithelial cell line (MLE 12) with TNFα (*24*), which increased the expression of an array of pro-inflammatory cytokines, C-C, and C-X-C chemokines (Fig. 3A-C and S8). Importantly, TH5487 decreased expression of the same genes to near pre-treatment levels (Fig. 3C, 3E, S8, S9, S10, S11 and S12). Inhibition was dose-dependent (Fig. 3D and S10) and observed also with the potent inflammatory agent lipopolysaccharide (LPS) (*25*) (Fig. 3F, S11 and S12). Crucially, TH5487 decreased TNFα- and LPS-induced gene expression also in diploid human airway epithelial cells (hSAECs; Fig. 3G-I, S9, S10 and S12).

ROS generate a localized increase in OGG1 substrates in guanine-rich promoter regions (*4*, *6*, *9*, *10*) including pro-inflammatory genes (*3*, *4*, *12*). Emerging evidence suggests that OGG1 binding to gene regulatory regions exerts an epigenetic role for 8-oxoG causing OGG1 to act as a modulator of gene expression (*3*, *4*, *6–11*). Guanine oxidation leads to sequential recruitment of OGG1 and downstream transcriptional effectors (*3*, *8–11*), such as nuclear factor kappa-B (NF-κB), which is the main driver of both TNFα- and LPS-induced pro-inflammatory gene expression (*26*). Consistent with the observation that TH5487 prevents OGG1 from engaging damaged DNA in vitro and in cells (Fig. 1E, 2D and 2E), we observed that TH5487 decreased the recruitment of OGG1 to regulatory regions of pro-inflammatory cytokines in TNFα-challenged cells (Fig. 3J). Consequently, binding of NF-κB to the same regulatory regions was significantly decreased by TH5487 in the chromatin of TNFα-exposed cells (Fig. 3K) and to its recognition sequence in nuclear extracts from mouse and human cells by TH5487 (Fig. 3L and S13A-C). In the presence of OGG1, TH5487 decreased NF-κB occupancy on 8-oxoG-containing DNA, whereas TH5487 alone was unable to inhibit NF-κB (Fig. S13D-E). Thus, TH5487 decreases pro-inflammatory

gene expression by perturbing DNA occupancy of NF-κB and potentially other OGG1-dependent transacting factors (*3*, *8–11*). TH5487 had no effect on the release of NF-κB from its inhibitory complex (Fig. S14A-C), but inhibited inflammatory gene expression similar to BMS-345541, an IκB kinase inhibitor (*27*) (Fig. S15A). Thus, both TH5847 and BMS-345541 inhibit NF-κB function: TH5487 by preventing NF-κB binding to promoters (Fig. 3K), and BMS-345541 by inhibiting NF-κB activation (Fig. S14A-C). This results in the same readout in the form of diminished induction of pro-inflammatory genes. The previously-developed OGG1 inhibitor O8 (*19*) did not affect gene expression (Fig. S15A), possibly because, in contrast to TH5487, it allows OGG1 binding to damaged DNA (*19*) (Fig. S15B-C).

In addition, TH5487 is metabolically relatively stable and well tolerated in mice (Table S7, S8, S9 and S10, Fig. S16A). To assess whether TH5487 could downregulate chemotactic (C-C and C-X-C) mediators (*28*) in vivo, we challenged mouse lungs with TNFα and profiled the gene expression of pro-inflammatory mediators. TNFα robustly induced expression of pulmonary pro-inflammatory genes, but a prophylactic injection of TH5487 decreased the expression levels by twofold or greater (Fig. 4A and 4B). Challenge with TNFα or LPS induced the robust recruitment of neutrophils to the airways, which was decreased by up to 85% ± 5% by the prophylactic intraperitoneal administration of TH5487 (Fig. 4C and S16B-G). We then administered TH5487 at different time points before or after challenge with TNFα and found that TH5487 reduced the pulmonary neutrophil count even when administered up to 9 h after TNFα challenge (Figure 4D and S17). Thus, TH5487 is efficacious in vivo, suggesting that the compound could be used for the treatment of inflammatory conditions. Finally, during the revision stage of this manuscript, another potent and structurally distinct OGG1 inhibitor was published (*29*). Even this compound has comparable anti-inflammatory effects (Fig. S18).

Thus, we have developed a pharmacologically useful OGG1 inhibitor that is a potent and selective active site binder that prevents OGG1 from engaging damaged DNA in vitro and in cells, resulting in a decreased pro-inflammatory gene expression by a mechanism that is distinct from other established therapeutic agents (Fig. S19). This is translated into a reduced neutrophil infiltration in mouse lungs challenged with TNFα or LPS, demonstrating that OGG1 inhibition may be a potentially useful strategy for the treatment of inflammation.

References and Notes

1. J. Cadet, T. Douki, J.-L. Ravanat, One-electron oxidation of DNA and inflammation processes. *Nat. Chem. Biol.* **2**, 348–349 (2006).

2. Y. Margolin, J.-F. Cloutier, V. Shafirovich, N. E. Geacintov, P. C. Dedon, Paradoxical hotspots for guanine oxidation by a chemical mediator of inflammation. *Nat. Chem. Biol.* **2**, 365–366 (2006).

3. L. Pan *et al.*, Oxidized Guanine Base Lesions Function in 8-Oxoguanine DNA Glycosylase-1-mediated Epigenetic Regulation of Nuclear Factor κB-driven Gene Expression. *J. Biol. Chem.* **291**, 25553–25566 (2016).

4. Y. Ding, A. M. Fleming, C. J. Burrows, Sequencing the Mouse Genome for the Oxidatively Modified Base 8-Oxo-7,8-dihydroguanine by OG-Seq. *J. Am. Chem. Soc.* **139**, 2569–2572 (2017).

5. I. Boldogh *et al.*, Activation of Ras Signaling Pathway by 8-Oxoguanine DNA Glycosylase Bound to Its Excision Product, 8-Oxoguanine. *J. Biol. Chem.* **287**, 20769–20773 (2012).

6. M. Seifermann, B. Epe, Oxidatively generated base modifications in DNA: Not only carcinogenic risk factor but also regulatory mark? *Free Radic. Biol. Med.* (2016), doi:10.1016/j.freeradbiomed.2016.11.018.

7. A. M. Fleming, Y. Ding, C. J. Burrows, Oxidative DNA damage is epigenetic by regulating gene transcription via base excision repair. *Proc. Natl. Acad. Sci.* **114**, 2604–2609 (2017).

8. S. Amente *et al.*, LSD1-mediated demethylation of histone H3 lysine 4 triggers Myc-induced transcription. *Oncogene*. **29**, 3691–3702 (2010).

9. V. Pastukh *et al.*, An oxidative DNA "damage" and repair mechanism localized in the VEGF promoter is important for hypoxia-induced VEGF mRNA expression. *Am. J. Physiol. - Lung Cell. Mol. Physiol.* **309**, L1367–L1375 (2015).

10. V. Pastukh, M. Ruchko, O. Gorodnya, G. L. Wilson, M. N. Gillespie, Sequence-specific oxidative base modifications in hypoxia-inducible genes. *Free Radic. Biol. Med.* **43**, 1616–1626 (2007).

11. B. Perillo *et al.*, DNA Oxidation as Triggered by H3K9me2 Demethylation Drives Estrogen-Induced Gene Expression. *Science*. **319**, 202–206 (2008).

12. X. Ba *et al.*, 8-Oxoguanine DNA Glycosylase-1 Augments Proinflammatory Gene Expression by Facilitating the Recruitment of Site-Specific Transcription Factors. *J. Immunol.* **192**, 2384–2394 (2014).

13. E. Touati *et al.*, Deficiency in OGG1 Protects against Inflammation and Mutagenic Effects Associated with H. pylori Infection in Mouse. *Helicobacter*. **11**, 494–505 (2006).

14. J. G. Mabley *et al.*, Potential role for 8-oxoguanine DNA glycosylase in regulating inflammation. *FASEB J.* **19**, 290–292 (2005).

15. G. Li *et al.*, 8-Oxoguanine-DNA glycosylase 1 deficiency modifies allergic airway inflammation by regulating STAT6 and IL-4 in cells and in mice. *Free Radic. Biol. Med.* **52**, 392–401 (2012).

16. A. Bacsi *et al.*, Down-regulation of 8-oxoguanine DNA glycosylase 1 expression in the airway epithelium ameliorates allergic lung inflammation. *DNA Repair*. **12**, 18–26 (2013).

17. A. Klungland *et al.*, Accumulation of premutagenic DNA lesions in mice defective in removal of oxidative base damage. *Proc Natl Acad Sci U A.* **96**, 13300–5 (1999).

18. A. E. Vidal, I. D. Hickson, S. Boiteux, J. P. Radicella, Mechanism of stimulation of the DNA glycosylase activity of hOGG1 by the major human AP endonuclease: bypass of the AP lyase activity step. *Nucleic Acids Res*. **29**, 1285–92 (2001).

19. N. Donley *et al.*, Small Molecule Inhibitors of 8-Oxoguanine DNA Glycosylase-1 (OGG1). *ACS Chem. Biol.* **10**, 2334–2343 (2015).

20. A. Banerjee, W. Yang, M. Karplus, G. L. Verdine, Structure of a repair enzyme interrogating undamaged DNA elucidates recognition of damaged DNA. *Nature*. **434**, 612–618 (2005).

21. R. Amouroux, A. Campalans, B. Epe, J. P. Radicella, Oxidative stress triggers the preferential assembly of base excision repair complexes on open chromatin regions. *Nucleic Acids Res.* **38**, 2878–2890 (2010).

22. L. Aguilera-Aguirre *et al.*, Innate Inflammation Induced by the 8-Oxoguanine DNA Glycosylase-1–KRAS–NF-κB Pathway. *J. Immunol.* **193**, 4643–4653 (2014).

23. J. A. Whitsett, T. Alenghat, Respiratory epithelial cells orchestrate pulmonary innate immunity. *Nat. Immunol.* **16**, 27–35 (2015).

24. G. D. Kalliolias, L. B. Ivashkiv, TNF biology, pathogenic mechanisms and emerging therapeutic strategies. *Nat. Rev. Rheumatol.* **12**, 49–62 (2016).

25. C. E. Bryant, D. R. Spring, M. Gangloff, N. J. Gay, The molecular basis of the host response to lipopolysaccharide. *Nat. Rev. Microbiol.* **8**, 8–14 (2010).

26. Q. Li, I. M. Verma, NF-κB regulation in the immune system. *Nat. Rev. Immunol.* **2**, 725–734 (2002).

27. J. R. Burke *et al.*, BMS-345541 Is a Highly Selective Inhibitor of IκB Kinase That Binds at an Allosteric Site of the Enzyme and Blocks NF-κB-dependent Transcription in Mice. *J. Biol. Chem.* **278**, 1450–1456 (2003).

28. A. Mantovani, R. Bonecchi, M. Locati, Tuning inflammation and immunity by chemokine sequestration: decoys and more. *Nat. Rev. Immunol.* **6**, 907–918 (2006).

29. Y. Tahara *et al.*, Potent and Selective Inhibitors of 8-Oxoguanine DNA Glycosylase. *J. Am. Chem. Soc.* **140**, 2105–2114 (2018).

Acknowledgements:

We are grateful to Dr T. Lundbäck and the Chemical Biology Consortium Sweden for invaluable assistance in the establishment, performance, and analysis of the high-throughput screen. We are grateful to Professors G. Dianov and S. Wallace and Drs J. Parsons and P. Herr for sharing expression vectors. We thank the Protein Science Facility at Karolinska Institute for the purification of DNA glycosylases for selectivity assays, K. Edfeldt, C. Sjögren, F. Pineiro and S. Eriksson for administrative and technical support. We thank Professors B. Dalhus, A. Klungland, and M. Bjørås for helpful discussions. The mass spectrometry analyses were performed at the Proteomics and Metabolomics Core Facility (PROMEC) at The Norwegian University of Science and Technology (NTNU) and the Central Norway Regional Health Authority. We thank the scientists at stations I04, and I24 of Diamond Light Source (UK) for their support during data collection (allocation MX15806).

Funding: This work was funded by the National Institute of Allergic and Infectious Diseases NIAID/AI062885 (IB), The Faculty of Medicine at the Norwegian University of Science and Technology and the Central Norway Regional Health Authority (A.S. and H.E.K., project no. 46056921), Svanhild and Arne Must's Fund for Medical Research (A.S. and H.E.K.). Vinnova (A.C.K and T.H.), The Knut and Alice Wallenberg Foundation and the Swedish Foundation for Strategic Research (T.H. and P.S.), Swedish Research Council (T.H. and P.S.), Swedish Cancer Society (T.H. and P.S.), the Swedish Children's Cancer Foundation (T.H.), the Swedish Pain Relief Foundation (T.H.), and the Torsten and Ragnar Söderberg Foundation (T.H.).

Author Contributions: T.V., A.C.K., W.H., and O.W. contributed equally to this work. A.C.K. O.W. ,T.K., D.I., P.I., and M.S contributed to medicinal chemistry experiments. W.H., X.B., L.P., and I.B. designed, analyzed, and performed animal and cell-culture experiments. T.V., A.C.K, W.H., O.M., B.M.F.H., S.K., C.v.N., C.B-B., C.K., M.A., I.B., and T.H. designed, performed, and analyzed cell biology experiments. T.V., A.C.K., L.P., X.B., O.L., A-S.J., A.J.J., E.W., E.J.H., C.B.J.P., M.G., and T.H. designed, performed, and analyzed biochemical and high-throughput experiments. G.M. and P.S. designed, performed, and analyzed the structural biology experiment. T.V., A.S., and H.E.K. designed,

performed, and analyzed LC–MS/MS experiments. A.C.K, A.M., J.A-W., and R.A.Z. designed, performed, and analyzed hydrogen–deuterium exchange experiments. P.B., P.A., A.C.K, C.G., K.S., T.P., and A.R. designed, performed, and analyzed ADME, pharmacology, and toxicology experiments. T.V., A.C.K., I.B., and T.H. wrote the manuscript. All authors discussed results and approved the manuscript.

Competing interests: T.V., A.C.K., O.W., T.K., and T.H. are listed as inventors on a provisional patent application No. 62/636983, covering OGG1 inhibitors. The patent is fully owned by a non-profit public foundation, the Helleday Foundation, and T.H. is a member of the foundation board developing OGG1 inhibitors towards the clinic. An inventor reward scheme is under discussion. The remaining authors declare no competing financial interests.

Data and materials availability: Mouse inflammatory cytokines & receptors PCR array data have been deposited in the Gene Expression Omnibus (GEO), NCBI, and is accessible through GEO series accession no. GSE106785 and GSE116809. The atomic coordinates and structure factors (codes 6G3X and 6G3Y) have been deposited in the Protein Data Bank (http://wwpdb.org). The supplementary materials section contains additional data.

Main text figure legends

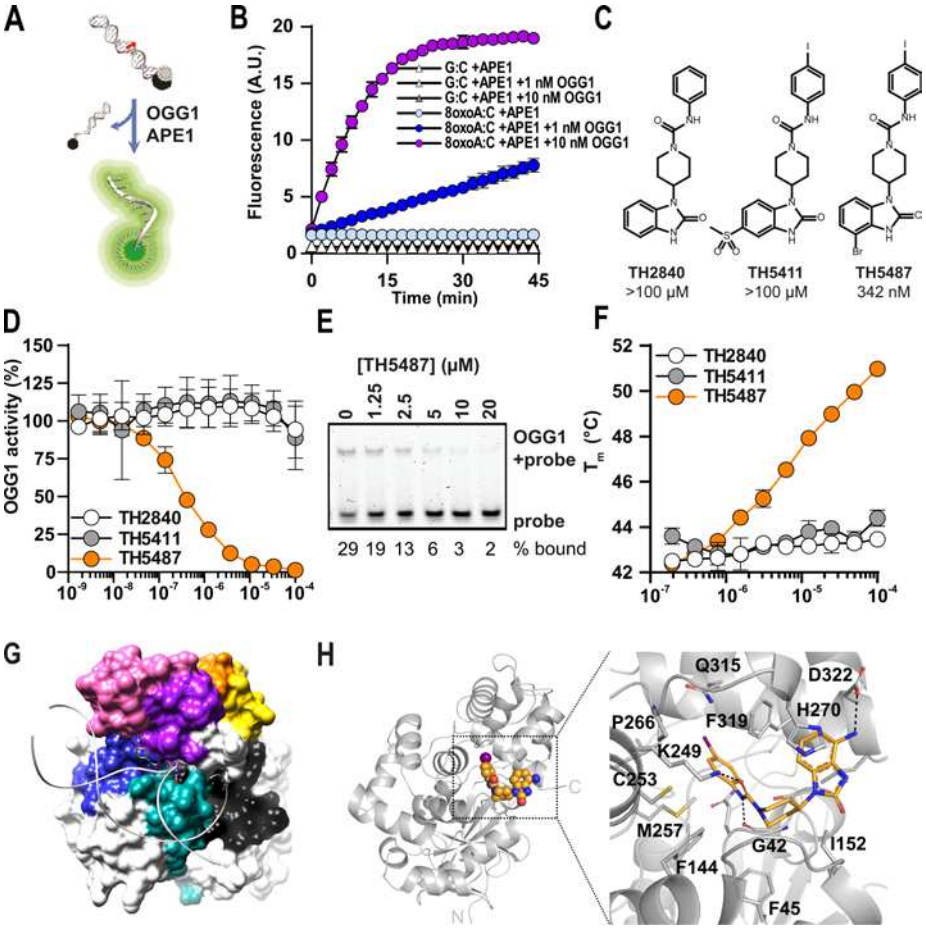

Fig. 1: Development and validation of OGG1 inhibitors (A) A fluorophore and a quencher on opposite strands are separated upon OGG1-mediated excision of 8-oxoA and APE1 incision at the resulting apurinic site, causing a local melting of the DNA helix. **(B)** Excision of 8-oxoA:C, but not undamaged substrates by OGG1 in the presence of APE1. Data represent average ± SD of three technical replicates, representative of four independent experiments. (**C)** Chemical structures of the OGG1 inhibitors described herein. **(D)** Inhibition curves: 0.8 nM OGG1 and 2 nM APE1 were incubated with 10 nM OGG1-substrate and different concentrations of the indicated compounds. Data are presented as average of four technical replicates from at least two independent experiments (n=2 for TH2840 and TH5411, n=33 for TH5487). **(E)** TH5487 precludes binding of OGG1 to damaged DNA. 10 nM of an OGG1 substrate duplex oligonucleotide was incubated with 100 nM OGG1 and the indicated concentrations of TH5487. This prevented the formation of OGG1–DNA complexes in a dose-dependent manner. The figure is representative of three independent experiments. **(F)** Differential scanning fluorimetry (DSF): OGG1 was incubated with SYPRO Orange and a dilution series of OGG1 inhibitors. TH5487, but not inactive analogues TH2840 and TH5411, confers the thermal stabilization of OGG1. Data are average ±SD of three technical replicates and are representative of three independent experiments. (**G)** Differences in deuterium uptake superimposed on an OGG1 model upon

TH5487 binding (PDB: 1EBM). Colored regions show peptides protected from deuterium exchange. The molecular surface of TH5487 is shown as a semi-transparent surface and DNA is displayed as a ribbon. **(H)** X-ray crystal structure of mouse OGG1 (gray) in complex with ligand (yellow). N- and C-termini are labeled. Close-up view of ligand binding. Important amino acid residues are marked; hydrogen bond interactions are shown with black dashed lines. Please note that the view in H is different from the one in G.

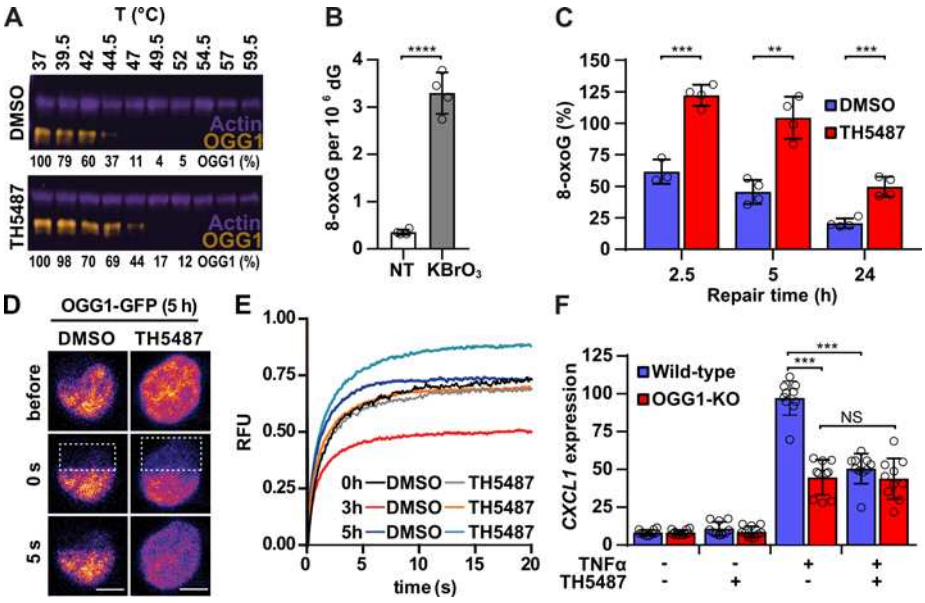

Fig. 2: TH5487 engages OGG1 in cells, inhibits DNA repair, and alters OGG1 chromatin dynamics. (A) Cellular thermal shift assay: Jurkat A3 cells were treated with 10 µM TH5487 and OGG1 thermal stability was analyzed by immunoblotting. Addition of 10 µM TH5487 to cultured cells increased the melting point of OGG1 by 3°C (n=2 independent experiments). **(B)** Induction of genomic 8-oxoG by $KBrO_3$: duplicate cultures of Jurkat A3 cells were treated for 1 h with 20 mM $KBrO_3$, and the level of 8-oxoG in genomic DNA determined by LC-MS/MS. $KBrO_3$ induced a >10-fold increase in genomic 8-oxoG. Data are presented as average ± SD of four replicates from two independent experiments. **(C)** Repair kinetics of genomic 8-oxoG: Cells treated with 20 mM $KBrO_3$ for 1 h were washed and released into medium containing 10 µM TH5487 or 0.1% DMSO. Duplicate samples were taken at the indicated time points and genomic content of 8-oxoG determined as in C. TH5487 induced a notable delay in repair kinetics at 2.5-, 5- and 24-h time points. Data are presented as average ± SD of four replicates from two independent experiments. **(D)** Fluorescence recovery after photobleaching (FRAP): Jurkat A3 cells expressing OGG1–GFP were treated with 16 mM $KBrO_3$, washed, and released into medium with 10 µM TH5487 or 0.1% DMSO. A nuclear region was bleached and recovery of fluorescence after photobleaching was recorded. Representative false-color images of DMSO- and TH5487-treated cells. **(E)** Quantification of FRAP experiments: 10 µM TH5487 increased the nuclear mobility of OGG1-GFP at 3 h and 5 h after $KBrO_3$ treatment. Quantifications of two (0 h) or three (3 h and 5 h) independent experiments are shown. **(F)** TH5487 inhibits TNFα-induced *CXCL1* gene expression in wild-type, but not OGG1 knock out HEK293T cells. Cells were treated with 0.05% DMSO or 5 µM TH5487 for 1 h and TNFα (20 ng/ml) for 30 min. *CXCL1* mRNA levels were determined with qPCR. Data are average ± SD from three independent experiments. $^{*}p < 0.05$, $^{**}p < 0.01$, $^{***}p < 0.001$, using unpaired two-sided t-test.

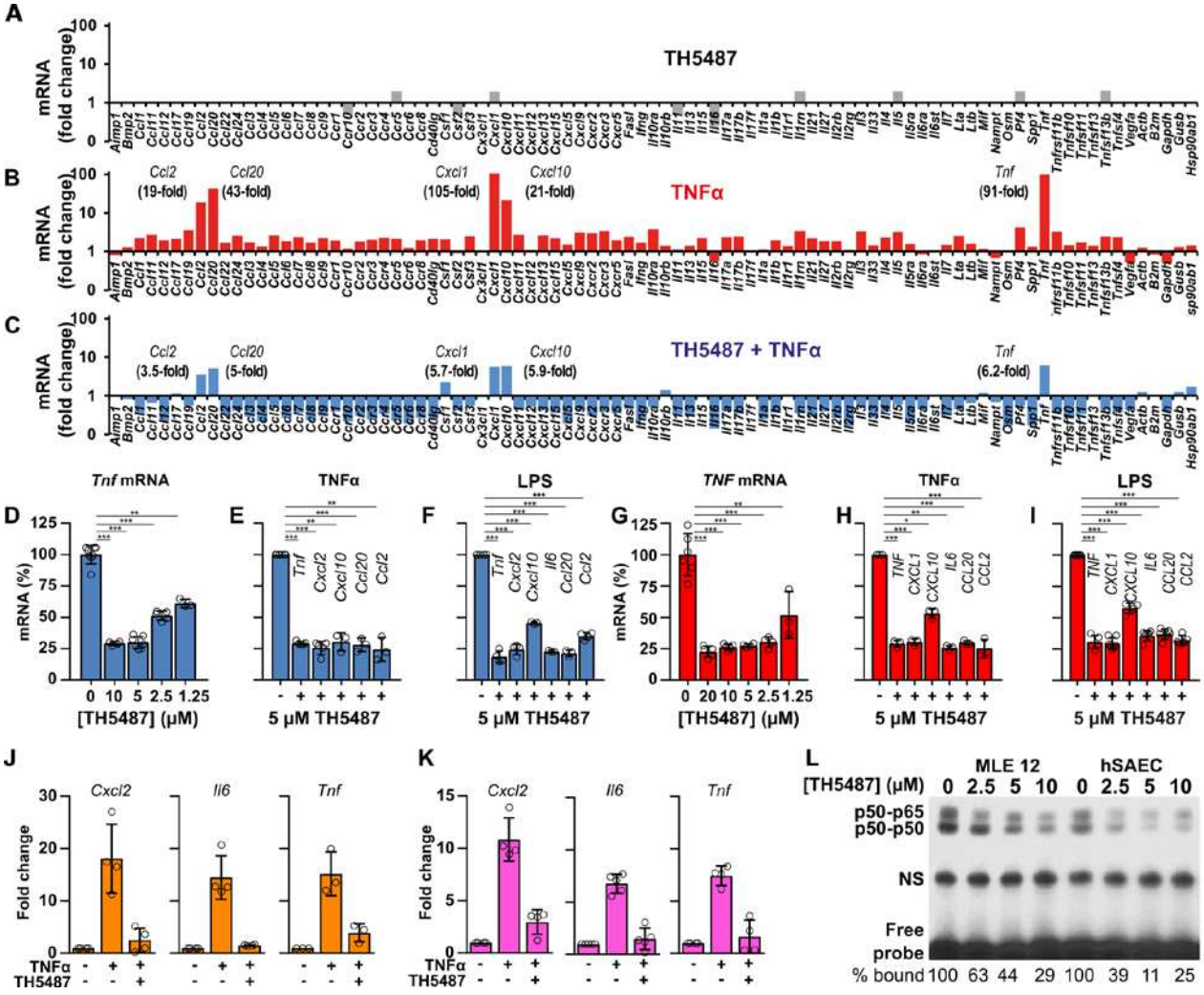

Fig. 3: Inhibition of pro-inflammatory gene expression and inflammation by TH5487 an active-site binder of OGG1. (A to **C)** The effect of TH5487 on basal (A) and TNFα-induced expression of an array of pro-inflammatory cytokines, chemokines and receptors (B, C) in mouse airway epithelial cells (MLE 12). Data analysis were performed according to the manufacturer's instructions using their web-based software package: http://sabiosciences.com/pcrarraydataanalysis.php. **(D)** The dose-dependent inhibition of TNFα-induced *Tnf* mRNA levels by TH5487 in MLE 12. **(E** and **F)**, TH5487 inhibits the TNFα- and LPS-induced expression of pro-inflammatory genes in MLE 12. **(G)** Dose-dependent inhibition by TH5487 of TNFα-induced expression of *TNF* in human airway epithelial cells (hSAECs). **(H** and **I)** TH5487 inhibits TNFα- or LPS-induced expression of pro-inflammatory genes in hSAECs. In A, B, C, E, F, H and I, parallel cultures of cells were treated with solvent or TH5487 (5 μM) for 1 h and TNFα (20 ng/ml for 30 min) or LPS (100 ng/ml for 1 h) was added. In D and G, decreasing concentrations of TH5487 were added prior to TNFα (20 ng/ml for 30 min). Changes in mRNA levels were determined by qRT-PCR. Data are presented as average ± SD of at least three independent experiments. **(J)** TH5487 decreases binding of OGG1 to promoters in chromatin. **(K)** TH5487 perturbs DNA occupancy of NF-κB in chromatin. In J and K, data are presented as average ± SD of four independent experiments. In J and K, MLE 12 cells were treated with solvent or 5 μM TH5487 for 1 h and exposed to TNFα (20 ng/ml) for 30 min. Chromatin was immunoprecipitated using antibody to epitope-tagged OGG1, or RelA/NF-κB. Fold changes in OGG1 and NF-κB binding

to the indicated proximal promoter regions were determined by qPCR. **(L)** TH5487 perturbs binding of NF-κB to 8-oxoG containing synthetic DNA in nuclear extracts from MLE 12 or hSAEC cells. Images are representative of three independent experiments. In D to L, $^{*}p < 0.05$, $^{**}p < 0.01$, $^{***}p < 0.001$, using unpaired two-sided t-test.

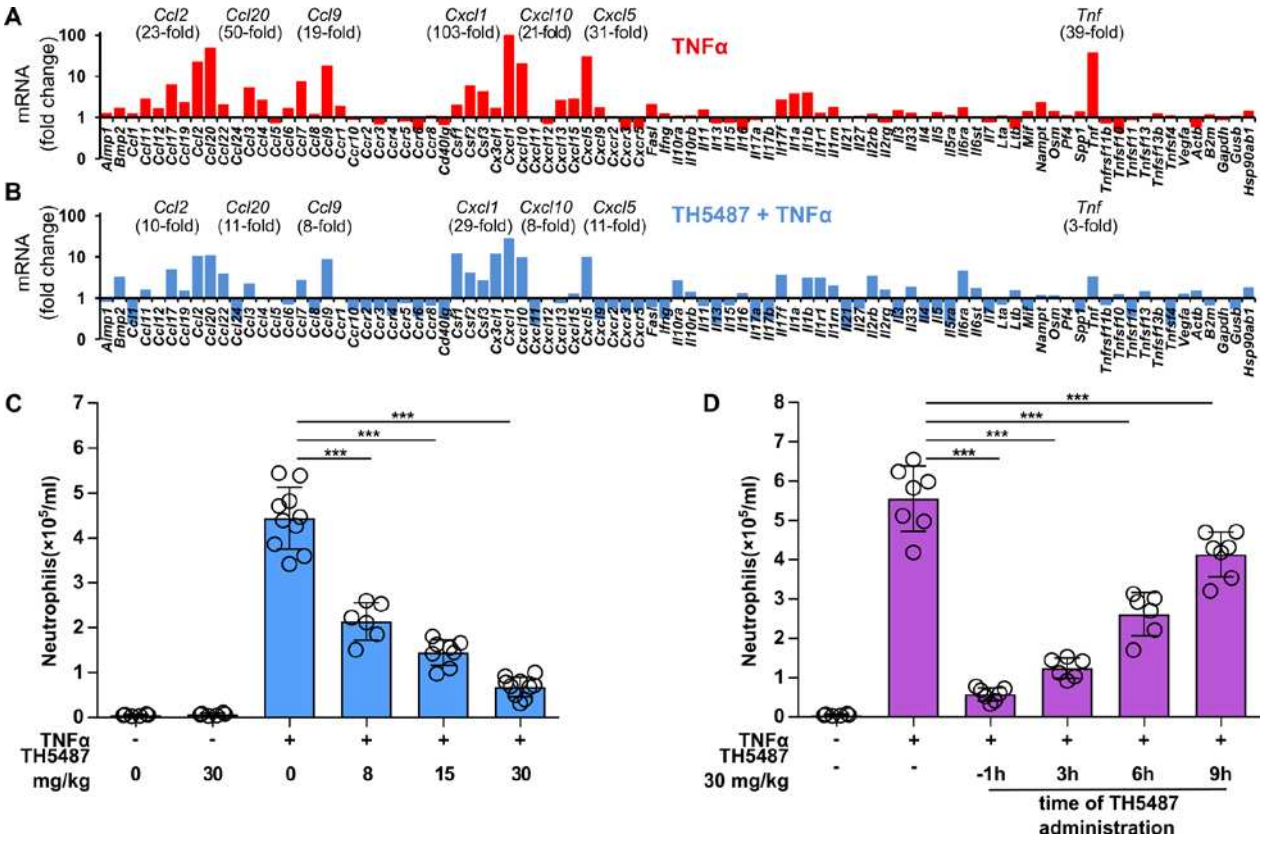

Fig. 4: TH5487 suppresses pro-inflammatory gene expression and lung inflammation in mice (A,B). Groups of mice were treated intraperitoneally with TH5487 (30 mg/kg) or vehicle and lungs were TNFα-challenged intranasally (20 ng/ml). The bars represent expression levels of mRNAs pooled from lungs of six individual mice. Target gene signals were normalized to housekeeping genes and all data analysis were performed according to the manufacturer's instructions using their web-based software package: http://sabiosciences.com/pcrarraydataanalysis.php (n=1). **(C)** Dose dependent inhibition of TNFα-induced neutrophilic inflammation by TH5487. Mice (50% ♀; 50% ♂) were treated intraperitoneally with increasing doses of TH5487 and challenged intranasally with TNFα. Sixteen hours after challenge, mice were euthanized and lavaged. Neutrophil numbers in bronchoalveolar lavage fluid were determined in a blinded fashion. **(D)** TH5487 interrupts TNFα-induced ongoing inflammatory processes. Randomly selected groups of mice (50% ♀; 50% ♂) were challenged intranasally with vehicle or 20 ng/lung TNFα, with TH5487 administered intraperitoneally 1 h before or 3 h, 6 h or 9 h thereafter. Sixteen hours post TNFα stimulation, mice were euthanized and lavaged. The levels of neutrophil infiltration were assessed as described for 4C. In C, D, $^{***}p < 0.001$, using unpaired two-sided t-test.

Supplementary Materials for

Small-molecule inhibitor of OGG1 suppresses pro-inflammatory gene expression and inflammation

Torkild Visnes[†], Armando Cázares-Körner[†], Wenjing Hao[†], Olov Wallner[†], Geoffrey Masuyer, Olga Loseva, Oliver Mortusewicz, Elisée Wiita, Antonio Sarno, Aleksandr Manoilov, Juan Astorga-Wells, Ann-Sofie Jemth, Lang Pan, Kumar Sanjiv, Stella Karsten, Camilla Gokturk, Maurice Grube, Evert J. Homan, Bishoy M.F. Hanna, Cynthia B. J. Paulin, Therese Pham, Azita Rasti, Catharina von Nicolai, Carlos Benitez-Buelga, Tobias Koolmeister, Dag Ivanic, Petar Iliev, Martin Scobie, Hans E. Krokan, Pawel Baranczewski, Per Artursson, Mikael Altun, Annika Jenmalm Jensen, Christina Kalderén, Xueqing Ba, Roman A. Zubarev, Pål Stenmark, Istvan Boldogh[3*], Thomas Helleday[1*]

†These authors contributed equally
* Correspondence to: sboldogh@umtb.edu (I.B.) and thomas.helleday@scilifelab.se (T.H.)

This PDF file includes:

Supplementary materials and methods
Figs. S1 to S20
Tables S1 to S13
Captions for Movie S1
References (30-58)

Other Suplementary Materials for this manuscript includes the following:

Supplementary Movie S1

Supplementary Material and Methods

Recombinant Proteins

The cDNA of human recombinant APE1 cloned into pET14b vector with *N*-terminal His_6-tag (a gift from Dr. Jason Parsons) was introduced into *Escherichia coli* strain BL21(DE3)pLysS. The transformed cells were grown in LB medium + 100 µg/ml ampicillin at 37°C overnight. LB medium was inoculated with the fresh overnight culture and bacteria were grown at 37°C to an $A_{600\ nm} \approx 0.8$. Then, the temperature was decreased to 30°C, APE1 expression was induced by addition of IPTG to 0.5 mM and cultivation was continued at 30°C for another 3 h. Cells were harvested by centrifugation and lysed in BugBuster protein extraction reagent (Millipore) supplemented with complete protease inhibitor cocktail (Roche) and Benzonase nuclease (Novagen) for 20 min at room temperature (RT). The suspension was centrifuged at 12000 × *g* for 20 min and the clear supernatant was loaded on a Ni–Sepharose column (HisTrap HP, GE Healthcare) equilibrated with 50 mM HEPES pH 7.5, 200 mM NaCl, 40 mM imidazole, 5% glycerol. Bound proteins were eluted using a linear gradient of imidazole (40 mM–500 mM) and analyzed by SDS–PAGE. Fractions containing APE1 protein were combined, dialyzed against 25 mM HEPES, pH 7.4, 25 mM NaCl, 5% glycerol, loaded onto an SP cation exchange column (GE Healthcare) and eluted with 25 mM – 800 mM NaCl gradient in 25 mM HEPES, pH 7.4, 25 mM NaCl, 5% glycerol. The purity of the final APE1 fractions was assessed by SDS–PAGE (Fig. S20) and verified by MALDI–TOF mass spectrometry analysis. The fractions with purified APE1 were dialyzed against 50 mM Tris-HCl pH 7.8, 50 mM KCl, 20% glycerol and protein concentration was determined by the Bradford method using Coomassie Plus Protein Assay Reagent and BSA as protein standard (Thermo Scientific). Aliquots of purified APE1 proteins were stored at −80°C.

The pNIC28–OGG1 construct expressing human recombinant OGG1 with N-terminal His_6-tag was transformed into Rosetta2pLysS *E. coli* competent cells. The transformed cells were grown in LB medium + 50 µg/ml kanamycin at 37 C overnight. Fresh overnight culture was inoculated into LB medium containing 50 µg/ml kanamycin, 0.8% glycerol, and 0.4% glucose and grown at 37°C to an $A_{600\ nm} \approx 0.9$ followed by a reduction in temperature to 18°C. After 1 h cultivation at 18°C, protein expression was induced by addition of 0.5 mM IPTG. Protein expression was continued for 18 h at 18°C. Cells were lysed using BugBuster protein extraction reagent (Millipore) with complete protease inhibitor cocktail (Roche), benzonase nuclease (Novagen) and 0.25 mg/ml of lysozyme (Sigma-Aldrich). After rotation for 20 min at RT, the suspension was centrifuged at 12000 × *g* for 20 min. The clear supernatant of cell lysate was loaded onto a Ni–Sepharose column (HisTrap HP, GE Healthcare) equilibrated with 25 mM potassium phosphate, pH 7.6, 250 mM NaCl, 10 mM imidazole and 5% glycerol buffer. The bound proteins were eluted with 50 mM–500 mM imidazole gradient in 25 mM potassium phosphate, pH 7.6, 250 mM NaCl, 5% glycerol buffer. The protein fractions were analyzed by SDS-PAGE using Mini-Protean 4%–15% TGX gel (Bio-Rad). The fractions with OGG1 protein were dialyzed against 25 mM potassium phosphate pH 7.4, 50 mM NaCl, and 10% glycerol at 4°C overnight. They were then loaded onto a cation-exchange column (SP HP, GE Healthcare) equilibrated with the same buffer and eluted with 50 mM–800 mM NaCl gradient. The purity of OGG1 protein was checked by SDS–

PAGE (Fig. S20) and protein concentration was determined by the Bradford method with Coomassie Plus Protein Assay Reagent and BSA as protein standard (Thermo Scientific). The sample with purified OGG1 protein was dialyzed against 25 mM potassium phosphate pH 7.4, 250 mM NaCl, 40% glycerol, aliquoted and stored at −20°C. *E.coli* formamidopyrimidine-DNA glycosylase (Fpg, M0240), single-strand selective monofunctional uracil-DNA glycosylase 1 (SMUG1, M0336), and methylpurine-DNA glycosylase (MPG, M0313) were purchased from New England Biolabs. ITPase, NEIL1, and TDG were purified by the Protein Science Facility at the Karolinska Institute, using C- and N-terminal histidine-tags, respectively. A synthetic gene fragment encoding mouse OGG1 was cloned into the pNIC28-vector and mouse OGG1 was purified as described for the human enzyme above. UNG2 was expressed from the pET28a vector (*30*) and purified essentially as described (*34*). Expression constructs of NUDT5, NUDT12, NUDT14, and NUDT15 in pNIC28 were kind gifts from SGC Stockholm. MTH1, SAMHD1, NUDT2, NUDT9 and NUDT18 were expressed from pET28a(+) (Novagen). Nudix proteins were expressed as N-terminally His-tagged in *E. coli* BL21(DE3) R3 pRARE2 at 18°C and were purified using HisTrap HP (GE Healthcare) followed by gel filtration using HiLoad 16/60 Superdex 75 (GE Healthcare) as decribed (*32*). NUDT2 was expressed at 18°C in BL21 DE3 (Life Technologies) and purified on HisTrap HP followed by cation exchange chromatography purification using HP monoQ column (GE Healthcare). dUTPase and dCTPase were expressed from pET28a(+) as *N*-terminally His-tagged in BL21 DE3 and BL21 DE3 pLysS (Life Technologies), respectively, and purified using HisTrap HP followed by cation exchange chromatography using HP monoQ (GE Healthcare). Purity of protein preparations was analyzed using SDS-PAGE followed by Coomassie staining. Purified proteins were aliquoted and stored at −80°C.

High throughput screening compatible OGG1 Glycosylase Activity Assay

The OGG1 activity assay was performed in black 384-well plates (Optiplate, PerkinElmer) using final concentrations of 25 mM Tris-HCl pH 8.0, 15 mM NaCl, 2 mM $MgCl_2$, 0.5 mM DTT, 0.0025% Tween-20, and 1:3000 dilution of dialyzed fish gelatin (Sigma G7765), 800 pM OGG1 enzyme, 2 nM APE1 and 10 nM 8-oxoA:C substrate in a final volume of 20 µl. The 8-oxodA:C substrate was a duplex oligonucleotide where 5′-FAM-TCTG CCA 8CA CTG CGT CGA CCT G-3′ was annealed to a 25% surplus of 5′-CAG GTC GAC GCA GTG CTG GCA GT-Dab-3′. “8” signifies 8-oxoA and “FAM” and “Dab” signify fluorescein and dabcyl (TriLink Biotech). Briefly, compounds dissolved in DMSO were dispensed using an Echo 550 (Labcyte), followed by transfer of enzyme and substrate solutions by a FlexDrop (PerkinElmer). The reactions were stopped by dispensing an equal volume of 0.1% SDS and 1 mM EDTA and read in an Envision plate reader using a 485-nm filter with a bandwidth of 14 nm for excitation and a 535-nm filter with a bandwidth of 25 nm for emission.

Compound Libraries

The screening for inhibitors of OGG1 was done at the Laboratories of Chemical Biology Karolinska Institutet (LCBKI), part of Chemical Biology Consortium Sweden, using a compound concentration of 10 µM in 384-well microtiter plates (black Optiplates, PerkinElmer). Compounds originating from Enamine were screened, along with an LCBKI in-house compound library (donated by Biovitrum AB). All assay plates

contained test compounds in columns 1-22, whereas negative and positive controls in column 23 and column 24 were used for normalization. In this layout, the negative controls represent the uninhibited enzyme, corresponding to empty wells or wells with the equivalent amount of DMSO as the compound containing wells, whereas the positive controls represent the completely inhibited enzyme, corresponding to the lack of OGG1.

Base Excision Repair Enzymes (BER) and DNA Intercalation Selectivity Assays

BER enzymes were assayed with a similar strategy as OGG1, using identical DNA sequences surrounding the substrate lesion and the same reaction buffer containing 2 nM APE1. Briefly, for UNG2, we used uracil with adenine in the opposite strand, 500 nM substrate DNA, and 300 pM UNG2. For SMUG1 and TDG, we used 375 nM and 10 nM substrate, respectively, containing uracil opposite guanine and 0.3 U SMUG1 enzyme *(*M0336 from New England Biolabs) or 33 nM TDG. For Fpg and NEIL1 we used thymidine glycol opposite adenine, 10 and 20 nM substrate DNA, respectively and 0.2 U Fpg (New England Biolabs, M0240) or 10 nM NEIL1. For MPG we used a substrate containing inosine opposite thymine at 10 nM concentration and 0.3 U MPG (New England Biolabs, M0313). For APE1 we pre-treated the UNG2-substrate with *E. coli* Uracil-DNA glycosylase (New England Biolabs M0280) to generate an AP-site opposite adenine, which was used at 10 nM concentration in the presence of 0.1 nM APE1. All assays were in the linear range, and less than 40% of the total substrate had been consumed at readout. DNA intercalation was measured by incubating 10 nM unlabeled, undamaged oligonucleotides in OGG1 reaction buffer in the presence of 62.5 nM Thiazole Orange (Sigma Aldrich 390062) as described (*33*).

NUDIX hydrolase, di- and triphosphatase selectivity assays

Enzyme-catalysed hydrolysis reactions were coupled to inorganic pyrophosphatase (PPase) or alkaline phosphatase from bovine intestinal mucosa (BIP), thereby releasing inorganic phosphate. The produced free phosphate was then detected using the malachite green assay (*34*). These conditions gave robust assays with Z′-factors between 0.5 and 1, and signal to background ratios above 3. Substrate concentration at the K_m value for the respective substrate was chosen if possible. Inhibition using 100 µM compound was tested in reaction buffer (100 mM Tris-Acetate pH 8.0, 10 mM magnesium acetate, 40 mM NaCl, 1 mM DTT, and 0.005% Tween-20) using conditions described in Table S3. Samplers were incubated with shaking at 22°C for 20 minutes. The reaction was then stopped by the addition of the malachite green reagent (*34*). SAMHD1 activity was measured following the established protocol (*35*). Absorbance was read at 630 nm using a Hidex Sense plate reader after a period of incubation with the MG reagent of 15 minutes. The experiment was performed with data points in triplicate and percentage inhibition was calculated relative to the signal of a DMSO treated control.

Target Engagement Assays

Differential scanning fluorimetry (*36*) and cellular thermal shift assay (*37*) was performed as described previously.

Binding Site Characterization by HDX MS

In-solution structural characterization of the OGG1/TH5487 complex was performed by comparing the local hydrogen/deuterium exchange kinetics between OGG1 alone and in the presence of the small molecule. The method involves the following steps:

Preparation of the OGG1/TH5487 complex. The OGG1/TH5487 interaction was initiated by mixing 48 µL of 0.3 mg/mL of OGG1 in 50 mM Tris-HCl, 10 mM NaCl, pH 7.5 with 1.4 µl of 1 mM TH5487 in DMSO (4× molar ligand excess), followed by 30 min incubating at room temperature. The control experiment was prepared in the same manner but using DMSO rather than TH5487. The HDX reaction was initiated by mixing 2 µL of protein complex (or control) with 18 µl of deuterated buffer consisting of 50 mM Tris-HCl, 10 mM NaCl, pH 7.5 in D_2O. The deuterium-labeling reaction was quenched by adding 30 µl of ice-cold 100 mM phosphate pH 2.3, 166 mM TCEP and 3.3 M urea. Each reaction was performed in triplicate using 30-sec, 1-min, 10-min, and 100-min deuteration labeling.

Local Deuterium Uptake Measurement by HDX LC MS. Samples were analyzed in a semi-automated HDX-MS system in which manually injected samples were automatically digested, cleaned and separated at 2°C. Deuterated samples were digested using an in-house packed 2.1 × 30-mm immobilized pepsin column followed by a 3-min desalting step using 0.05% TFA at 350 µl/min. Peptic peptides were then separated by a 2 mm I.D × 50-mm length HALO C18/1.8 µm column using a 20 min/2%–90% acetonitrile gradient in 0.3% formic acid at 100 µl/min. An Orbitrap XL mass spectrometer (Thermo Fisher Scientific) operated at 60,000 resolution at *m/z* 400 was used for analysis. The HDExaminer software (Sierra Analytics, USA) was used to process all HDX-MS data. Peptides exhibiting a statistically significant decrease in HDX kinetics in presence of the small molecule were identified as candidates for the binding site.

X-ray crystallography

Crystals of mOGG1 (20 mg/ml) were obtained from a sitting-drop vapor diffusion setup against 0.12 M Ethylene glycols, 0.1 M Buffer System 3 pH 8.5, and 50% v/v Precipitant Mix 4 (Morpheus screen (*38*), Molecular Dimensions, UK). Samples for co-crystallization were prepared by pre-incubation of mOGG1 (18 mg/ml) with 2 mM–4 mM of the ligands. The mOGG1:TH5675 complex was obtained with 0.09 M Halogens, 0.1 M Buffer System 2 pH 7.5, 50 % v/v Precipitant Mix 3 (Morpheus screen (*38*), Molecular Dimensions, UK). A 200-nl drop of sample was mixed with an equal amount of reservoir and incubated at 16°C. Crystals grew within 1 week and were cryo-cooled in liquid nitrogen for data collection. Diffraction data were collected at station I04, and I24 of Diamond Light Source (Oxon, UK). The complete dataset (between 2.06 and 2.5 Å) was collected from single crystals at 100 K for each complex. Raw data images were processed and scaled with xia2 (*39*), DIALS (*40*), and Aimless (*41*) using the CCP4 suite 7.0 (*42*). Molecular replacement was performed with the coordinates of human OGG1 (PDB code 1EBM), to determine initial phases for structure solution in Phaser (*43*). The working models were refined using Refmac5 (*44*) and manually adjusted with Coot (*45*). Validation was performed with MolProbity (*46*). Crystallographic data statistics are summarized in supplementary table S6. Figures were drawn with PyMOL (Schrödinger, LLC, New York).

Fluorescence recovery after photobleaching

Jurkat A3 cells stably expressing GFP-tagged wildtype OGG1 were centrifuged, resuspended in PBS and seeded onto Poly-L-Lysine coated µ-dish (ibidi). After 10 min, PBS was removed and fresh RPMI medium supplemented with 25 mM HEPES and 16 mM $KBrO_3$ added to the cells for 1 h. A3 cells were subsequently released into medium containing either 0.1% DMSO or 10 µM TH5487 for indicated time periods and transferred to a Zeiss LSM780 confocal microscope equipped with a UV-transmitting Plan-Apochromat 40x/1.30 Oil DIC M27 objective. eGFP was excited with a 488 nm Ar laser line. The microscope was equipped with a heated environmental chamber set to 37°C.

For FRAP analysis, half of each nucleus was selected using the Regions tool of the ZEN software (ZEN, Zeiss, Germany) and photobleached with the 488 nm Ar-laser set to maximum power at 100% transmission using five iterations at scan speed 8 (5 µs). Before and after bleaching, confocal image series were recorded at 100 ms time intervals (20 prebleach and 200 postbleach frames) with a frame size of 256 × 256 pixels and a pixel size of 110 nm, bidirectional scanning and a pinhole setting of 2.52 Airy units. Mean fluorescence intensities of the bleached region were corrected for background and for total nuclear loss of fluorescence over the time course. For the quantitative evaluation of photobleaching experiments, data of at least 19 nuclei from two or three independent experiments were averaged and the mean curve and the standard error of the mean calculated using Microsoft Excel software. Graphs were displayed using GraphPad Prism.

Genomic 8-oxoG analysis

Cells were treated with 20 mM $KBrO_3$ for 1 h in complete medium and treated as indicated. Genomic DNA from 5×10^6 cells was purified using the EZNA tissue DNA kit (Omega Biotek, D3396). Prior to nucleoside analysis, RNA in the DNA isolates was degraded by incubating samples with 8 µg of RNase (Sigma-Aldrich) in 10 mM ammonium bicarbonate (pH 7.0), 1 mM $MgCl_2$, and 0.1 mM deferoxamine mesylate (DFO; Santa Cruz Biotechnologies) at 37°C for 30 min. DFO chelates ferric iron, which can catalyze DNA oxidation by the Fenton reaction in vitro during sample preparation and result in artefactually high oxidative lesion levels. DFO is therefore used to reduce background 8-oxoG levels (*47–49*). Free nucleosides and nucleotides were then removed from samples by centrifugation through 30-kDa cut-off columns (Merck) and re-dissolved in UHPLC-grade water.

After RNAse pre-treatment, 15 µg DNA was hydrolyzed in 50 µl containing 0.8 U nuclease P_1 from *Penicillium citrinum* (Sigma-Aldrich), 80 U Benzonase® nuclease (Sigma-Aldrich), 0.2 U alkaline phosphatase from *E. coli* (Sigma-Aldrich), and 1.25 pmol $^{15}N_3{}^{13}C_2$-8-oxoG (Cambridge Isotopes) in 10 mM ammonium acetate (pH 5.5), 1 mM $MgCl_2$, 0.1 mM $ZnCl_2$, and 0.4 mM DFO at 37°C for 1 h. The reactions were stopped by chilling on ice, and proteins were precipitated by the addition of three volumes ice-cold acetonitrile and centrifugation at 16,000 × *g* for 30 min. The supernatants were then lyophilized at –80°C to dryness. Finally, the samples were re-dissolved in 30 µl of water for LC/MS/MS analysis, of which 5 µl was diluted 5,000-fold

to measure unmodified nucleosides and 20 µl was used to measure 8-oxoG. All analyses were performed with an Agilent 6495 triple quadrupole LC/MS/MS system with an Agilent EclipsePlusC18 RRHD column (2.1 × 150 mm, 1.8-µm particle size). The mobile phases were (A) UHPLC-grade water and (B) UHPLC-grade methanol, both containing 0.1 %UHPLC-grade formic acid. The unmodified nucleoside HPLC method used a flow rate of 300 µl/min with an isocratic flow of 24% B for 2.3 min. The 8-oxoG HPLC method used a flow rate of 300 µl/min with 5% B to 2.5 min, ramp to 13% B at 3 min, ramp to 17.16% B at 5.5 min, hold at 35 % B from 5.5 to 7 min, ramp to 5% at 8 min, and equilibration with 5% B from 7 to 11.5 min. The mass transitions used were 284.1 → 168; 289.1 → 173; 252.1 → 136; 228.1 → 111.9; 268.1 → 152; and 243.1 → 127 m/z for 8-oxoG, $^{15}N_3{}^{13}C_2$-8-oxoG, dA, dC, dG, and dT, respectively.

Chemicals and Antibodies

For OGG1 detection, we used a monoclonal rabbit anti-OGG1 antibody (Ab) from Abcam (ab124741, EPR4664(2)), or a rabbit polyclonal OGG1 antibody from Novus (NB100-106). Loading controls were monoclonal rabbit anti-GAPDH (CellSignaling Technologies Cat #2118, 14C10), or monoclonal mouse anti-actin from Abcam (ab6276, AC-15). OGG1 inhibitor O8 was purchased from Sigma-Aldrich (Cat # SML1697), mouse anti-FLAG Ab M2 (MilliporeSigma (Cat # F1804); chromatin immunoprecipitation (ChIP)-quality rabbit anti-NF-κB/RelA (Cat # sc-372X), and control rabbit IgG (Cat # sc-2025) were bought from Santa Cruz Biotech (Santa Cruz, CA); rabbit anti-phospho-NF-κB/RelA(Ser276) (cat #3037); recombinant TNFα (cat no. H8916) MilliporeSigma; recombinant human (r)NF-kB/p50 (cat no. AG-40T-0021-C002); human rNF-kB/p65 (cat no. AG-40T-0020-C002), Adipogen, San Diego, CA; recombinant OGG1 GenWay (Cat # GWB-P1370E, San Diego, CA); 4-(2′-aminoethyl)amino-1,8-dimethylimidazo[1,2-a]quinoxaline (BMS345541; cat no. CAS 445430-58-0-Calbiochem) MilliporeSigma. *E. coli* lypopolysacharide (LPS) (from strain O111:B4) and LightShift chemiluminescent EMSA kit (Cat # 20148) were purchased from ThermoFisher Scientific.

Mammalian Expression

The human OGG1 coding sequence excluding the stop codon was cloned from the pNIC28-OGG1 construct into the SalI-XhoI restriction site of the pENTR1A no CCDB (w48-1) vector (addgene # 17398), which had been modified to contain EGFP in the XhoI-XbaI site (a kind gift from Dr. P Herr). The K249Q mutation was created by site-directed mutagenesis. Both constructs were transferred into the pLenti PGK Puro DEST (w529-2) (addgene # 19068), using the Gateway LR Clonase II system (Invitrogen # 11791-020). The plasmids were packaged into lentiviral particles and transduced into Jurkat A3 cells and selected using 1 µg/ml puromycin for 7 days. The wild-type OGG1 was cloned into pCMV-N-FLAG expression plasmid (MilliporeSigma) and the sequence identity of N-terminal FLAG-tagged OGG1 was confirmed by direct sequencing (*50*). Transfection was performed using LipofectAMINE 2000 (Invitrogen) according to the manufacturer's instruction.

CRISPR/Cas9 knockout of OGG1

OGG1 was knocked out essentially as described (51). Briefly, two OGG1 targeting sequences 5′-GATGCGGGCGATGTTGTTGTTGG-3′ and 5′-AACAACATCGCCCGCATCACTGG-3′ were cloned into pSpCas9(BB)-2A-Puro plasmid. Following transfection into HEK293T cells, cells were treated with 2 μg/ml of puromycin for 96 h and re-seeded into 96-well plates at a density of 0.5 cells/well. Out of 768 wells, 70 clones were established, of which three displayed reduced OGG1 expression (Fig. S7D). Knockouts were validated by Sanger sequencing of the targeted region, followed by analysis using Tracking of Indels by Decomposition (TIDE) (https://tide.nki.nl/) (52).

Cell culture and maintenance

The A3 and MLE 12 cell lines were acquired from the American Type Culture Collection (ATCC). A3 (ATTC CRL-2570) was grown in RPMI medium supplemented with 10% fetal bovine serum (FBS). An immortalized type 2 mouse lung epithelial cell line (MLE 12; ATCC CRL-2110) was grown in DMEM containing 2% fetal bovine serum (FBS). FBS (HyClone Cat #: SH30084) was obtained from GE Healthcare Life Sciences. All media were supplemented with penicillin (100 units/ml; Gibco, Life Technologies,Inc.) and streptomycin (100 g/ml; Gibco, Life Technologies, Inc.). The human telomerase and cyclin-dependent kinase 4-immortalized human normal small epithelial cell line (hSAEC) were kindly provided by Dr. JD Minna (Hamon Center for Therapeutic Oncology Research, Department of Internal Medicine Pharmacology, University of Texas Southwestern Medical Center, Dallas, TX, USA). These cells display characteristics of normal airway epithelial cells including morphology, epithelial cell markers cytokeratins 7, 14, 17, and 19, the stem cell marker p63, p16(INK4a) and have an intact p53 checkpoint pathway (*53*). hSAECs were cultured in small airway epithelial growth media (SAGM^{TM}, Cat # CC-3119), supplemented with Bulletkit (Cat # CC-4124) containing 52 μg/ml bovine pituitary extract, 0.5 ng/ml human recombinant epidermal growth factor (EGF), 0.5 μg/ml epinephrine, 1 μg/ml hydrocortisone, 10 μg/ml transferrin, 5 μg/ml insulin, 0.1 ng/ml retinoic acid (RA), 6.5 ng/ml triiodothyronine, 50 μg/ml gentamicin/amphotericin-B (GA-1000), and 50 μg/ml fatty acid-free bovine serum albumin (BSA). Cells were regularly tested for mycoplasma contamination (https://microbiology.utmb.edu/centers/tccf-tissue-culture-core-facility). Cell lines identity was determined using Short Tandem Repeat (STR) analysis (https://scmm.utmb.edu/cores/genomics-core/sequencing) as suggested by the ATCC Standard Development Organization.

Absorption, Distribution, Metabolism, and Excretion (ADME) properties

The kinetic solubility, utilizing test compound from 10 mM DMSO stock solution, was measured at a final compound concentration of 100 μM and 1% DMSO. The test compound was added to 100 mM potassium phosphate buffer and incubated at 37°C for at least 20 hours in a heater-shaker. After incubation, the samples were centrifuged at 3,000 × *g* at 37°C for 30 min to pellet insoluble material and an aliquot of the supernatant was taken for analysis. After dilution of the sample, the concentration of dissolved compound was quantified by LC–MS/MS analysis.

Metabolic stability was determined in 0.5 mg/ml human (pooled) or mouse (pooled) liver microsomes at a compound concentration of 1 µM in 100 mM phosphate buffer pH 7.4 in a total incubation volume of 500 µl. The reaction was initiated by addition of 1 mM NADPH. At various incubation times (i.e., at 0, 5, 10, 20, 40 and 60 min), a sample was withdrawn from the incubation and the reaction was terminated by addition of ice-cold acetonitrile. The amount of parent compound remaining was analyzed by LC–MS/MS.

Plasma protein binding was determined by equilibrium dialysis of drug in plasma against an isotonic buffer. Pooled human plasma was provided by the Uppsala Academic Hospital and was collected from two male and two female donors (non-smoking). 0.2 ml of the plasma test solution (10 µM final compound concentration) was transferred to the membrane tube in a rapid equilibrium dialysis (RED) insert. Isotonic phosphate buffer (0.35 ml) pH 7.4 was added to the other side of the membrane. The 96-well base plate is then sealed with an adhesive plastic film (Scotch Pad) to prevent evaporation. The sample is incubated with rapid rotation (900 rpm) on a Kisker rotational incubator at 37°C for 4 h to achieve equilibrium. After incubation, the contents of each plasma and buffer compartment were removed and mixed with equal volumes of control buffer or plasma as appropriate to maintain matrix similarity for analysis. The samples were then sealed, centrifuged and the supernatant is analyzed by mass spectrometry (LC–MS/MS). The following LC–MS/MS system was used: Waters XEVO TQ triple-quadrupole mass spectrometer (electrospray ionization, ESI) coupled to a Waters Acquity UPLC (Waters Corp.). For chromatographic separation a general gradient was used (1% mobile phase B to 90% over 2 min total run) on a C18 BEH 1.7 µm column 2 × 50mm (Waters Corp.). Mobile phase A consisted of 5% acetonitrile 0.1% formic acid and mobile phase B 100% acetonitrile 0.1% formic acid. The flow rate was 0.5 ml/min. 5 µl of the sample were injected. When analyzing plasma protein binding and solubility samples a standard curve between 1 nM–1000 nM is prepared.

Pharmacokinetics, blood and serum parameters

Pharmacokinetic parameters were determined in compliance with EU 2010/63 directive and approved by the regional experimental animal ethical committee in Stockholm (N484/12). The animals were housed under sterile conditions and were provided with enrichment and free access to food and water. The environmental conditions, temperature, humidity, cage size and light cycle were according to laboratory animal guidelines and regulations. Animals were acclimatized for 1 week before initiation of study. Groups of 7-week-old female C57Bl/6N mice (Charles River laboratories) were administrated either one single dose orally (30 mg/kg) or intravenously (10 mg/kg), according to body weight. Blood was collected in EDTA-coated collection tubes (Sarstedt, Helsingborg, Sweden) at different time points. Three animals were used for each time point. Plasma was separated from by centrifugation at 2,000 × g for 10 min. Pharmacokinetic parameters were calculated using PK Solutions 2.0™ Noncompartmental Pharmacokinetics Data Analysis Software.

To establish blood and serum parameters, six C57Bl/6N (Charles River laboratories, three male and three female) in vehicle and treatment group were administered either vehicle or 30 mg/kg TH5487 by intraperitoneal injection once a day for 5 consecutive days. Twenty-four hours after the last injection, blood was collected by orbital bleeding

to measure whole blood parameters. Serum was subjected to various clinical chemistry assays to detect any toxic effects to major organs. Blood and serum profiles were measured by Adlego Biomedical AB, Solna, Sweden.

In vivo inflammation experiments

In vivo inflammation experiments were performed according to the NIH Guide for Care and Use of Experimental Animals and approved by the University Texas Medical Branch (UTMB) Animal Care and Use Committee (approval no. 0807044B). Eight-week-old female and male BALB/c mice (The Jackson Laboratory, Bar Harbor, ME, USA) housed in pathogen-free conditions in the animal research facility of the UTMB (Galveston, Texas) were used for these studies. Randomly selected groups of mice (50% ♂ and 50%) were challenged intranasally (i.n.) with TNFα (20 ng per mouse) or 20 ng LPS, per lung in 60 µl of pH-balanced saline solution (pH: 7.4) under mild anesthesia (*54*) one hour after intraperitoneal administration of TH5487 (30, 15, and 8 mg per kg, in a 200-µl volume without anesthesia) or vehicle only (5% DMSO, 10% Tween 80 in saline). In controls, mice were challenged alone with TNFα (20 ng), LPS (100 ng) or saline (60 µl). Independent groups of mice were intraperitoneally injected with TH5487 (30 mg per kg) dissolved in 5% DMSO and 10% Tween 80 in saline. During a 48-h observation period, there were no signs of toxicity observed as determined by well-established clinical illness grading scale (0 = healthy; 1 = barely ruffled fur; 2 = ruffled fur but active; 3 = ruffled fur and inactive; 4 = ruffled fur, inactive, and hunched; 5 = dead).

Evaluation of airway inflammation

Evaluation of airway inflammation was performed essentially as described (*22*). Briefly, tracheae were cannulated, and lungs were lavaged by two instillations of 0.6 ml of ice-cold PBS. Broncho-alveolar lavage fluid (BALF) samples were centrifuged (800 × *g* for 5 min at 4ºC), and the resulting supernatants were stored at −80°C for further analysis. Total cell counts in the BALF were determined from an aliquot of the cell suspension using a hemocytometer. Differential cell counts were performed on cytocentrifuge preparations (Shandon Cytospin^{R} 4 Cytocentrifuge, Thermo Scientific, Waltham, MA). Cells were stained with Modified Wright–Giemsa using HEMA-TEK 2000 Slide Stainer (Protocol^{TM}) for differential cell counts. Differential cell counts were performed in a blind fashion by two independent researchers counting 1000 cells from each animal. Randomly selected fields were photographed using an OLYMPUS Microscope System BX53P microscope with a built-in digital CCD color camera DP73WDR.

RNA isolation and quantitative real-time PCR (qRT-PCR)

RNA was extracted using an RNeasy kit (Qiagen) per the manufacturer's recommendations. Briefly, DNaseI-treated total RNA was loaded onto an RNeasy column and subjected to washes with RW1 and RPE buffers. RNA was eluted with the RNase-free water included in the kit. The RNA concentration was determined spectrophotometrically on an Epoch Take-3™ system (Biotek, Winooski, VT) using Gen5 v2.01 software. The quality of the total RNA was confirmed via the 260/280 nm ratio, which varied from 1.9 – 2.0. One microgram of RNA was reverse-transcribed using

a SuperScript® III First-Strand Synthesis System (Invitrogen, Life Technologies). qRT-PCR reactions were performed in triplicate using SYBR Green PCR Master Mix (BioRad) in an CFX 96 real-time PCR detection system (Bio Rad). The transcript levels were evaluated using the $2^{-\Delta\Delta Ct}$ method (*55*) using Microsoft Excel. The validated primers were obtained from Integrated DNA Technologies (San Diego, CA USA) and the sequences may be found in Supplementary Table S11.

Gene expression profiling

Parallel cultures of cells were treated with TH5487 (5 μM) or mock-treated (0.05% DMSO) for 1 h and then exposed to TNFα for 30 minutes (20 ng/ml). Total RNA was isolated with RNeasy Mini Kit followed by DNase I treatment. RNA from three independent cultures were pooled and cDNA were synthesized using Superscript® III First Strand Synthesis System (Invitrogen). cDNA was mixed with equal amounts of 2X iTaq Universal SYBR Green Supermix (BioRad) and 20 μl of reaction mixture was added to each well of the Mouse Inflammatory Cytokines & Receptors PCR Array (PAMM-011ZA) to determine changes in mRNA levels. The qRT-PCR was performed using an ABI PRISM® 7000 Sequence Detection System. The normalization used the average of the following housekeeping genes: beta-D-glucuronidase (*Gusb*), beta-2 microglobulin (*B2M*), heat shock protein 90 Alpha (cytosolic) family class A member 1 (*Hsp90ab1*), glyceraldehyde-3-phosphate dehydrogenase (*Gapdh*), and actin cytoplasmic 1 (*Actb*). Target gene signals normalized to housekeeping genes as described above (*55*). The normalization and all the data analysis were performed according to the manufacturer's instructions using their web-based software package: http://sabiosciences.com/pcrarraydataanalysis.php. The full lists of gene names are in the legend of Supplementary Figure S8.

Electrophoretic Mobility Shift Assay (EMSA)

To evaluate OGG1 binding to damaged DNA, electrophoretic mobility shift assays were performed by incubating 10 nM duplex oligo containing 8-oxoG with 100 nM OGG1 enzyme in 25 mM TrisHCl pH 8.0, 15 mM NaCl, 2 mM $MgCl_2$ and 0.5 mM DTT, supplemented with 5% glycerol and OrangeG as loading dye. The duplex oligo had the sequence 5′-FAM-TGT ATC GAT ACC XTC AAC CTC GAG GAA TT-3′, where "X" signifies 8-oxoG (GeneLink). The complementary sequence, in 25% excess, had the sequence 5′-AAT TCC TCG AGG TTG ACG GTA TCG ATA CA-3′. Samples were incubated with OGG1, TH5487, and DNA for 15 minutes on ice, then separated at 200 V for 45 minutes in a 7.5% polyacrylamide gel (0.5 × TBE, 5% glycerol).

To assess NF-κB binding to synthetic DNA, mock- and TNFα-exposed cells were harvested and nuclear extracts (NEs) were prepared using CelLytic™ NuCLEAR™ extraction kit (NXTRACT, MilliporeSigma) and EMSAs were performed as described (*3*). In brief, protein concentrations of NEs were assessed using the protein assay kit (Bio-Rad). Probes (10 fmol) were mixed with NE (2 μg) in buffer containing 2 mM HEPES (pH 7.5), 4 mM KCl, 1 mM dithiothreitol (DTT), 0.25 mM $MgCl_2$, 0.01% Nonidet P-40, 50 ng/μL of poly(dI-dC), and 1 mg/ml BSA. EMSAs for recombinant NF-κB subunits (RelA(p65R) and/or p50R) were first annealed in 10 mM Tris (pH 7.5), 5 mM NaCl, 1 mM DTT, 1 mM EDTA and 1 mg/ml BSA at 37°C for 1 h. The mixture was incubated with 8-oxo(G) (G*) and NF-κB-binding site containing synthetic double-stranded

oligonucleotides DNA (probe; Dharmacon Inc, GE Healthcare, Lafayette, CO, USA) for 15 min at 4°C (Supplementary Table S12). Unlabeled probe was used for competition experiments. Samples were resolved on a 6% DNA retardation gel (Invitrogen) in 0.25 × TBE buffer. Visualization of NF-κB-DNA complexes was carried out with LightShift chemiluminescent EMSA kit (Thermo Scientific).

To validate the effect of TH5487 on binding of OGG1 to the duplex DNA probe, 10 nM OGG1 in 10 mM Tris (pH 7.5), 5 mM NaCl, 1 mM DTT, and 1 mM EDTA were incubated with TH5487 for 30 min and mixture was added to duplex DNA probes (10 fmol) lacking or containing 8-oxoG for 15 min at 4°C. Sequences of synthetic DNA are identical to those used in NF-κB EMSA. EMSA and visualization of OGG1-DNA complexes were carried out using LightShift chemiluminescent EMSA kit (Thermo Scientific). Band intensities were quantified using ImageJ v1.51 (U. S. National Institutes of Health, Bethesda, Maryland, USA).

Immunoprecipitation and Western blotting

Cells (1×10^7 per time point) were exposed to TNFα (20 ng/ml) and lysed using buffer from Cell Signaling Technology (Cat # 9803; 50 mM TrisHCl, pH 7.5, 150 mM NaCl, 1 mM EDTA, 1 mM EGTA, 1% Nonidet P-40, 2.5 mM sodium pyrophosphate, 1 mM glycerophosphate, 1 mM $Na3VO_4$, 1 mM NaF, and 20 μg/ml aprotin/leupeptin/ phenylmethanesulfonyl fluoride). Cell lysates were centrifuged at 14,000 × *g* at 4°C for 30 minutes. The pre-cleared (on protein A agarose; MilliporeSigma; Cat # 16-125; for 1 h) supernatants were incubated with antibody against RelA for 12 h and then protein A agarose slurry (50%) for 3 h with continuous rotation. The immunoprecipitates were then washed with lysis buffer and resolved by sodium dodecyl sulfate–polyacryamide gel electrophoresis (SDS–PAGE). Proteins were transferred, and nitrocellulose membranes were blocked with 5% non-fat dry milk in TBST (20 mM Tris base, 500 mM NaCl, and 0.05% Tween-20, pH 7.5) and then incubated for 3 h with anti-phospho-RelA antibody (1:1000 dilution) and subsequently with horseradish peroxidase-conjugated secondary antibody (1:4000 dilution; SouthernBiotech, Birmingham, AL, USA). The signals were detected using the ECL Plus chemiluminescent detection system (GE Life Sciences, Bucking Hampshire, UK). After stripping membranes were probed with antibody to RelA (Santa Cruz (Sc-8008). Even loading was confirmed using the GAPDH antibody (Cat # 14C10; Cell Signaling Technology).

Chromatin immunoprecipitation (ChIP)

ChIP assays were performed as described by "ChIP-sequencing guidelines and practices" of the ENCODE (http://encodeproject.org/ENCODE/) and modENCODE consortia using slight modifications. Briefly, Flag-OGG1-transfected cells (10^7) (*3*) were stimulated with TNFα (20 ng/ml) for 0 or 30 min and DNA/protein were cross-linked with 1% paraformaldehyde and sheared (average 300 bp) with 30-second pulses using Cole-Parmer's GEX 130 Ultrasonic processor (Vernon Hills, IL, USA) set to 30% of maximum power. DNA-protein complexes were immunoprecipitated using protein A- or G-agarose (Millipore, Corporation Billerica, MA, USA) with ChIP quality antibodies (Abs) [NF-κB-RelA, Cat # sc-372X; IgG, Cat # sc-2027; Santa Cruz Biotech (Santa Cruz, CA); anti-FLAG Ab, Cat # F1804, SigmaMillipore (Cambridge, MA)], using a ChIP-IT® Express Chromatin Immunoprecipitation Kits (ActiveMotif, Cat # 53008). The

precipitates were washed three times, de-cross-linked and subjected to qPCR, using the primer sequences in Supplementary Table S13. ChIP-qPCR calculations were performed as described previously (*56*). In brief, the ChIP-ed DNA signal was divided by the IgG-ChIP-ed signal, representing the ChIP-DNA signal as the fold increased relative to the IgG signal. This method was based on the assumption that the ChIP of a specific Ab contains both specific signal and background, whereas the ChIP of IgG represents the background alone.

Synthetic Chemistry Experimental Section

General Information.

All reagents and solvents were purchased from Sigma-Aldrich, Combi-Blocks, Thermo Fischer Scientific, or VWR and were used without purification. Unless otherwise stated, reactions were performed without care to exclude air or moisture. Analytical thin-layer chromatography was performed on silica gel 60 F-254 plates (E. Merck) and visualized under a UV lamp. Flash column chromatography was performed in a Biotage® SP4 MPLC system using Merck silica gel 60 Å (40–63 µm mesh). ^{1}H and ^{13}C NMR spectra were recorded on a Bruker DRX-400 MHz spectrometer. Chemical shifts are expressed in parts per million (ppm) and referenced to the residual solvent peak. Analytical LC–MS were performed on an Agilent MSD mass spectrometer connected to an Agilent 1100 system with: Method ST1090A3: Column ACE 3 C8 (50 × 3.0 mm); H_2O (+ 0.1% TFA) and MeCN were used as mobile phases at a flow rate of 1 ml/min, with a gradient from 10% – 90% in 3 min; or Method B0597X3: Column Xterra MSC18 (50 × 3.0 mm); H_2O (containing 10 mM NH_4HCO_3; pH = 10) and MeCN were used as mobile phases at a flow rate of 1 ml/min, with a gradient of 5% – 97% in 3 min. For LC–MS, detection was made by UV (254 or 214 nm) and MS (ESI+). Preparative LC was performed on a Gilson system using Waters C18 OBD 5 µm column (30 × 75 mm) with water buffer (50 mM NH_4HCO_3 at pH 10) and acetonitrile as mobile phases using a flow rate of 45 ml/min. All final compounds were assessed to be >95% pure by LC–MS analysis.

Synthesis of TH5487 (4-(4-Bromo-2-oxo-3H-benzimidazol-1-yl)-N-(4-iodophenyl)piperidine-1-carboxamide).

Step 1. Tert-butyl 4-(3-bromo-2-nitro-anilino)piperidine-1-carboxylate.

A mixture of tert−butyl 4−aminopiperidine−1−carboxylate (3000 mg, 15.0 mmol), 1-bromo-3-fluoro-2-nitro-benzene (3000 mg, 13.6 mmol), and diisopropylethylamine (4.75 ml, 16.4 mmol) was stirred in a sealed vial at 120°C for 16 h. The mixture was concentrated and purified by silica gel chromatography using a gradient of DCM (0% – 100%) in hexane. Yield 4140 mg (80%). LCMS $[M\text{-isobutene+H}]^+$ 344. ^{1}H-NMR (400 MHz, CHLOROFORM-*d*) δ ppm 7.14 (dd, *J*=8.5, 7.6 Hz, 1 H), 6.96 (dd, *J*=7.9, 1.3 Hz, 1 H), 6.76 – 6.79 (m, 1 H), 4.02 (m, 2 H), 3.49 – 3.57 (m, 1 H), 2.99 (m, 2 H), 1.97 – 2.05 (m, 2 H), 1.42 – 1.49 (m, 11 H). ^{13}C-NMR (100 MHz, CHLOROFORM-*d*) δ ppm 154.6, 142.2, 136.7, 132.9, 121.8, 116.5, 112.7, 79.9, 49.9, 42.1, 31.7, 28.4.

Step 2. Tert-butyl 4-(2-amino-3-bromo-anilino)piperidine-1-carboxylate.

A mixture of tert-butyl 4-(3-bromo-2-nitro-anilino)piperidine-1-carboxylate (1845 mg, 4.61 mmol) and $NiCl_2$ (120 mg. 0.922 mmol) was suspended in acetonitrile (20 ml) and water (2.0 ml) and cooled to 4°C, then $NaBH_4$ (698 mg, 18.4 mmol) was added

portion wise. The mixture was then diluted with DCM (30 ml) and decanted. The mixture was poured into $NaHCO_3$ (20 mL) and extracted with DCM (3 × 30 ml). The combined organics were dried, filtered, and concentrated and then purified by silica gel chromatography using a gradient of EtOAc (0% – 40%) in hexane. Yield: 1400 mg (82%). LC-MS $[M\text{-isobutene}+H]^+$ 314. ^{1}H-NMR (400 MHz, CHLOROFORM-*d*): δ (ppm) 7.00 – 7.06 (m, 1 H), 6.68 – 6.75 (m, 1 H), 6.62 – 6.68 (m, 1 H), 4.06 (br. s., 2 H), 3.35 – 3.47 (m, 1 H), 2.91 (m, 2 H), 1.96 – 2.11 (m, 2 H), and 1.47 (m, 11 H).

Step 3. Tert-butyl 4-(4-bromo-2-oxo-3H-benzimidazol-1-yl)piperidine-1-carboxylate.

A mixture of tert-butyl 4-(2-amino-3-bromo-anilino)piperidine-1-carboxylate (550 mg, 1.48 mmol), and diisopropylethylamine, was stirred in DCM at 4°C, then trichloromethyl carbonochloridate (0.090 ml, 0.74 mmol) in DCM (10 ml) was added dropwise. The resulting mixture was stirred 10 min and was then concentrated and purified by silica gel chromatography using a gradient of MeOH (0% – 8%) in DCM. Yield: 530 mg (90%). LC–MS $[M\text{-isobutene}+H]^+$ 340. ^{1}H-NMR (400 MHz, CHLOROFORM-*d*): δ (ppm) 8.37 (br. s., 1 H), 7.20 (dd, *J*=8.1, 0.8 Hz, 1 H), 7.05 – 7.09 (m, 1 H), 6.93 – 6.99 (m, 1 H), 4.45 (tt, *J*=12.5, 4.1 Hz, 1 H), 4.33 (m, 2 H), 2.86 (m, 2 H), 2.29 (m, 2 H), 1.79 – 1.88 (m, 2 H), 1.51 (s, 9 H). ^{13}C-NMR (100 MHz, CHLOROFORM-d): δ (ppm) 154.7, 154.3, 129.7, 127.8, 124.0, 122.2, 108.2, 102.7, 80.0, 51.1, 43.4, 29.1, and 28.5.

Step 4. 7-Bromo-3-(4-piperidyl)-1H-benzimidazol-2-one;2,2,2-trifluoroacetic acid.

In a 100-ml flask tert-butyl 4-(4-bromo-2-oxo-3H-benzimidazol-1-yl)piperidine-1-carboxylate (530 mg, 1.33 mmol) was stirred in DCM (40 ml) at 20°C, then TFA (3.0 ml) was slowly added. The mixture was stirred until the reaction was complete according to LC–MS after which the solvents were removed by co-evaporation with 2-propanol. The crude material was dried by means of a vacuum oven. No further purification was done. Yield: 550 mg (quant.) LC–MS $[M+H]^+$ 296.

Step 5. 4-(4-Bromo-2-oxo-3H-benzimidazol-1-yl)-N-(4-iodophenyl)piperidine-1-carboxamide (TH5487).

A suspension of 7-bromo-3-(4-piperidyl)-1H-benzimidazol-2-one 2,2,2-trifluoroacetic acid (500 mg, 1.23 mmol) and diisopropylethylamine (0.25 mL, 1.44 mmol) was stirred in DCM (20 ml). Then 1-iodo-4-isocyanato-benzene (300 mg, 1.23 mmol) in DCM (5.0 ml) was slowly added. The mixture was stirred in a sealed vial at 50°C for 30 min and another 2 h at 20°C. The solid that precipitated was collected by filtration and was washed sequentially with DCM, water, MeOH, and DCM. The solid was then suspended in boiling MeOH and collected by filtration (this was repeated once). Yield 412 mg (76%). LC–MS $[M+H]^+$ 541. ^{1}H-NMR (400 MHz, DMSO-d_6): δ (ppm) 11.31 (s, 1 H), 8.69 (s, 1 H), 7.53 – 7.59 (m, 2 H), 7.33 – 7.39 (m, 2 H), 7.25 (d, *J*=7.9 Hz, 1 H), 7.16 (d, *J*=7.6 Hz, 1 H), 6.95 (t, *J*=8.1 Hz, 1 H), 4.34 – 4.45 (m, 1 H), 4.28 (m, 2 H), 2.93 (m, 2 H), 2.26 (m, 2 H), 1.74 (m, 2 H). 13C-NMR (100 MHz, DMSO-d6): δ (ppm) 154.4, 153.4, 140.7, 136.9, 130.3, 127.8, 123.2, 121.9, 121.7, 107.7, 101.0, 84.5, 50.5, 43.4, and 28.5.

Synthesis of TH5411 (N-(4-iodophenyl)-4-(5-methylsulfonyl-2-oxo-3H-benzimidazol-1-yl)piperidine-1-carboxamide)

Step 1. Tert-butyl 4-(4-methylsulfonyl-2-nitro-anilino)piperidine-1-carboxylate.

A mixture of tert−butyl 4−aminopiperidine−1−carboxylate (421 mg, 2.1 mmol), 1-fluoro-4-methylsulfonyl-2-nitro-benzene (438 mg, 2 mmol), and diisopropylethylamine (0.350 ml, 2.01 mmol) was stirred at 120°C for 16 h. The mixture was cooled, concentrated and then purified by silica gel chromatography using a gradient of DCM (0% – 100%) in hexane. Yield 537 mg (67%). LC–MS $[M\text{-isobutene+H}]^+$ 344. ^{1}H-NMR (400 MHz, CHLOROFORM-*d*) δ ppm 8.79 (d, *J*=2.2 Hz, 1 H), 8.44 – 8.51 (m, 1 H), 7.90 (ddd, *J*=9.2, 2.2, 0.6 Hz, 1 H), 7.01 (d, *J*=9.2 Hz, 1 H), 4.01 – 4.11 (m, 3 H), 3.70 – 3.80 (m, 1 H), 3.06 (s, 5 H), 2.04 – 2.12 (m, 2 H), 1.55 – 1.66 (m, 2 H), 1.48 (s, 9 H). ^{13}C-NMR (100 MHz, CHLOROFORM-*d*) δ ppm 154.5, 146.6, 133.6, 131.1, 128.3, 126.9, 114.7, 80.1, 49.9, 44.7, 41.9, 31.5, and 28.4.

Step 2. Tert-butyl 4-(5-methylsulfonyl-2-oxo-3H-benzimidazol-1-yl)piperidine-1-carboxylate.

A mixture of tert-butyl 4-(4-methylsulfonyl-2-nitro-anilino)piperidine-1-carboxylate (537 mg, 1.34 mmol) and Pd/C (50 mg) was stirred in THF (15 ml) under an atmosphere of H_2 provided by a balloon. After complete reaction diisopropylethylamine (0.470 ml, 2.69 mmol) and bis(trichloromethyl) carbonate (140 mg, 0.471 mmol) in DCM (10 mL) was added dropwise. The resulting mixture was stirred 10 min and was then concentrated and purified by silica gel chromatography using a gradient of MeOH (0% – 8%) in DCM. Yield 420 mg (79%). LC–MS $[M+H]^+$ 396. ^{1}H-NMR (400 MHz, CHLOROFORM-*d*) δ ppm 9.87 (br. s., 1 H), 7.68 – 7.72 (m, 2 H), 7.27 – 7.30 (m, 1 H), 4.51 (tt, *J*=12.5, 4.2 Hz, 1 H), 4.37 (m, 2 H), 3.08 (s, 3 H), 2.85 – 2.95 (m, 2 H), 2.33 (m, 2 H), 1.87 (m, 2 H), and 1.52 (s, 9 H).

Step 3. 6-Methylsulfonyl-3-(4-piperidyl)-1H-benzimidazol-2-one.

In a 100-ml flask tert-butyl 4-(5-methylsulfonyl-2-oxo-3H-benzimidazol-1-yl)piperidine-1-carboxylate (420 mg, 1.06 mmol) was stirred in DCM (20 mL) at 20°C, then TFA (2.00 mL) was slowly added. The mixture was stirred for 10 min after which the solvents were removed by co-evaporation with 2-propanol. The crude material was dried by means of a vacuum oven. No further purification was done. Yield: 433 mg (quant.) LC–MS $[M+H]^+$ 296.

Step 4. N-(4-iodophenyl)-4-(5-methylsulfonyl-2-oxo-3H-benzimidazol-1-yl)piperidine-1-carboxamide (TH5411).

A suspension of 6-methylsulfonyl-3-(4-piperidyl)-1H-benzimidazol-2-one (41 mg, 0.10 mmol) and diisopropylethylamine (0.014 ml, 0.10 mmol) was stirred in DCM (2 ml). Then 1-iodo-4-isocyanato-benzene (25 mg, 0.10 mmol) was added and the resulting mixture was stirred at 50°C for 3 h. The crude reaction mixture was then purified by silica gel chromatography using a gradient of MeOH (0-10%) in DCM. Yield 46 mg (85%). LC-MS $[M+H]^+$ 541. ^{1}H-NMR (400 MHz, DMSO-*d*6) δ ppm 11.38 (br. s., 1 H), 8.70 (s, 1 H), 7.54 – 7.60 (m, 3 H), 7.47 – 7.52 (m, 1 H), 7.44 (br. s, 1 H), 7.36 (br. d, J=8.5 Hz, 2 H), 4.41 – 4.52 (m, 1 H), 4.25 – 4.34 (m, 2 H), 3.17 (s, 3 H), 2.88 – 3.00 (m, 2 H), 2.20 – 2.34 (m, 2 H), 1.72 – 1.81 (m, 2 H). ^{13}C-NMR (100 MHz, DMSO-*d*6) δ ppm 154.4, 153.9, 140.6, 136.9, 133.3, 132.8, 128.3, 121.7, 120.3, 108.5, 107.2, 84.6, 50.6, 44.2, 43.4, and 28.6.

Synthesis of TH2840 4-(2-oxo-2,3-dihydro-1H-1,3-benzodiazol-1-yl)-N-phenylpiperidine-1-carboxamide).

A mixture of 3-(4-piperidyl)-1H-benzimidazol-2-one (57 mg, 0.26 mmol) and phenyl isocyanate (0.028 mL, 0.26 mmol) was stirred at 20°C for 15 min. The reaction mixture was then filtered and the solid was washed with DCM. Yield: 80 mg (91%). LC–MS $[M+H]^+$ 337. ^{1}H-NMR (400 MHz, DMSO-d_6) δ ppm 10.86 (s, 1 H), 8.59 (s, 1 H), 7.46 – 7.51 (m, 2 H), 7.19 – 7.27 (m, 2 H), 6.96 – 7.01 (m, 3 H), 6.93 (tt, *J*=7.4, 1.1 Hz, 1 H), 4.39 (tt, *J*=12.4, 4.0 Hz, 1 H), 4.25 – 4.34 (m, 2 H), 2.89 – 2.98 (m, 2 H), 2.31 (br. dd, *J*=12.5, 4.0 Hz, 1 H), 2.25 (br. dd, *J*=12.5, 4.0 Hz, 1 H), 1.69 – 1.76 (m, 2 H). ^{13}C-NMR (100 MHz, DMSO-d_6) δ ppm 154.8, 153.7, 140.7, 129.3, 128.3, 128.3, 121.6, 120.6, 120.4, 119.6, 108.8, 108.4, 50.1, 43.5, and 28.7.

Synthesis of TH5675 (4-(4-amino-2-oxo-3H-benzimidazol-1-yl)-N-(4-iodophenyl)piperidine-1-carboxamide).

Step 1. N,N-dibenzyl-3-fluoro-2-nitro-aniline.

A mixture of 1,3-difluoro-2-nitro-benzene (320 mg, 2.0 mmol), dibenzylamine (390 mg, 2.0 mmol), and diisopropylethylamine (0.35 mL, 2.0 mmol) was stirred in 2-propanol (1.0 ml) at 70°C for 4 days. The mixture was then poured into HCl (2 M) and extracted with DCMx3. The combined organics were concentrated and purified by silica gel chromatography using a gradient of DCM (0% – 30%) in isohexane to afford N,N-dibenzyl-3-fluoro-2-nitro-aniline. Yield 600 mg (89%). LC–MS $[M+H]^+$ 337. ^{1}H-NMR (400 MHz, CHLOROFORM-*d*) δ ppm 7.22 – 7.36 (m, 11 H), 6.83 – 6.90 (m, 2 H), and 4.20 (s, 4 H).

Step 2. tert-butyl 4-[3-(dibenzylamino)-2-nitro-anilino]piperidine-1-carboxylate.

A mixture of N,N-dibenzyl-3-fluoro-2-nitro-aniline (600 mg, 1.78 mmol), tert-butyl 4-aminopiperidine-1-carboxylate (600 mg, 3.0 mmol), and diisopropylethylamine (0.54 ml, 3.1 mmol) was stirred in 2-propanol (6.0 mL) at 120°C for 3 days. The mixture was then poured into HCl (2 M) and extracted with DCMx3. The combined organics were concentrated and purified by silica gel chromatography using a gradient of MeOH (0% – 8%) in DCM to afford tert-butyl 4-[3-(dibenzylamino)-2-nitro-anilino]piperidine-1-carboxylate. Yield 640 mg (69%). LC–MS $[M+H]^+$ 517. ^{1}H-NMR (400 MHz, DMSO-*d6*) δ ppm 7.18 – 7.32 (m, 10 H), 7.13 (t, *J*=8.2 Hz, 1 H), 6.61 (d, *J*=8.2 Hz, 1 H), 6.55 (d, *J*=7.3 Hz, 1 H), 5.51 (d, *J*=7.9 Hz, 1 H), 4.04 (s, 4 H), 3.82 – 3.93 (m, 2 H), 3.42 – 3.53 (m, 1 H), 2.82 (br. s., 2 H), 1.75 – 1.84 (m, 2 H), 1.39 (s, 9 H), and 1.27 – 1.36 (m, 2 H).

Step 3 and 4. tert-butyl 4-[4-(dibenzylamino)-2-oxo-3H-benzimidazol-1-yl]piperidine-1-carboxylate.

To a mixture of tert-butyl 4-[3-(dibenzylamino)-2-nitro-anilino]piperidine-1-carboxylate (640 mg, 1.2 mmol) and $NiCl_2$ (32 mg, 0.25 mmol) in acetonitrile (9 ml) and water (1 ml) was added $NaBH_4$ (187 mg, 4.9 mmol) slowly. After complete addition, the mixture was stirred for 30 min after which DCM (10 ml) was added. The mixture was then decanted into $NaHCO_3$ and was then extracted with DCM × 3. The combined organics were dried ($MgSO_4$) and filtered. To the filtrate was then added diisopropylethylamine (0.43 ml, 2.5 mmol) and trichloromethyl carbonochloridate (0.074 ml, 0.62 mmol). The resulting mixture was stirred 30 min and was then concentrated and

purified by silica gel chromatography using a gradient of MeOH (0% – 10%) in DCM to afford tert-butyl 4-[4-(dibenzylamino)-2-oxo-3H-benzimidazol-1-yl]piperidine-1-carboxylate. Yield 670mg (86%). ^{1}H-NMR (400 MHz, CHLOROFORM-*d*) δ ppm 7.24 – 7.39 (overlapping m, 10 H), 6.93 (s, 1 H), 6.80 – 6.86 (m, 1 H), 6.71 – 6.76 (m, 1 H), 4.17 – 4.46 (m, 7 H), 2.74 – 2.90 (m, 2 H), 2.16 – 2.33 (m, 2 H), 1.70 – 1.82 (m, 2 H), and 1.50 (s, 9 H).

Step 5. tert-butyl 4-(4-amino-2-oxo-3H-benzimidazol-1-yl)piperidine-1-carboxylate.

A mixture of tert-butyl 4-[4-(dibenzylamino)-2-oxo-3H-benzimidazol-1-yl]piperidine-1-carboxylate (110 mg, 0.21 mmol), Pd/C (20 mg) and cyclohexene (1 ml) in dioxane (3 ml) was stirred under nitrogen atmosphere at 120°C for 16 h. The mixture was then concentrated and purified by silica gel chromatography using a gradient of MeOH (0% – 10%) in DCM which afforded tert-butyl 4-(4-amino-2-oxo-3H-benzimidazol-1-yl)piperidine-1-carboxylate. Yield 57 mg (83%). LC–MS [M-isobutene+H]$^{+}$ 277. ^{1}H-NMR (400 MHz, CHLOROFORM-*d*) δ ppm 11.10 (br. s, 1 H), 6.94 – 7.00 (m, 1 H), 6.82 – 6.93 (m, 2 H), 4.18 – 4.47 (m, 3 H), 2.74 – 2.95 (m, 2 H), 2.12 – 2.36 (m, 2 H), 1.74 – 1.83 (m, 2 H), and 1.52 (s, 9 H).

Step 6. 7-amino-3-(4-piperidyl)-1H-benzimidazol-2-one.

A mixture of tert-butyl 4-(4-amino-2-oxo-3H-benzimidazol-1-yl)piperidine-1-carboxylate (50 mg, 0.15 mmol) and TFA (1.0 ml) was stirred in DCM (1.0 ml) at 20°C for 1 h. The solvent was then removed by co-evaporation with 2-propanol and the crude residue was purified by preparative LC which afforded 7-amino-3-(4-piperidyl)-1H-benzimidazol-2-one. Yield 14 mg (40%). LC–MS [M+H]$^{+}$ 233. ^{1}H-NMR (400 MHz, DMSO-*d6*) δ ppm 10.24 (br. s., 1 H), 6.72 (t, *J*=7.9 Hz, 1 H), 6.55 (d, *J*=7.9 Hz, 1 H), 6.30 (dd, *J*=7.9, 0.6 Hz, 1 H), 4.86 – 4.93 (m, 2 H), 4.15 (tt, *J*=12.3, 4.3 Hz, 1 H), 2.98 – 3.08 (m, 2 H), 2.49 – 2.58 (overlapping m, 2 H), 2.09 – 2.21 (m, 2 H), and 1.50 – 1.58 (m, 2 H).

Step 7. 4-(4-amino-2-oxo-3H-benzimidazol-1-yl)-N-(4-iodophenyl)piperidine-1-carboxamide (TH5675).

In a reaction tube, 7-amino-3-(4-piperidyl)-1H-benzimidazol-2-one (12 mg, 0.052 mmol) was suspended in DCM (3.0 ml), then 1-iodo-4-isocyanato-benzene (13 mg, 0.052 mmol) was added and the resulting mixture was stirred at 20°C for 16 h. The precipitate that formed was collected by filtration and was washed with DCM and water. No further purification was performed. Yield 16.7 mg (65%). LC–MS [M+H]$^{+}$ 478. ^{1}H-NMR (400 MHz, DMSO-*d6*) δ ppm 10.27 (s, 1 H), 8.69 (s, 1 H), 7.54 – 7.59 (m, 2 H), 7.32 – 7.38 (m, 2 H), 6.72 (t, *J*=8.0 Hz, 1 H), 6.46 (d, *J*=8.0 Hz, 1 H), 6.30 (dd, *J*=8.0, 0.8 Hz, 1 H), 4.91 (s, 2 H), 4.22 – 4.37 (m, 3 H), 2.86 – 2.97 (m, 2 H), 2.18 – 2.31 (m, 2 H), and 1.65 – 1.73 (m, 2 H). ^{13}C-NMR (100 MHz, DMSO-d_6) δ ppm 154.5, 153.3, 140.7, 136.9, 131.8, 129.7, 121.7, 121.3, 114.5, 106.9, 97.8, 84.6, 50.0, 43.6, and 28.7.

Synthesis of SU268 (4'-(*N*-(1-(cyclopropanecarbonyl)-1,2,3,4-tetrahydroquinolin-7-yl)sulfamoyl)-[1,1'-biphenyl]-3-carboxamide)

SU268 was prepared by the method of Tahara et al. (*29*).

Statistical analysis

The data are expressed as the mean±SD. Results were analyzed for significant differences using unpaired, two-tailed Student's *t*-tests using Microsoft Excel procedures. Differences were considered significant at $p<0.05$ (*$p<0.05$, **$p<0.01$, ***$p<0.001$, ****$p< 0.0001$). IC_{50} and EC_{50} were calculated using Microsoft Excel program (2014) and XLfit software (IDBS, United Kingdom).

Supplementary Figures

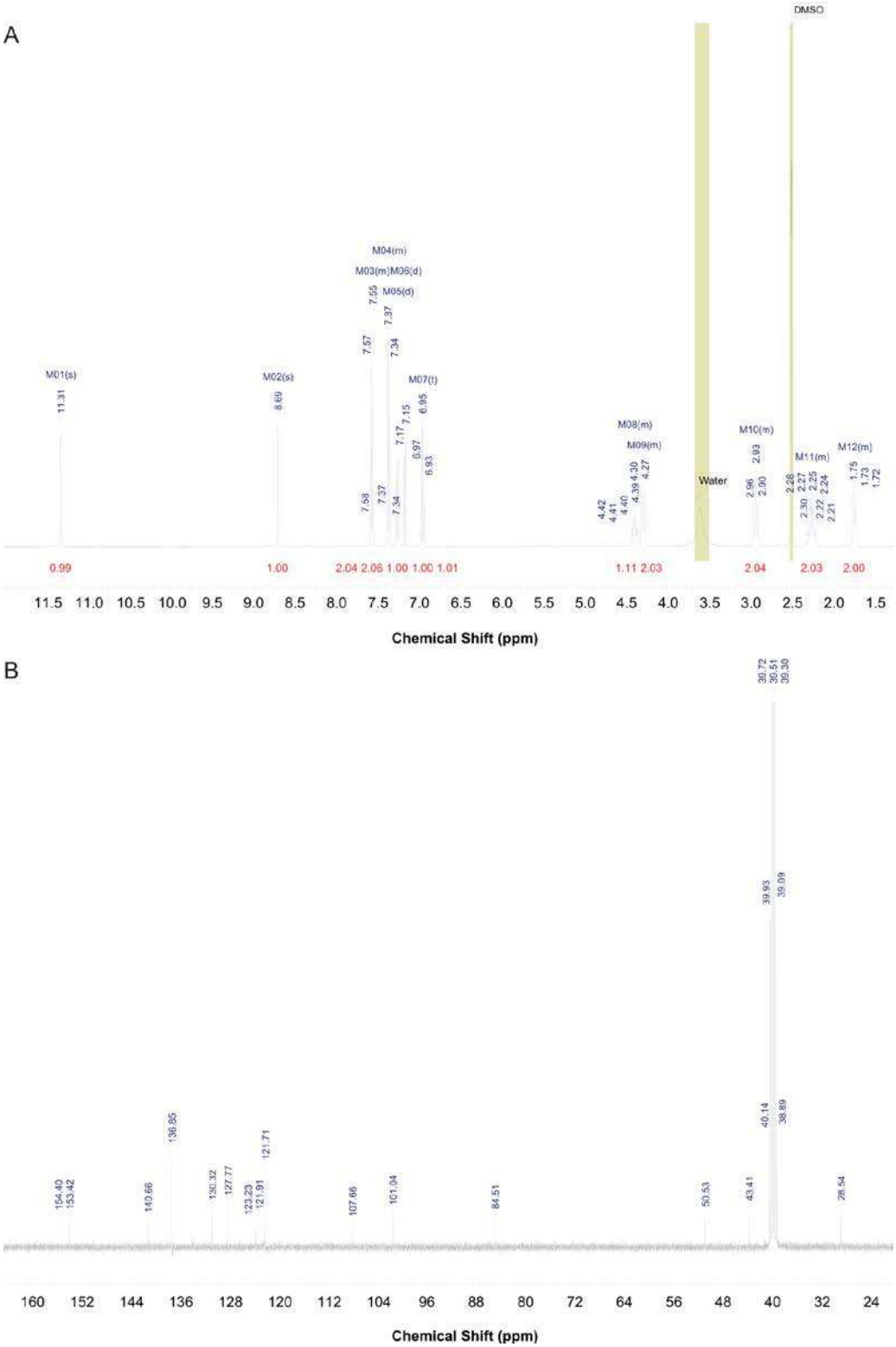

Supplementary Fig. S1: (A) ^{1}H NMR of TH5487. **(B)** ^{13}C NMR of TH5487. Chemical shifts (δ) are shown in parts per million.

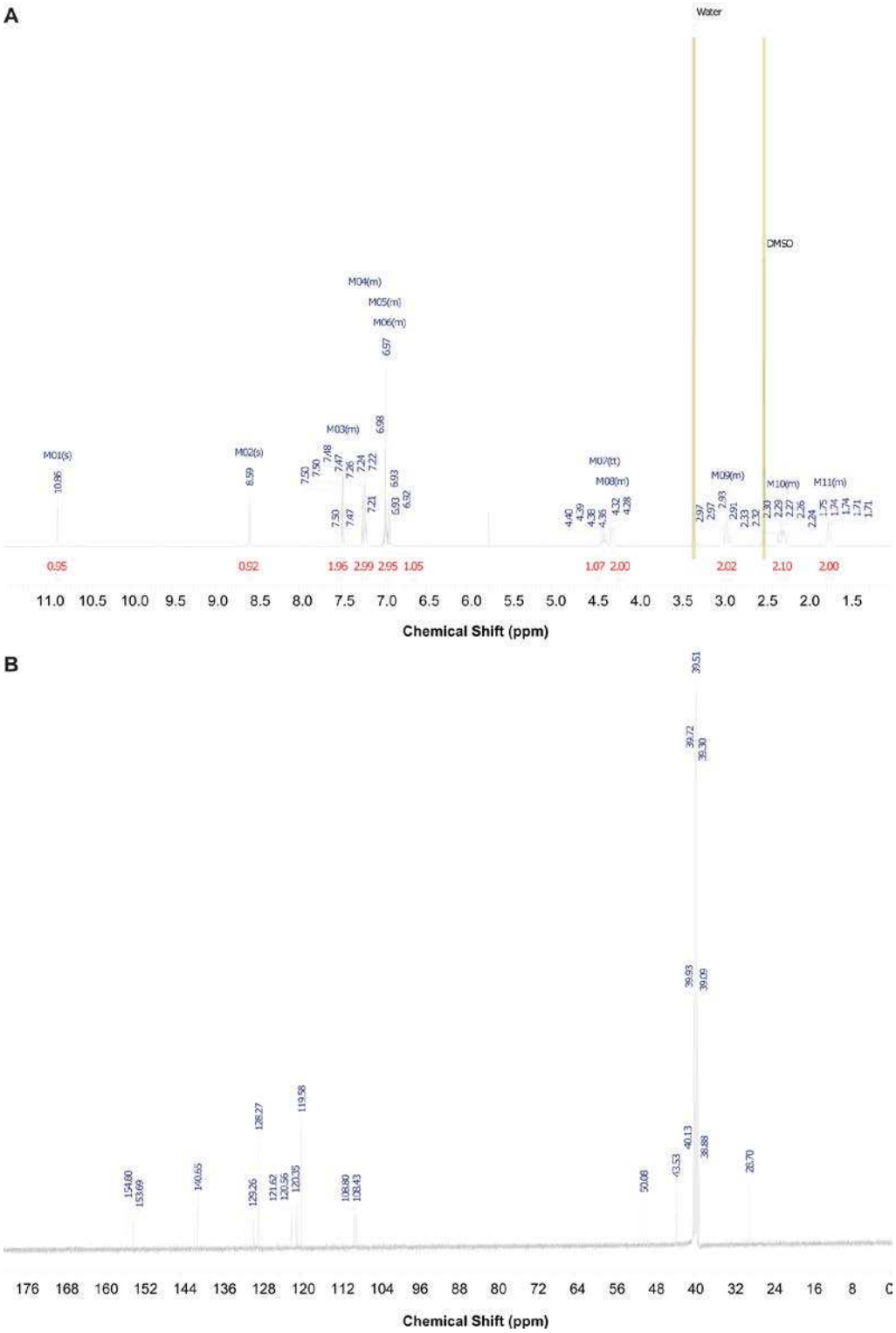

Supplementary Fig. S2: NMR spectra of TH2840. (A) ^{1}H NMR spectrum of TH2840. **(B)** ^{13}C NMR spectrum of TH2840. Chemical shifts (δ) are shown in parts per million.

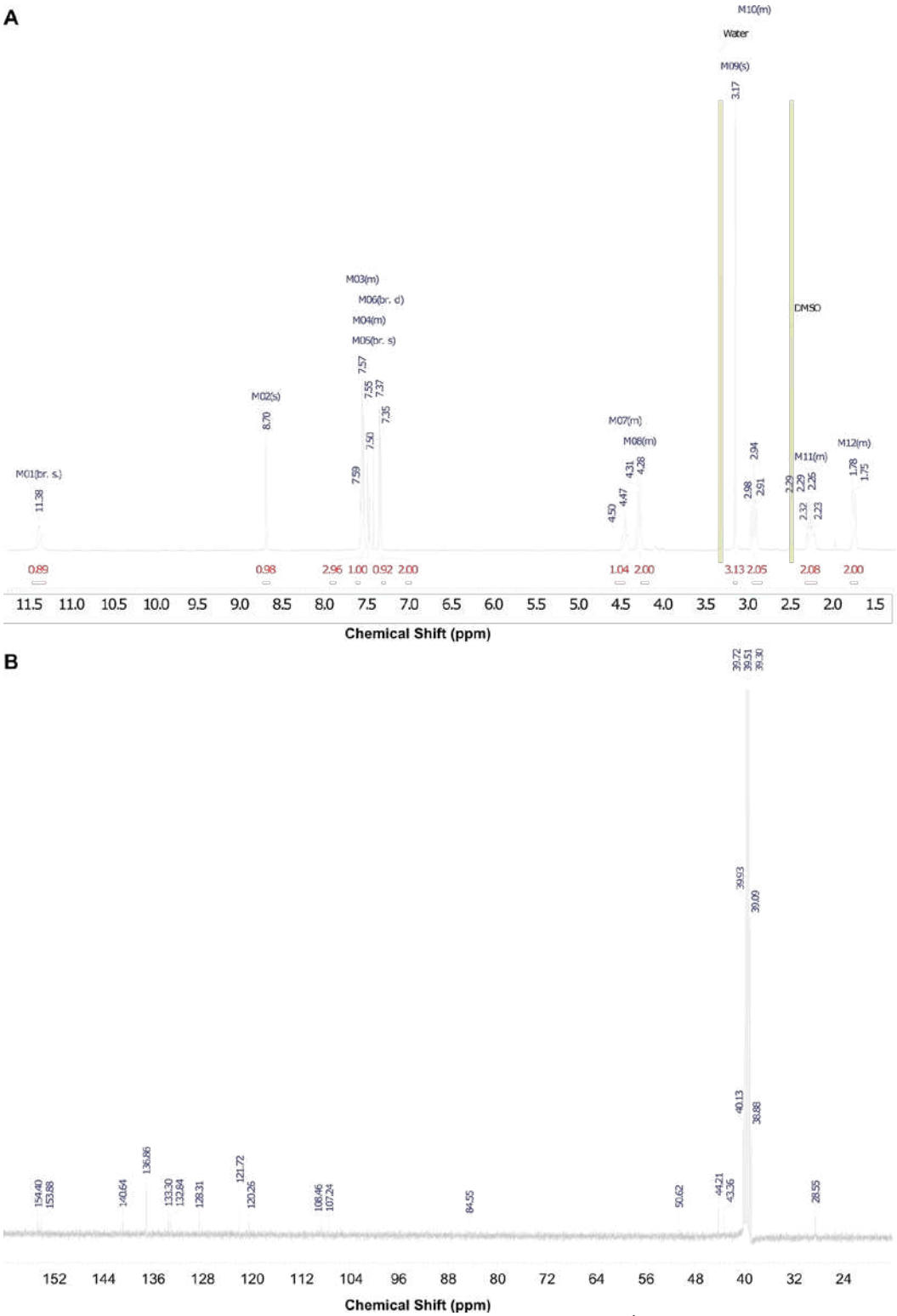

Supplementary Fig. S3: NMR spectra of TH5411. (A) ^{1}H NMR-spectrum of TH5411. **(B)** ^{13}C-NMR spectrum of TH5411. Chemical shifts (δ) are shown in parts per million.

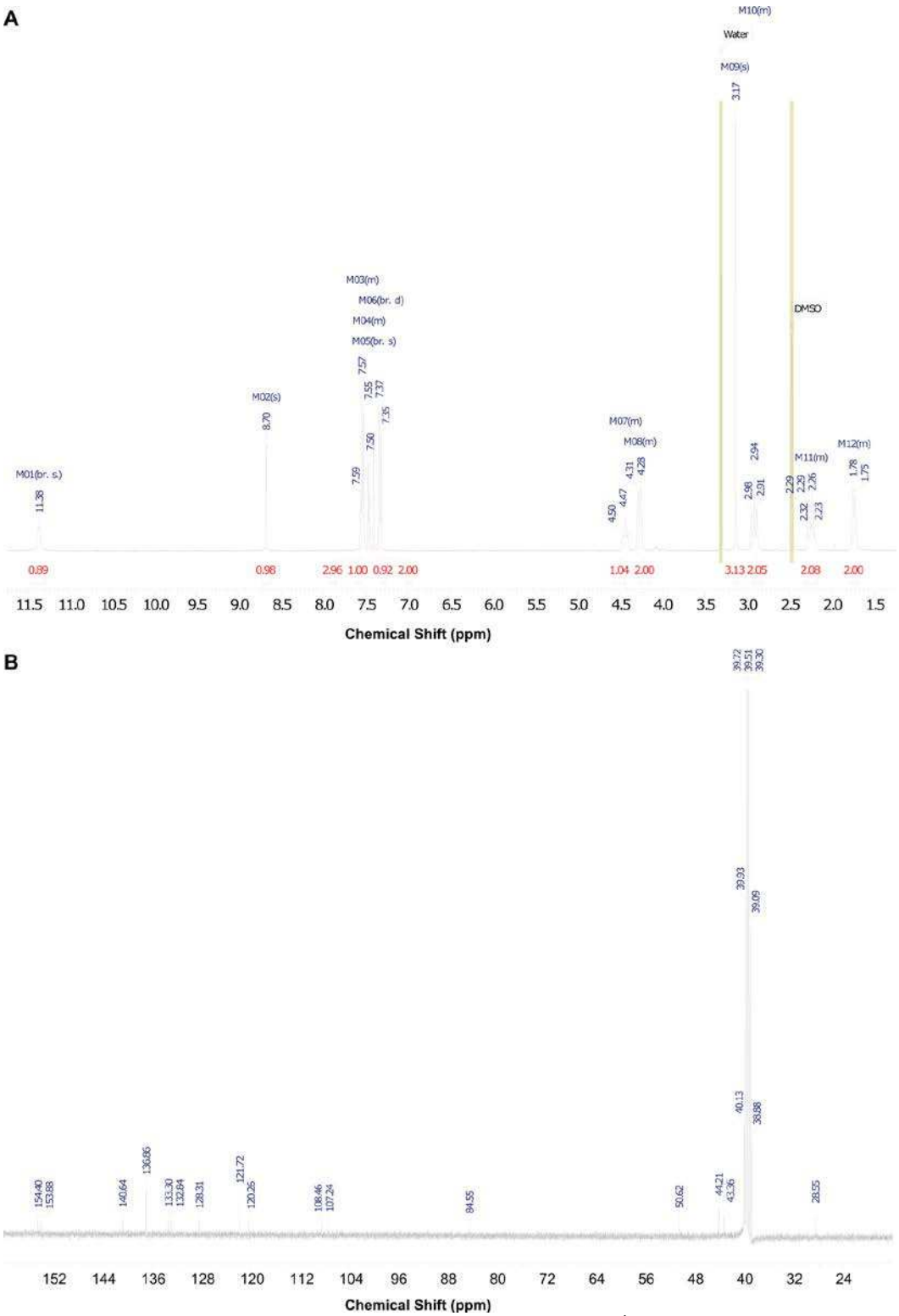

Supplementary Fig. S3: NMR spectra of TH5411. (A) ^{1}H NMR-spectrum of TH5411. **(B)** ^{13}C-NMR spectrum of TH5411. Chemical shifts (δ) are shown in parts per million.

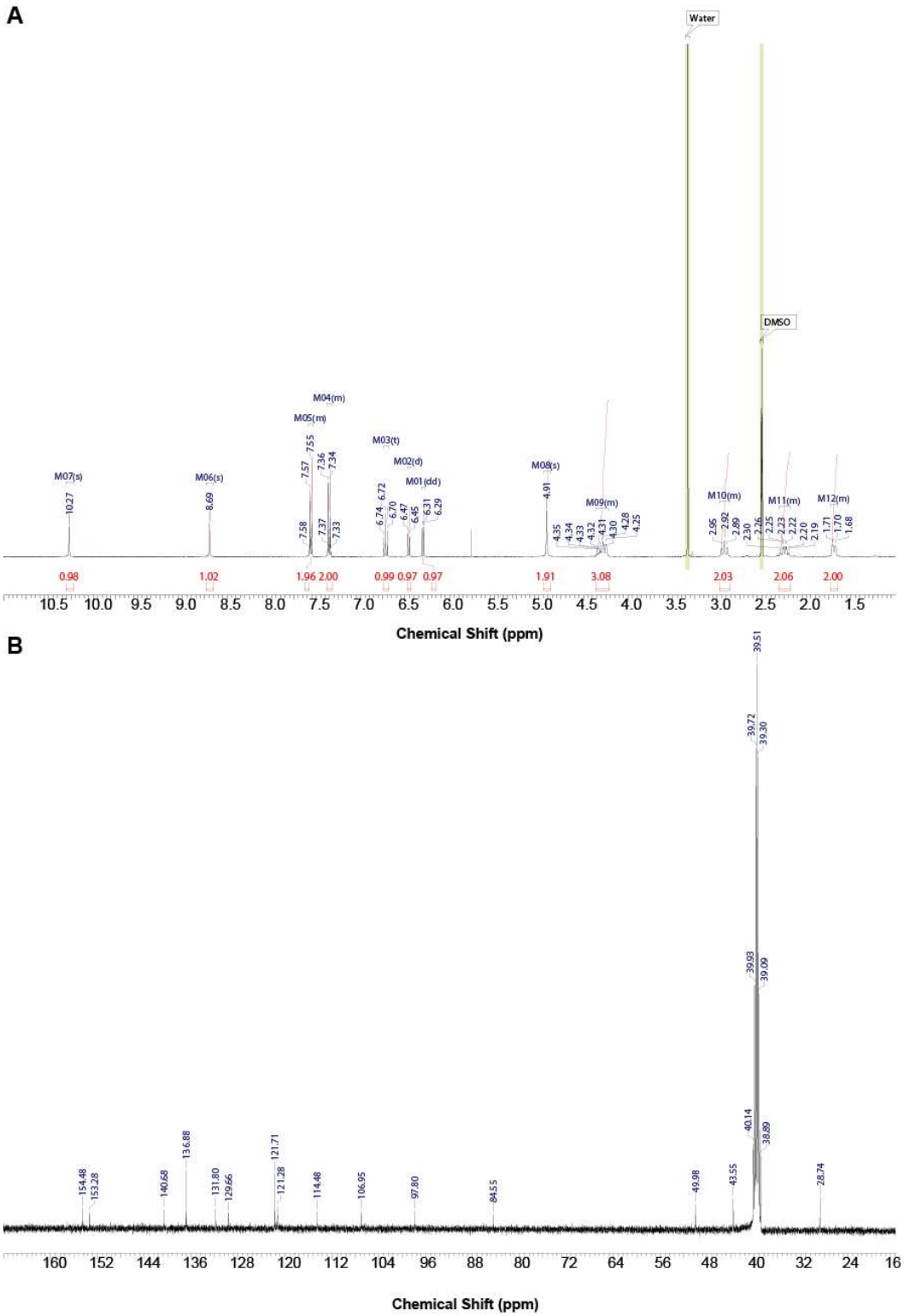

Supplementary Fig. S4: NMR spectra of TH5675. A, ^{1}H NMR-spectrum of TH5675. **B,** ^{13}C-NMR spectrum of TH5675. Chemical shifts (δ) are shown in parts per million.

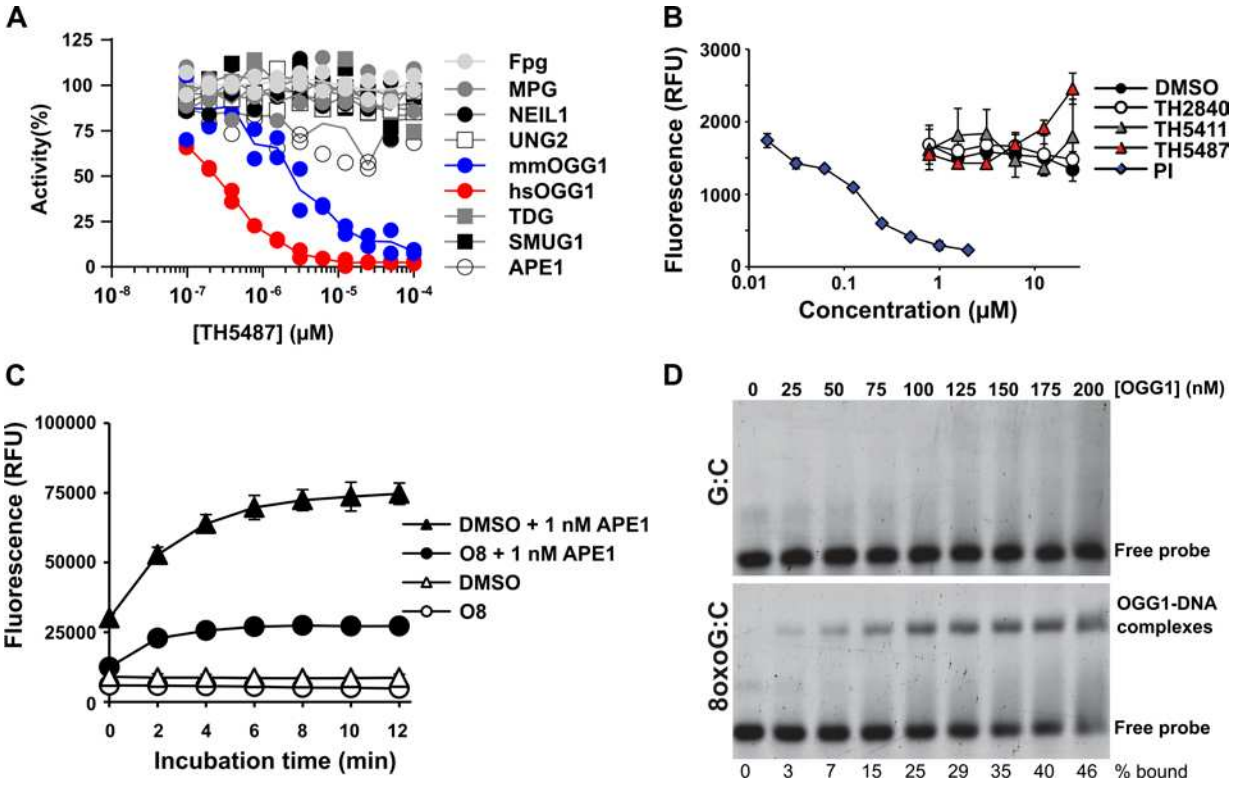

Supplementary Fig. S5: Selectivity of OGG1 inhibitors on DNA repair enzymes and DNA intercalation. (A) Selectivity of TH5487 on DNA repair enzymes. The indicated base excision repair enzymes were incubated with a dilution series of TH5487 and suitable fluorescence reporter substrates. Fluorescence was recorded when total substrate conversion was less than 30%. Shown are average of duplicate reactions, representative of independent experiments (n=33 for hsOGG1, n=3 for UNG2, APE1, and NEIL1, n=2 for Fpg, SMUG1, APE1, and MPG, and n=1 for TDG and mmOGG1). **(B)** DNA intercalation assay. 10 nM DNA oligo was incubated with 150 nM thiazole orange and the indicated concentrations of OGG1 inhibitors or propidium iodide as positive control. DNA intercalation causes a loss of fluorescence due to thiazole orange being out-competed from binding DNA. The known intercalator propidium idodide (PI) was used as positive control. Data are average ± SD of three technical replicates, representative of two independent experiments. **(C)** O8 inhibits signal generation from AP-site substrates in the absence of OGG1. 10 nM AP-site substrate pre-incubated or not with 10 µM O8 was digested with 1 nM APE1 enzyme and fluorescence were recorded as a function of time. Pre-incubation with 10 µM O8 resulted in a plateau in fluorescence values, indicating that the O8 compound may react with the aldehyde-containing AP-site substrate. The AP-site substrate was prepared from an identical substrate as that used in the OGG1 assay, except that 8-oxoA was replaced with uracil, which was subsequently converted into an AP-site using *E. coli* uracil-DNA glycosylase. Data are average ± SD of three technical replicates and are representative of two independent experiments. **(D)** Electrophoretic mobility shift assay. 10 nM of a duplex oligonucleotide containing 8-oxoG or a canonical guanine opposite cytosine was incubated with increasing concentrations of OGG1 and separated on a polyacrylamide gel. Binding of OGG1 to

damaged DNA results in a slower migrating band. 100 nM OGG1 was used in subsequent experiments.

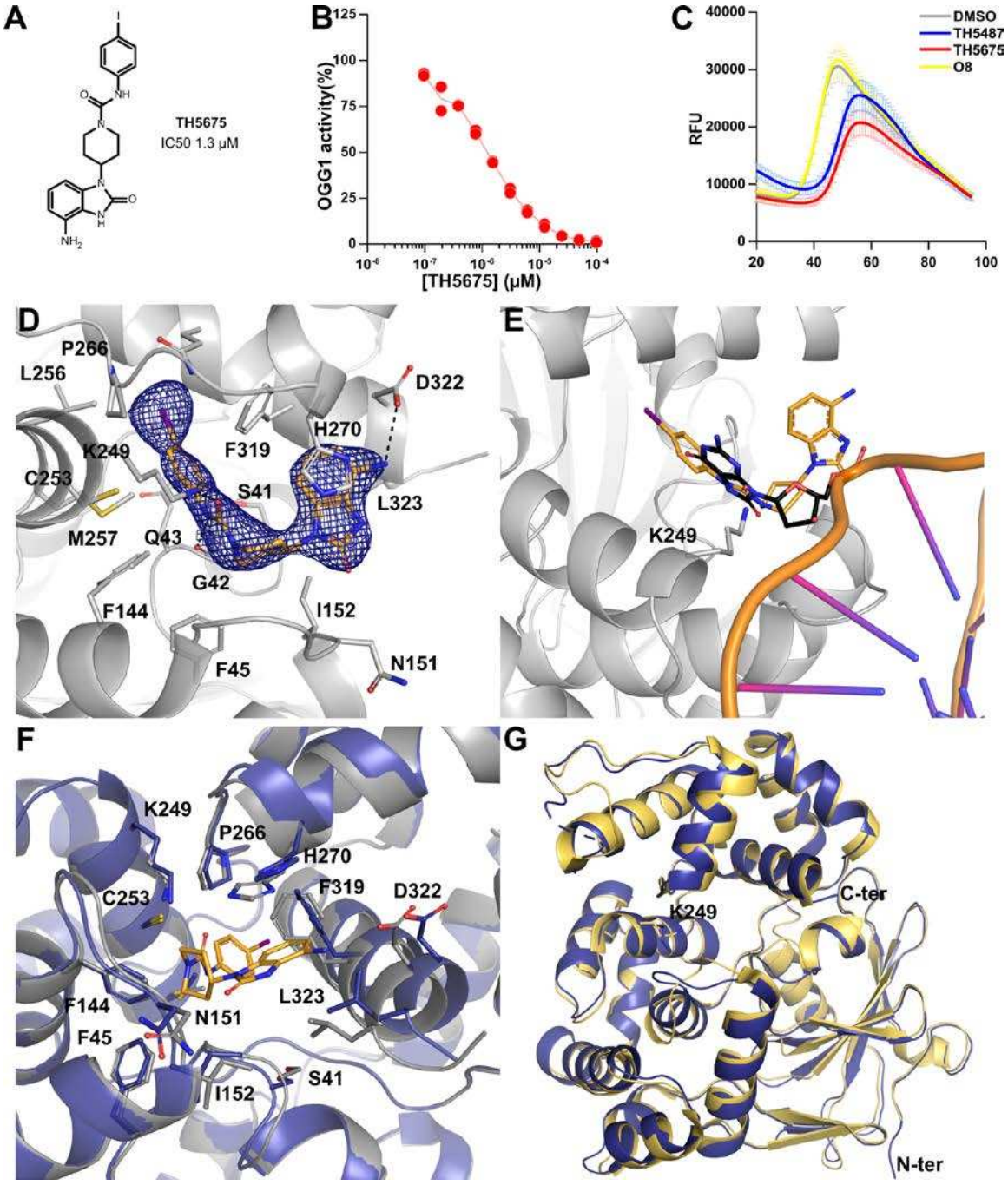

Supplementary fig. S6: Co-crystals of murine OGG1 in complex with the OGG1 inhibitor TH5675. (A) Chemical structure of TH5675, an OGG1 inhibitor with an IC_{50} value of 1.3 µM. **(B)** Inhibition curve for TH5675. Data are presented as average of two technical replicates, representative of two independent experiments. **(C)** OGG1 melting curve in the presence of the indicated OGG1 inhibitors. 100 µM of the indicated compounds were incubated with 4 µM OGG1 in the presence of SYPRO Orange. Thermal protein denaturation causes an increase in fluorescence, that is shifted by ~7°C by TH5487 and TH5675 compared to DMSO (p<0.001, using unpaired two-sided t-test).

Data are presented as average ± SD of 12 technical replicates, representative of two independent experiments. (**D**) Close-up view of ligand TH5675 (orange) binding to mOGG1. Important residues in the binding site are marked, hydrogen bond interactions are shown in black dashed line. Unbiased simulated annealing omit map for the ligand at 1σ. (**E**) Comparison between the binding of ligand TH5675 (orange) and 8-oxoG-containing DNA (black). The structure of mOGG1:TH5675 was superposed with human OGG1 (PDB 1EBM) bound to a substrate oligonucleotide (cartoon depiction). The guanine base of TH5675 occupies a different position to what was observed in the substrate-bound structure (of PDB 1EBM). (**F**) Superposition of native mOGG1 structure (blue) with the TH5675 complex (gray). Binding of the inhibitor causes a local conformational change where the surrounding pocket closes around the ligand (Movie S1). In particular, residues H270, F319 and L323 are seen to change position. (**G**) Comparison of native mouse (blue) and human (gold, PDB 1KO9) OGG1 crystal structures. The two homologues share 90% sequence identity and have identical tertiary structure.

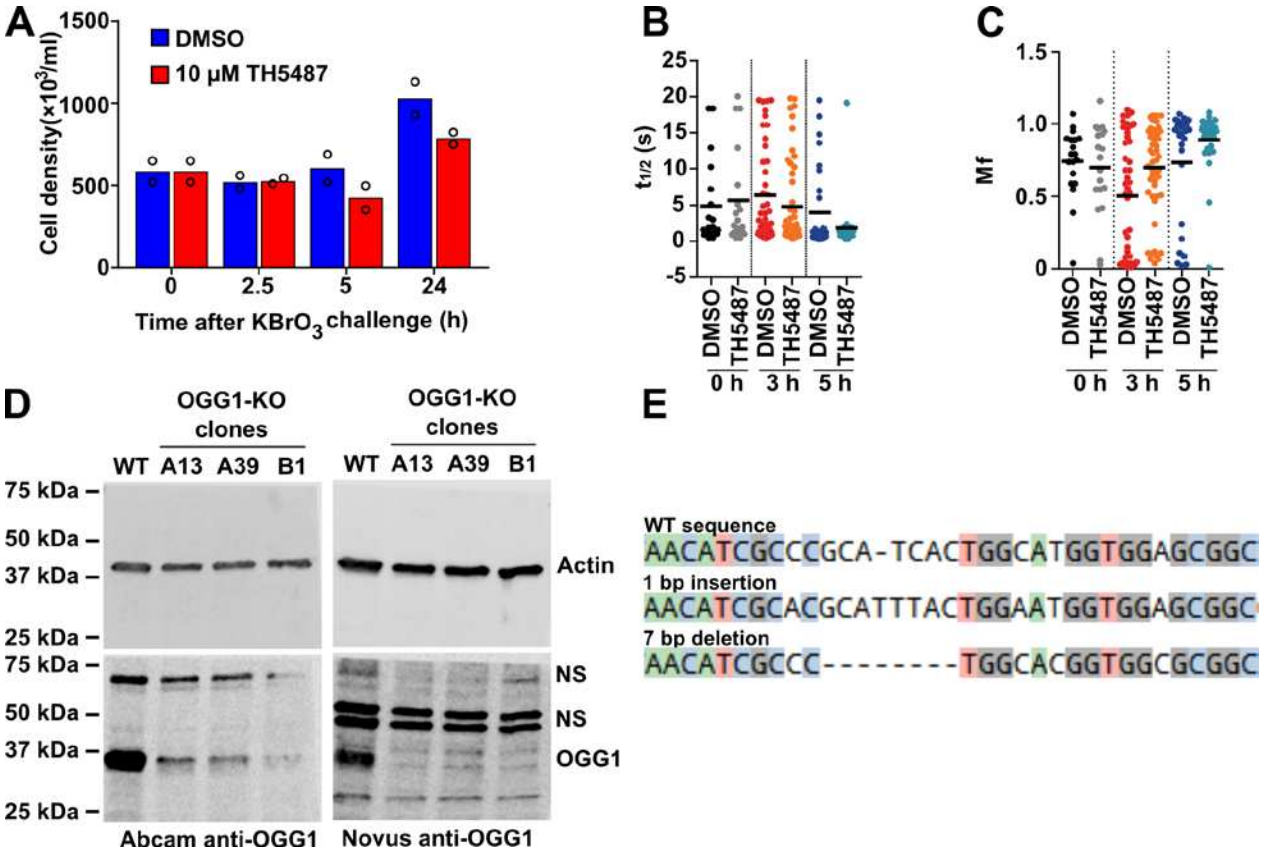

Supplementary Fig. S7: (A) Cell numbers following exposure to $KBrO_3$ and recovery in the presence of DMSO or TH5487. Duplicate cultures of cells were exposed to 20 mM $KBrO_3$ for 1 h, released into 0.1% DMSO (blue bars) or 10 µM TH5487 (red bars) and one of the duplicates counted at the time of harvest for LC-MS/MS (Fig. 2C). The bars represent the average of two independent experiments. **(B)** Quantification of the half-life of recovery ($t_{½}$) at the indicated time points. **(C)** Quantification of the mobile fraction (Mf) at the indicated time points. **(D)** Validation of CRISPR-Cas9 OGG1 knockout in HEK293T cells by immunoblot. Three out of 70 clones displayed lower OGG1 levels using antibodies raised against OGG1 from Abcam (left panels) or Novus (right panels). NS indicates non-specific bands. **(E)** Sanger sequencing of the targeted *OGG1* exon. Genomic DNA from clone B1 was PCR-amplified and Sanger-sequenced. Deconvolution using TIDE (*52*) revealed a 1-bp insertion and a 7-bp deletion. Clone B1 was used for subsequent experiments.

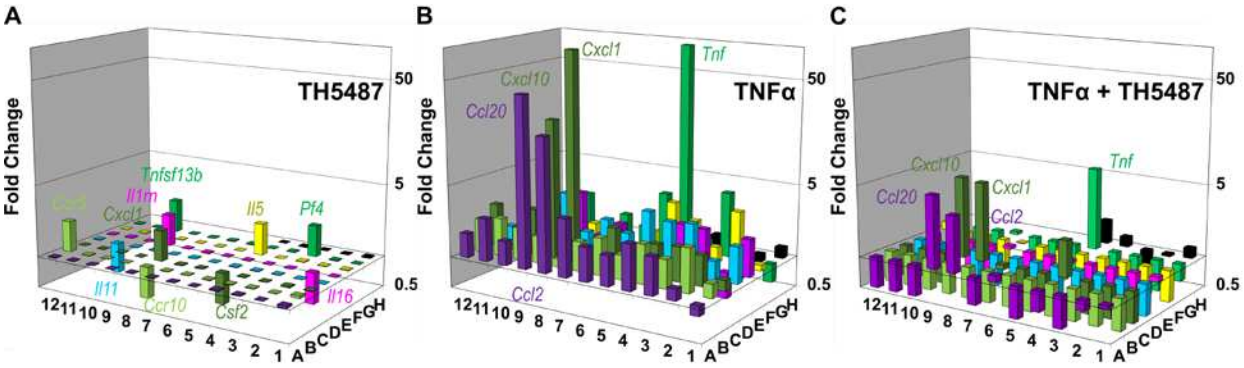

Supplementary Fig. S8: TH5487-mediated inhibition of TNFα-induced expression of pro-inflammatory mediators. MLE 12 cells were treated with TH5487 (5 μM) for 1 h and TNFα-exposed (20 ng per ml) 30 min. In controls, cells were treated with solvent (0.05% DMSO) for the same time period. RNAs were isolated and pooled from three independent experiments (n=3) followed by qRT-PCR using the Mouse Inflammation Cytokines and RT^2 profiler PCR Arrays (PAMM-011ZA, SA Biosciences/Qiagen). The normalization and statistical analysis were performed by using their web-based software package: http://sabiosciences.com/pcrarraydataanalysis.php. Expression levels of selected genes were confirmed as shown in Supplementary Fig. S11, upper panels). Left panel: Effect of TH5487 on basal gene expression (TH5487 vs. solvent). Middle panel: TNFα-induced expression of cytokines, C-C, C-X-C motif chemokines and their receptors (TNFα vs. solvent). Right panel: Inhibition of TNFα-induced gene expression by TH5487 (TH5487+TNFα vs. solvent). Data is deposited to NCBI, and is accessible through GEO series accession no. GSE106785. **Abbreviations:** PAMM-011ZA (MOUSE INFLAMMATION ARRAY): *Aimp1*, Aminoacyl tRNA synthetase complex-interacting multifunctional protein 1; *Bmp2*, Bone morphogenetic protein 2; *Ccl1*, Chemokine (C-C motif) ligand 1; *Ccl11*, Chemokine (C-C motif) ligand 11; *Ccl12*, Chemokine (C-C motif) ligand 12; *Ccl17*, Chemokine (C-C motif) ligand 17; *Ccl19*, Chemokine (C-C motif) ligand 19; *Ccl2*, Chemokine (C-C motif) ligand 2; *Ccl20*, Chemokine (C-C motif) ligand 20; *Ccl22*, Chemokine (C-C motif) ligand 22; *Ccl24*, Chemokine (C-C motif) ligand 24; *Ccl3*, Chemokine (C-C motif) ligand 3; *Ccl4*, Chemokine (C-C motif) ligand 4; *Ccl5*, Chemokine (C-C motif) ligand 5; *Ccl6*, Chemokine (C-C motif) ligand 6; *Ccl7*, Chemokine (C-C motif) ligand 7; *Ccl8*, Chemokine (C-C motif) ligand 8; *Ccl9*, Chemokine (C-C motif) ligand 9; *Ccr1*, Chemokine (C-C motif) receptor 1; *Ccr10*, Chemokine (C-C motif) receptor 10; *Ccr2*, Chemokine (C-C motif) receptor 2; *Ccr3*, Chemokine (C-C motif) receptor 3; *Ccr4*, Chemokine (C-C motif) receptor 4; *Ccr5*, Chemokine (C-C motif) receptor 5; *Ccr6*, Chemokine (C-C motif) receptor 6; *Ccr8*, Chemokine (C-C motif) receptor 8; *Cd40lg*, CD40 ligand; *Csf1*, Colony stimulating factor 1 (macrophage); *Csf2*, Colony stimulating factor 2 (granulocyte-macrophage); *Csf3*, Colony stimulating factor 3 (granulocyte); *Cx3cl1*, Chemokine (C-X3-C motif) ligand 1; *Cxcl1*, Chemokine (C-X-C motif) ligand 1; *Cxcl10*, Chemokine (C-X-C motif) ligand 10; *Cxcl11*, Chemokine (C-X-C motif) ligand 11; *Cxcl12*, Chemokine (C-X-C motif) ligand 12; *Cxcl13*, Chemokine (C-X-C motif) ligand 13; *Cxcl15*, Chemokine (C-X-C motif) ligand 15; *Cxcl5*, Chemokine (C-X-C motif) ligand 5; *Cxcl9*, Chemokine (C-

X-C motif) ligand 9; *Cxcr2*, Chemokine (C-X-C motif) receptor 2; *Cxcr3*, Chemokine (C-X-C motif) receptor 3; *Cxcr5*, Chemokine (C-X-C motif) receptor 5; *Fasl*, Fas ligand (TNF superfamily, member 6); *Ifng*, Interferon gamma; *Il10ra*, Interleukin 10 receptor alpha; *Il10rb*, Interleukin 10 receptor, beta; *Il11*, Interleukin 11; *Il13*, Interleukin 13; *Il15*, Interleukin 15; *Il16*, Interleukin 16; *Il17a*, Interleukin 17A; *Il17b*, Interleukin 17B; *Il17f*, Interleukin 17F; *Il1a*, Interleukin 1 alpha; *Il1b*, Interleukin 1 beta; *Il1r1*, Interleukin 1 receptor, type I; *Il1rn*, Interleukin 1 receptor antagonist; *Il21*, Interleukin 21; *Il27*, Interleukin 27; *Il2rb*, Interleukin 2 receptor, beta chain; *Il2rg*, Interleukin 2 receptor, gamma chain; *Il3*, Interleukin 3; *Il33*, Interleukin 33; *Il4*, Interleukin 4; *Il5*, Interleukin 5; *Il5ra*, Interleukin 5 receptor, alpha; *Il6ra*, Interleukin 6 receptor, alpha; *Il6st*, Interleukin 6 signal transducer; *Il7*, Interleukin 7; *Lta*, Lymphotoxin A; *Ltb*, Lymphotoxin B; *Mif*, Macrophage migration inhibitory factor; *Nampt*, Nicotinamide phosphoribosyltransferase; *Osm*, Oncostatin M; *Pf4*, Platelet factor 4; *Spp1*, Secreted phosphoprotein 1; *Tnf*, Tumor necrosis factor; *Tnfrsf11b*, Tumor necrosis factor receptor superfamily, member 11b (osteoprotegerin); *Tnfsf10*, Tumor necrosis factor (ligand) superfamily, member 10; *Tnfsf11*, Tumor necrosis factor (ligand) superfamily, member 11; *Tnfsf13*, Tumor necrosis factor (ligand) superfamily, member 13; *Tnfsf13b*, Tumor necrosis factor (ligand) superfamily, member 13b; *Tnfsf4*, Tumor necrosis factor (ligand) superfamily, member 4; *Vegfa*, Vascular endothelial growth factor A; *Actb*, Actin, beta; *B2m*, Beta-2 microglobulin; *Gapdh*, Glyceraldehyde-3-phosphate dehydrogenase; *Gusb*, Glucuronidase, beta; *Hsp90ab1*, Heat shock protein 90 alpha (cytosolic), class B member 1; MGDC, Mouse Genomic DNA Contamination.

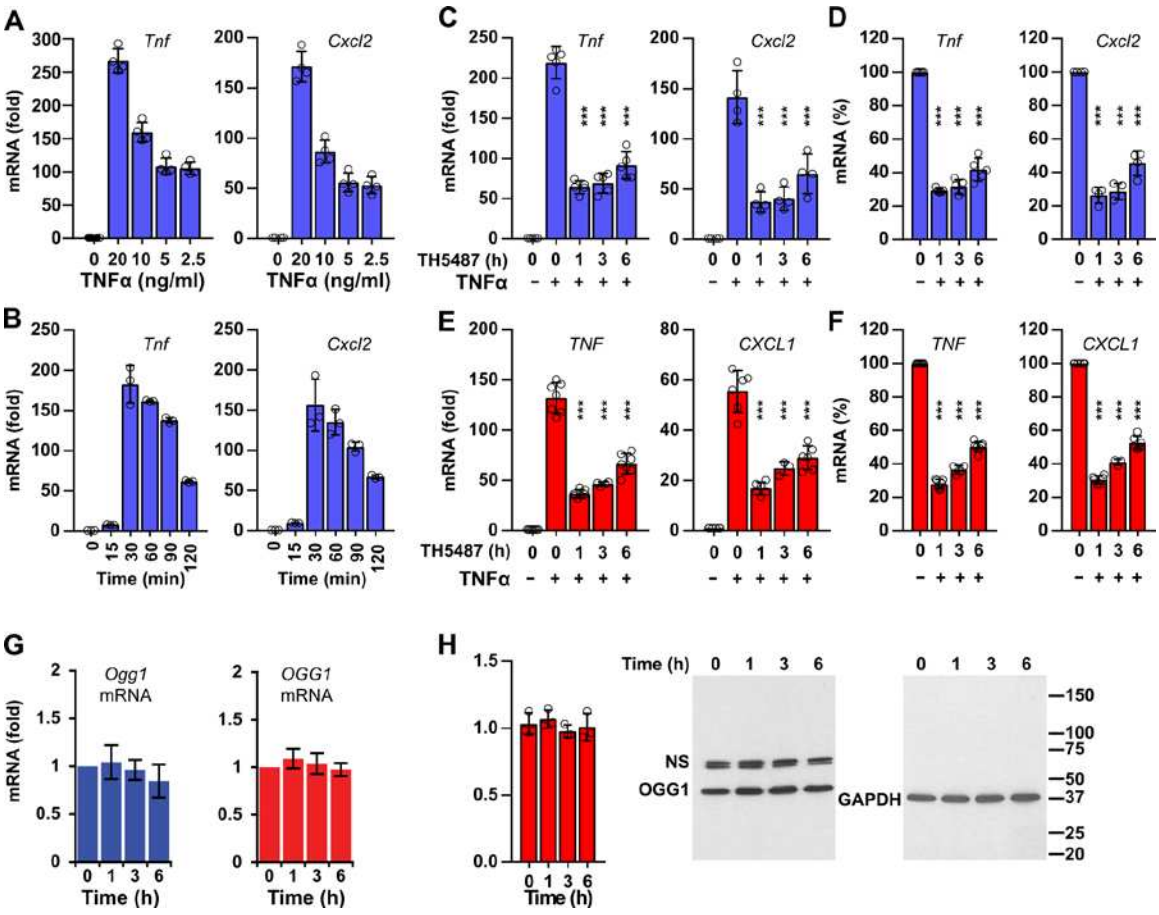

Supplementary Fig. S9: Dose and time dependent effects of TH5487 on expression of inflammatory mediators and OGG1. (A) Dose-dependent inhibition by TH5487 on expression of *Tnf* and *Cxcl2* in response to TNFα Parallel cultures of MLE 12 cells were exposed to the indicated doses TNFα for 30 min. mRNA levels of *Tnf* and *Cxcl2* were measured by qRT-PCR. **(B)** Kinetics of Tnf and Cxcl2 expression after TNFα exposure. MLE 12 cells were exposed to 20 ng/ml TNFα for the indicated times. mRNA levels were measured with qRT-PCR. **(C-F)** Effect of a single TH5487 dose on gene expression as a function of time in mouse (MLE 12) and human (hSAEC) cells. Parallel cultures of cells were pre-treated with TH5487 (5 μM) for 0 h, 1 h, 3 h or 6 h and TNFα (20 ng/ml) was added for 30 min. Mouse *Tnf* and *Cxcl2* and human *TNF* and *CXCL1* mRNA levels were assessed with qRT-PCR. TH5487 is ~15% less efficient after 6 h pre-incubation. $^{**}p < 0.01$, $^{***}p < 0.001$ using unpaired two-sided t-test, where samples are compared to the 0 h time point added TNFα. **(G)** TH5487 does not alter the expression of OGG1 in mouse and human cells. MLE 12 (left panel) and hSAEC (right panel) were treated with 5 μM TH5487 for 0 h, 1 h, 3 h and 6 h. mRNA encoding OGG1 protein were measured by qRT-PCR (n = 3). **(H)** TH5487 treatment does not change OGG1 protein expression levels. hSAEC were treated with 5 μM TH5847 for the indicated times and OGG1 protein levels were assessed by immunoblot analysis. An autoradiogram representative of three independent experiments is shown. NS signifies non-specific. Band intensities were quantified using Image J (version 5.0) software and fold changes in densities were

calculated using MS Excel. In A-G, bars represent average values ± SD and are derived from at least three independent experiments. *Tnf*, mouse tumor necrosis factor; *Cxcl2*, mouse chemokine (C-X-C Motif) ligand 2 (macrophage inflammatory protein 2-alpha).

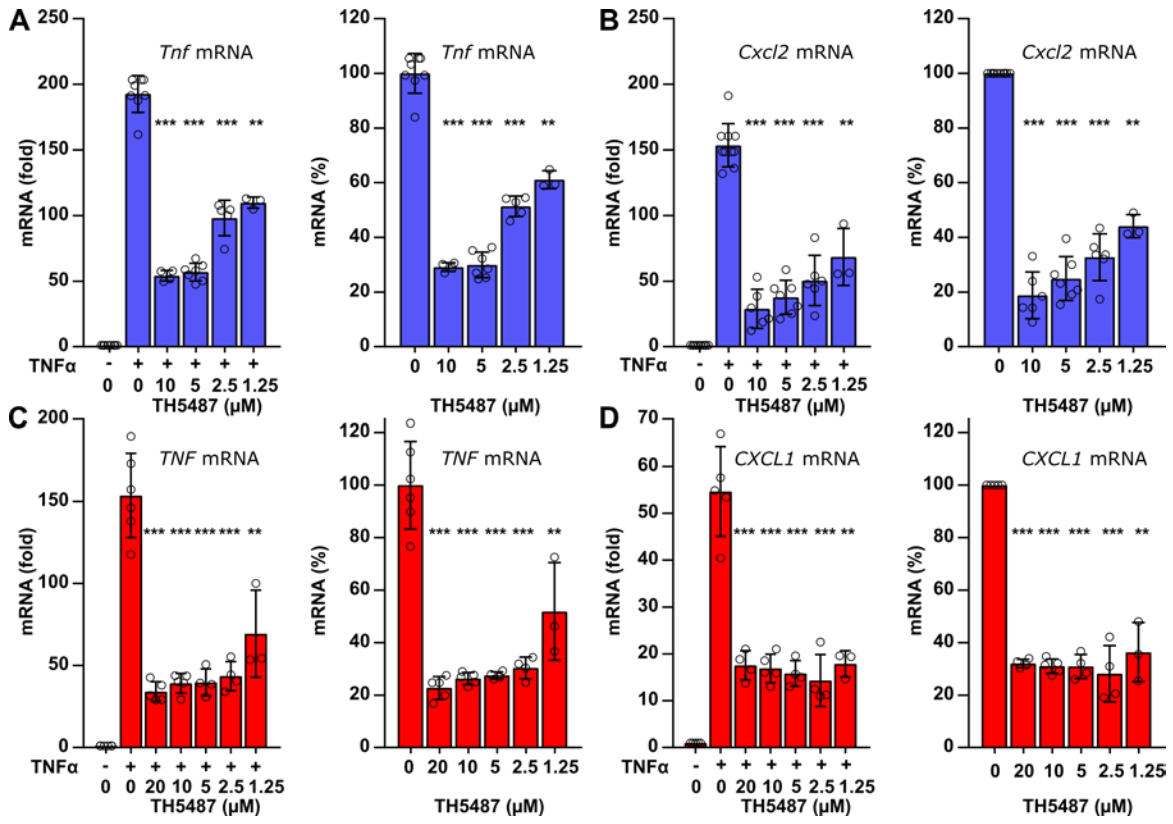

Supplementary Fig. S10: Cell-type and dose-dependent inhibition of pro-inflammatory gene expression by TH5487. **(A** and **B)**, MLE 12 cells were pretreated with the indicated doses of TH5487 for 1 h and TNFα (20 ng per ml) was added for 30 min. **(C** and **D)**, hSAECs were pretreated with the indicated doses of TH5487 for 1 h and TNFα (20 ng per ml) was added for 30 min. A to D, Changes in mRNA levels were determined by qRT-PCR. A to D: left panels show changes in fold, right panels are depicting percentage of inhibition as function of TH5487 dose. The data correspond to the average of three independent experiments, and the error bars indicate ± SD (n = 3). $^{**}p < 0.01$, $^{***}p < 0.001$ using unpaired, two-sided t-test, and the data were compared to the sample added TNFα at 0 h. Abbreviations: *Tnf*: mouse tumor necrosis factor; *TNF*: human tumor necrosis factor; *Cxcl2*: mouse chemokine (C-X-C Motif) ligand 2 (macrophage inflammatory protein 2-alpha); *CXCL1*: human chemokine (C-X-C Motif) ligand 1 (macrophage inflammatory protein 1-alpha).

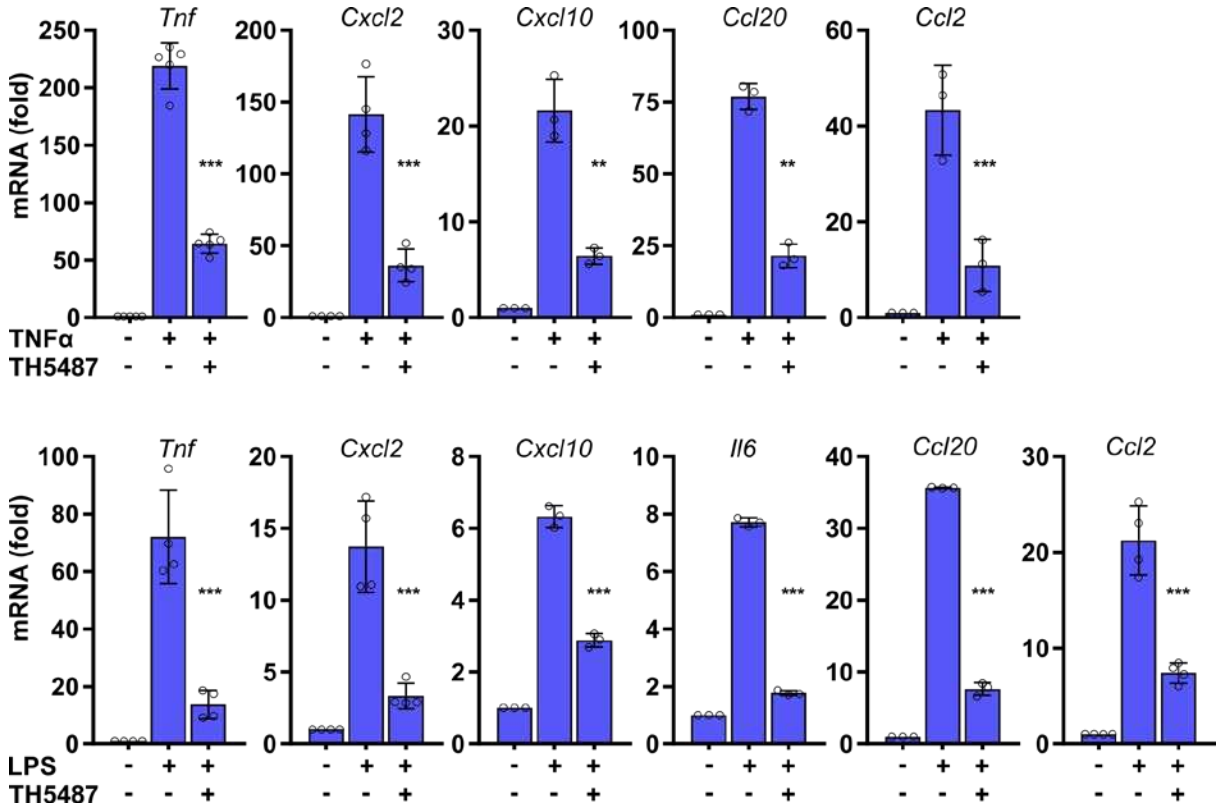

Supplementary Fig. S11: TH5487 decreases TNFα- and LPS-induced expression of *Tnf*, C-X-C and C-C chemokines, as well as interleukin in mouse cells. Parallel cultures of mouse (MLE 12) airway epithelial cells were treated with solvent (0.05% DMSO in PBS) or TH5487 (5 μM) for 1 h and then cells were TNFα (upper panels) or LPS-exposed (lower panels) for 30 min or 1 h, respectively. Changes in mRNA levels were determined by qRT-PCR. The data correspond to the average of at least three independent experiments and the error bars indicate standard deviation. Genes were selected based on their key roles in an immediate cellular innate immune response. $^{**}p < 0.01$, $^{***}p < 0.001$ using unpaired, two-sided t-test, where TH5487-treated samples were compared to samples with LPS or TNFα. Abbreviations: *Tnf*: Tumor necrosis factor; *Cxcl2*: Chemokine (C-X-C Motif) ligand 2 (Macrophage inflammatory protein 2-alpha); *Ccl20*: C-C motif chemokine ligand 20 (Macrophage inflammatory protein 3 alpha); *Ccl2*: C-C motif chemokine ligand 2 (Monocyte chemotactic and activating factor); *Cxcl10*: C-X-C motif chemokine ligand 10 (10 kDa interferon gamma-induced protein); *Il6*: Interleukin 6 (Interferon, beta 2).

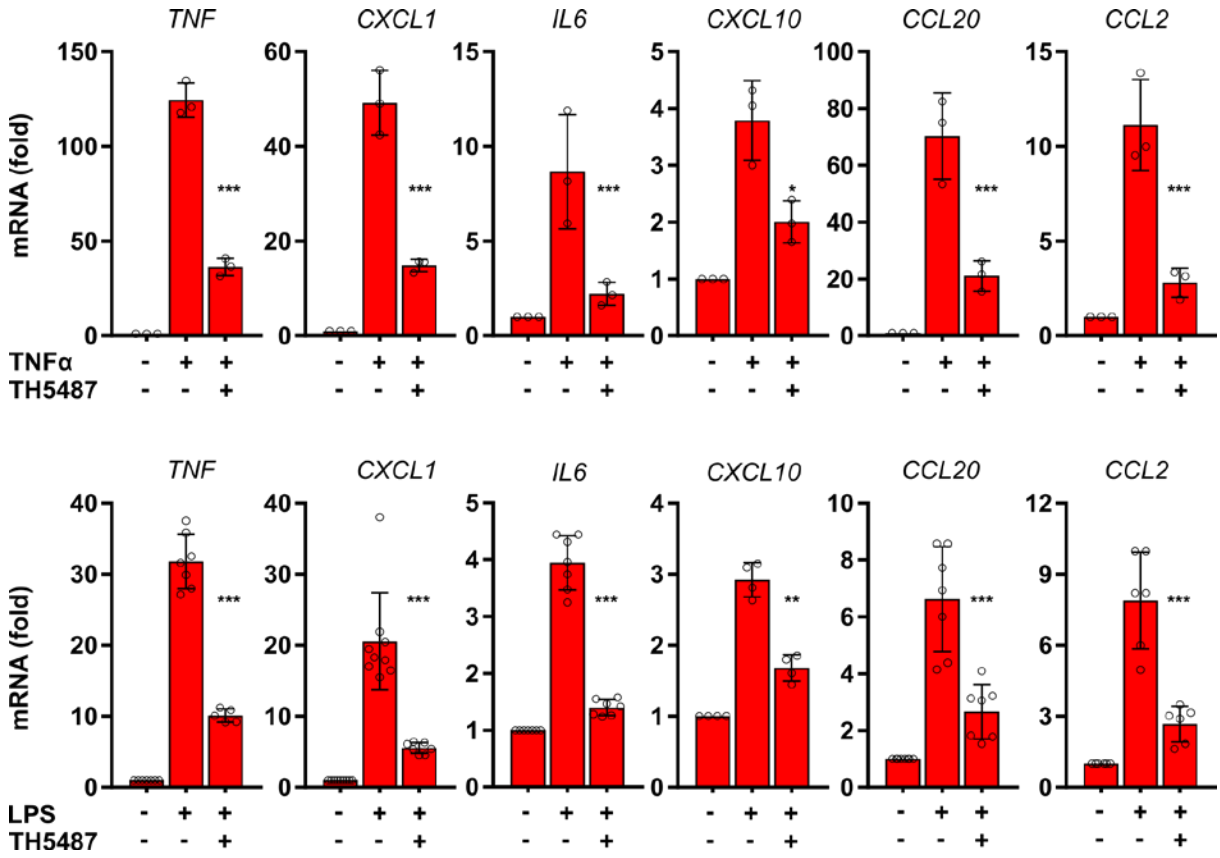

Supplementary Fig. S12: TH5487 decreases TNFα- and LPS-induced expression of *TNF*, C-X-C and C-C chemokines, as well as interleukin in human cells. Parallel cultures of human (hSAECs) airway epithelial cells were treated with solvent (0.05% DMSO in PBS) or TH5487 (5 μM) for 1 h and then TNFα (upper panels) or LPS (lower panels)-exposed for 30 min or 1 h, respectively. Changes in mRNA levels were determined by qRT-PCR. The data correspond to the average of at least three independent experiments and the error bars indicate standard deviation. Genes were selected based on their key roles in an immediate cellular innate immune response. $^{**}p < 0.01$, $^{***}p < 0.001$ using unpaired two-sided t-test, where TH5487-treated samples were compared to samples with LPS, or TNFα. Abbreviations: *TNF*: Tumor necrosis factor; *CXCL1*: Chemokine (C-X-C Motif) ligand 1 (Macrophage inflammatory protein 1 alpha); *CCL20*: C-C motif chemokine ligand 20 (Macrophage inflammatory protein 3 alpha); *CCL2*, C-C motif chemokine ligand 2 (Monocyte chemotactic and activating factor); *CXCL10*: C-X-C motif chemokine ligand 10 (10 kDa interferon gamma-induced protein); *IL6*: Interleukin 6 (Interferon, beta 2).

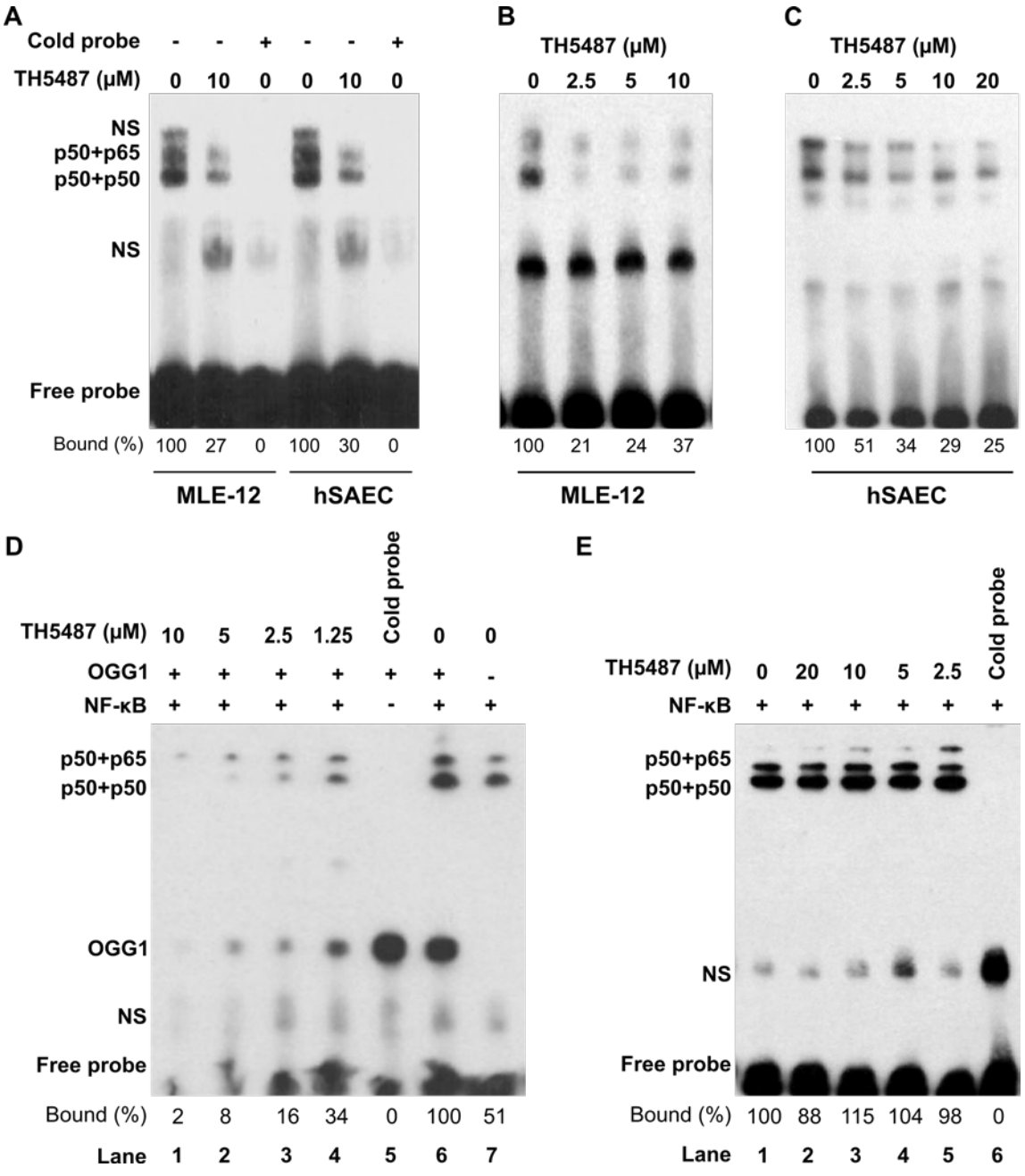

Supplementary Fig. S13: TH5487 decreases NF-κB DNA occupancy to 8-oxoG containing synthetic DNA in crude nuclear extracts (NE). (A) TH5487 decreases binding of NF-κB to 8-oxoG –containing oligo. MLE 12 and hSAECs were TNFα (20 ng/ml) exposed for 30 min and nuclear extracts were isolated using CelLytic™ NuCLEAR™ extraction kit (MilliporeSigma). Two micrograms of NE was incubated with the indicated concentrations TH5487 for 60 min and added to DNA probes containing 8-oxoG (10 fmol) for 15 min at 4°C. Samples were separated on a 6% non-denaturing gel at 4°C. The DNA probes were visualized using LightShift chemiluminescent EMSA kit (Thermo Scientific). The DNA sequence of the probe is based on the human *TNF* promoter (−224 to −193) and contains 8-oxoG in sense strand

8-bp upstream of an NF-κB binding site (Supplementary Table S12). (**B** and **C**), **Binding of NF-κB to 8-oxoG–containing oligo based on the mouse *Cxcl2* promoter.** MLE 12 cells and hSAECs were exposed to TNFα (20 ng/ml) for 30 min. NE from both cell lines were prepared as in panel a. Two micrograms of nuclear extracts from MLE 12 (B) or hSAEC (C) was incubated with the indicated doses TH5487 for 60 min and added to probe (10 fmol) and EMSA was carried out as in panel A. The DNA sequence is based on the sequence of the mouse *Cxcl2* promoter (−65 to –34 bp) and contains 8-oxoG in anti-sense strand 9 bp down-stream from an NF-κB binding site. Oligo sequences are shown in Supplementary Table S12. NS, non-specific. **(D) OGG1 increases NF-κB binding to 8-oxoG-containing DNA, whereas TH5487 perturbs it.** OGG1, the indicated concentrations of TH5487, and homo- or heterodimeric NF-κB were added to 10 fmol of a 8-oxoG- and NF-κB binding motif-containing double stranded DNA probe for 10 min. and separated on a non-denaturating polyacrylamide gel. In lanes 1–4, equimolar amounts of recombinant p50 (55 fmol) and RelA(p65) (55 fmol) were annealed in binding buffer (10 mM Tris (pH 7.5), 5 mM NaCl, 1 mM DTT and 1 mM EDTA) at 37°C for 60 min. OGG1 (10 nM) was incubated with the indicated doses TH5487 for 30 min. In lane 5, NF-κB binding was competed out using 100-fold excess DNA without 8-oxoG. In lane 6, OGG1 increased NF-kB DNA occupancy. In lane 7, NF-κB DNA occupancy in absence of OGG1. For more information, see (*3*). **(E) In the absence of OGG1, TH5487 does not inhibit NF-κB binding to 8-oxoG-containing DNA**. Equimolar amounts of recombinant p50 (55 fmol) and RelA(p65) (55 fmol) were annealed as in legend to D. A mixture of homo (p50–p50) and heterodimeric (p50–p65) NF-κB was incubated with various concentrations of TH5487 for 60 min and added to 8-oxoG- and NF-κB binding motif-containing double stranded DNA probes (10 fmol) for 10 min at 4^{o}C. In lane 6, NF-κB binding was competed out by an 100-fold excess unlabeled probe. In D to E, samples were resolved on a 6% non-denaturing DNA retardation gel in Tris/Borate/EDTA (TBE) buffer at 4°C. NF-κB-DNA complexes were visualized using LightShift Chemiluminescent EMSA kit (Thermo Scientific). NF-κB binding was competed out using 100-fold excess of unlabeled double stranded DNA probe. Probe sequence is derived from *TNF* promoter (Supplementary Table S12). NS, non-specific. For more information, see (*3*). Band intensities for the p50+p65 and p50+p50 bands were quantified using Image J (v1.52) software and percentage changes in densities were calculated using MS Excel.

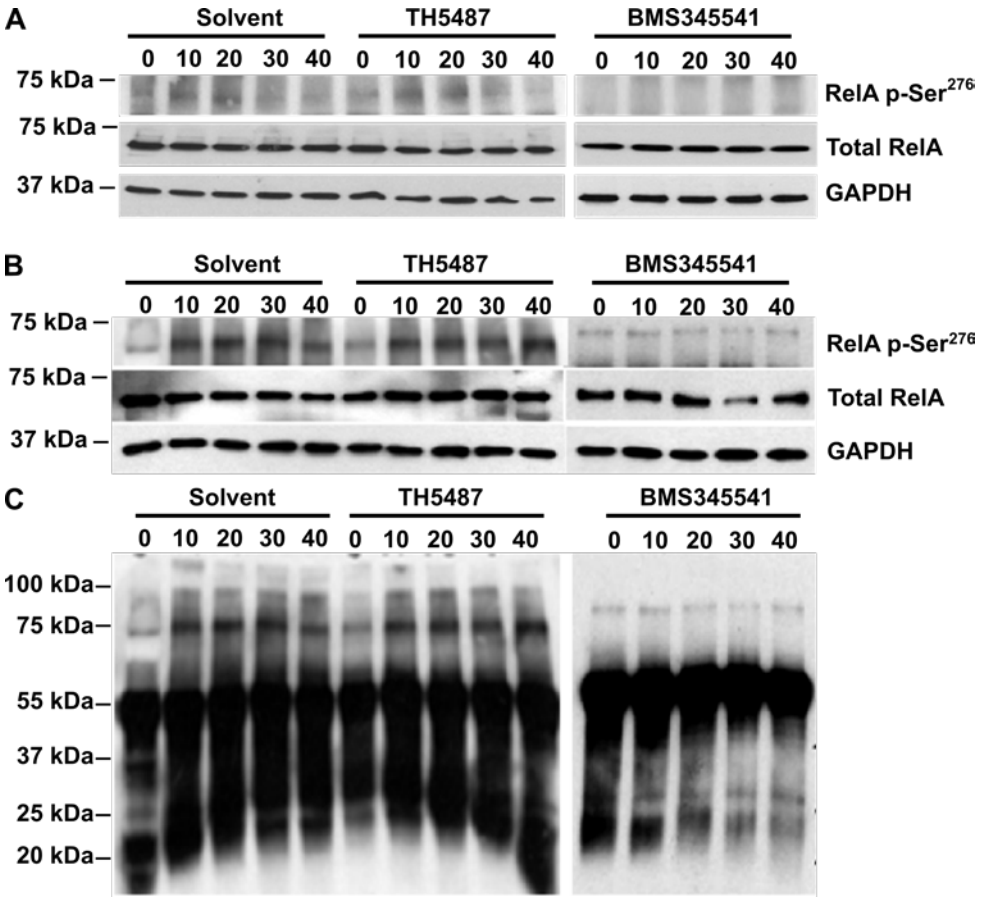

Supplementary Fig. S14: TH5487 does not inhibit NF-κB activation. (A) Direct assessment of NF-κB activation by determining changes in RelA phosphorylation at serine 276 in TH5487 treated cells. MLE 12 cells were treated with TH5487 (5 μM) or BSM345541 (5 μM) for 1h and TNFα (20 ng/ml) was added for the indicated times. Whole cell extracts were isolated and 20 μg protein per lane were fractionated by 4%–20% SDS-PAGE. Phosphorylated RelA (serine residue at 276) (57) was detected by immunoblot analysis using anti-phospho RelA antibody. Loading controls were total RelA (anti-RelA Ab; middle panel) and glyceraldehyde 3-phosphate dehydrogenase (GAPDH, lower panel). In controls, inhibition of I kappa B-alpha by BSM345541(27) prevented the release and phosphorylation of RelA. **(B) Assessment of NF-κB activation via RelA phosphorylation by immunoprecipitation after TH5487 treatment of cells.** MLE 12 cells were treated as in A. At indicated times, cell extracts were made and clarified by centrifugation. Then, 500 μg protein equivalent of supernatants were incubated with rabbit RelA antibody. Protein A agarose was subsequently added with continuous rotation. The immunoprecipitates were then washed and equal amounts were resolved by 4%–20% SDS–PAGE. Proteins transferred to nitrocellulose membranes were subjected to immunoblot analysis using a rabbit antibody to phospho-RelA (Fig. B upper panel). After stripping, membranes were probed with antibody to RelA (mouse, Fig. B middle panel). Even loading was confirmed by testing membranes with GAPDH antibody

(rabbit; Fig. B lower panel). In controls, inhibition of I kappa B-alpha by BSM345541 (27) prevented phosphorylation of RelA. **(C)**, Full-size gels are shown after probing membranes with phosphor-RelA antibody (rabbit). BMS345541: N-(1,8-Dimethylimidazo[1,2-a]quinoxalin-4-yl)-1,2-ethanediamine hydrochloride.

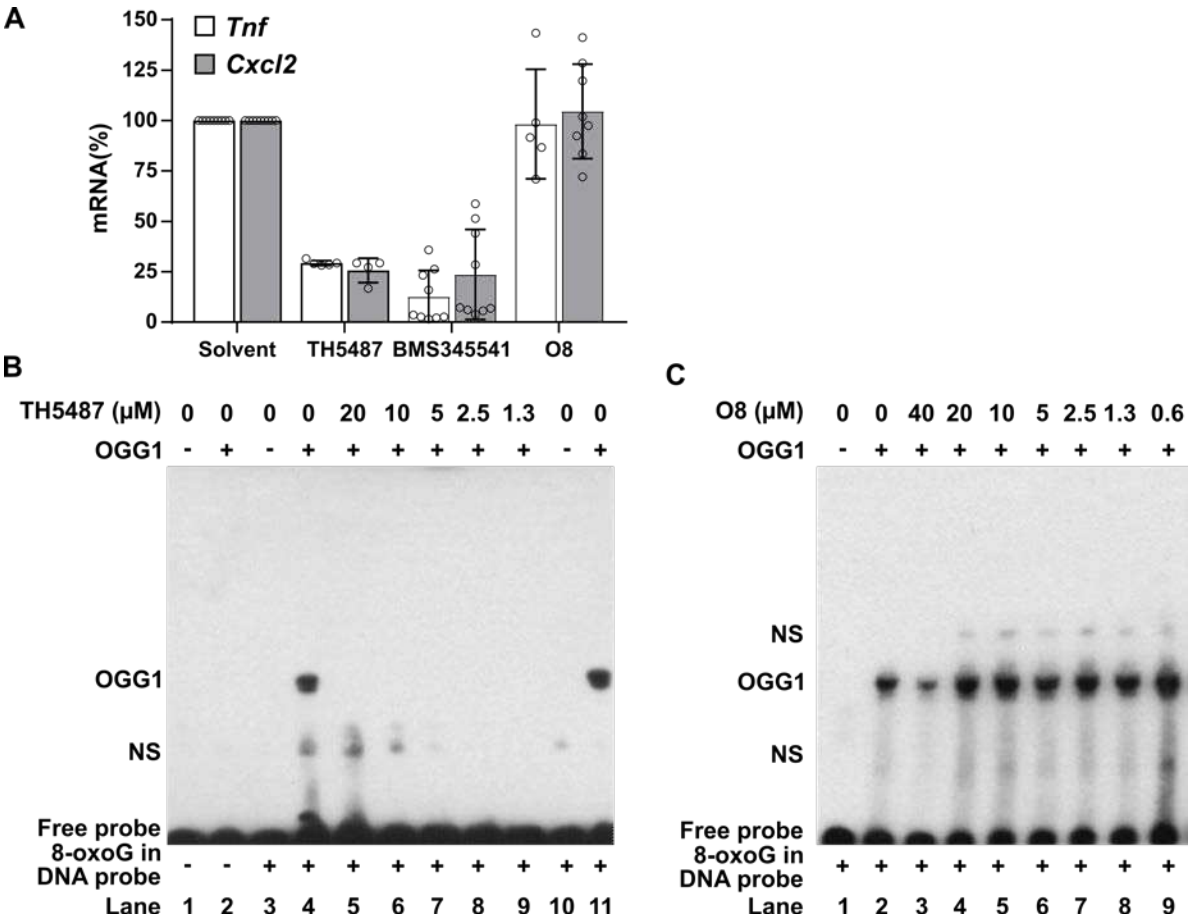

Supplementary Fig. S15: (A) Inhibition of *Tnf* and *Cxcl2* expression by TH5487, IKK inhibitor BMS345541, and the O8 compound. Parallel cultures of MLE 12 cells were pre-treated with TH5487 (5 μM), BSM345541 (27) (5 μM) or O8 (19) (5 μM) for 1 h. Cells were mock-exposed to solvent or TNFα (20 ng/ml) for 30 min. Levels of *Tnf* and *Cxcl2* mRNA were determined by qRT-PCR. Data are average ± SD, representative of independent experiments (TH5487 n = 5, BMS345541 n= 6; O8 n = 5 independent experiments). The error bars indicate standard deviations. ***$p<0.001$ using unpaired, two-sided t-test, and data were normalized and compared to the solvent control sample. BMS345541: N-(1,8-Dimethylimidazo[1,2-a]quinoxalin-4-yl)-1,2-ethanediamine hydrochloride; O8: 3,4-Dichloro-benzo[b]thiophene-2-carboxylic acid hydrazide.
(B) TH5487 inhibits binding of OGG1 to 8-oxoG-containing DNA. 10 nM OGG1 were incubated with the indicated doses TH5487 for 30 min at 37°C and added to double-stranded DNA probe (10 fmol) with and without 8-oxoG for 10 min at 4oC. Samples were separated by a non-denaturating polyacrylamide electrophoresis. Lane 1, probe only; lane 2, OGG1 and probe without 8-oxoG; lane 3, 8-oxoG-containing probe alone; lane 4, OGG1 and 8-oxoG-containing probe, lane 5–9 TH5487 prevents OGG1 binding to 8-oxoG-containing probe; lane 10, 8-oxoG-containing probe alone (replica of lane 3); lane 11, replica of lane 4. NS, non-specific.

(C) O8 does not inhibit binding of OGG1 to 8-oxoG-containing DNA. 10 nM OGG1 was incubated with the indicated doses of O8 for 30 min at 37°C then added to 8-oxoG-containing double stranded DNA probe for 10 min at 4°C. Lane 1: probe alone; lane 2: OGG1 and 8-oxoG-containing probe; lanes 3-9: O8 does not inhibit the interaction between OGG1 and an 8-oxoG-containing probe. NS: non-specific. In **B** and **C**, the 8-oxoG-containing probe was synthesized based on the sequence of the human TNF promoter (–224 to −193 bp, Supplementary Table S12).

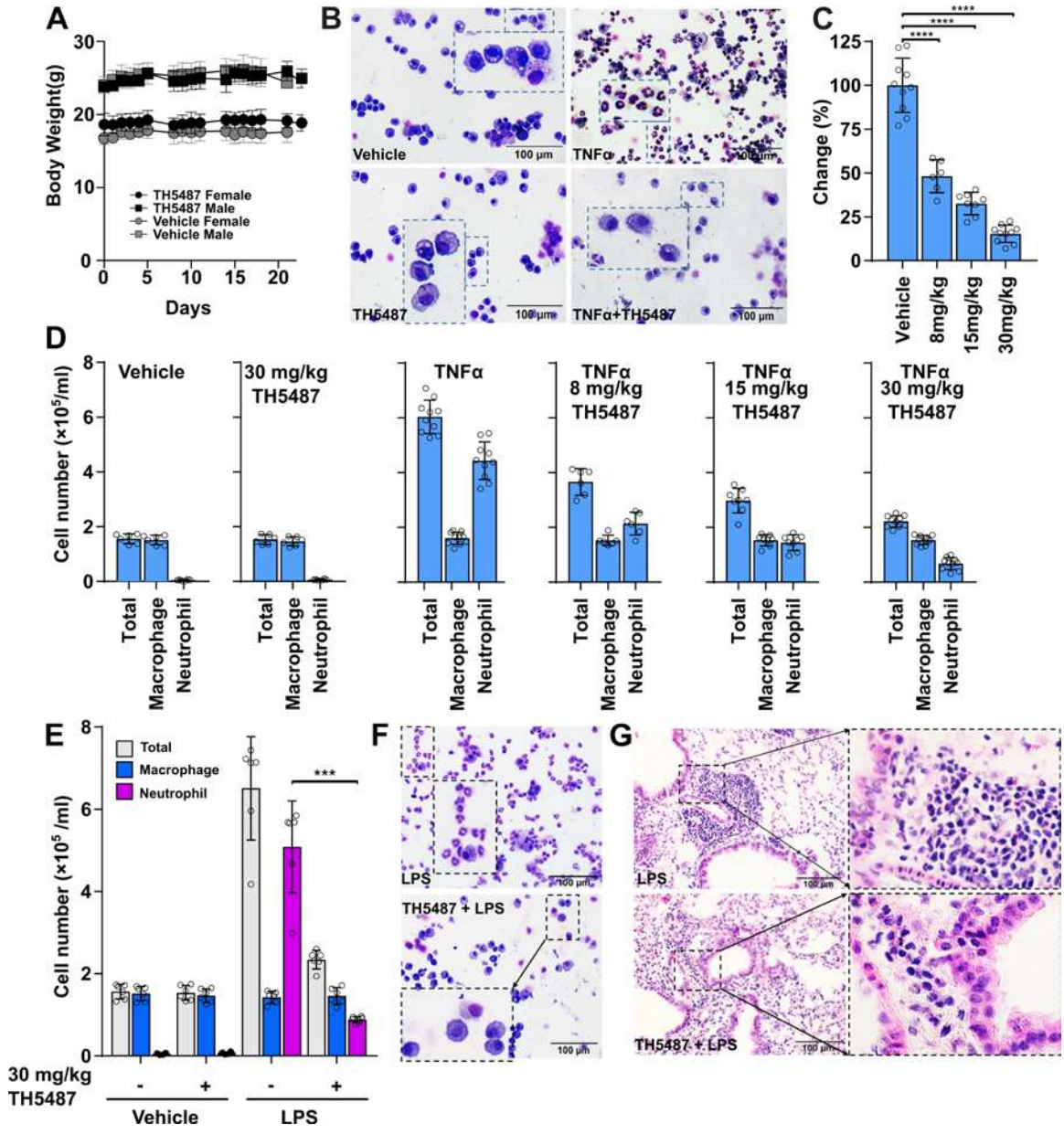

Supplementary Fig. S16: Inhibition of TNFα and LPS-induced lung inflammation by TH5487. (A) Long term TH5487 administration does not affect mouse body weight. Mice were administered 20–40 mg/kg TH5487 orally once every day on weekdays. At the start of the treatment the dose was 20 mg/kg TH5487, which was subsequently raised to 40 mg/kg after the first week (n=3–6 per treatment group). Average values ± SD are shown. No overt behavioral changes or signs of toxicity were observed, and the experiment was not stopped due to toxicity in any of the groups. **(B)** Visual depiction of cells in bronchoalveolar lavage fluids. Challenge with TNFα (20 ng per lung) induces infiltration of neutrophils, whereas the samples from TH5487-treated animals are dominated by macrophages. Ten to sixteen randomly selected field of view per cytospon slide were photographed using a WHN10×/22 eyepiece and a 20× objective (field of view is 1.1 mm, and camera correction is 0.63) on an OLYMPUS Microscope System BX53P.

(**C** to **D**), Inhibition of TNFα-induced lung inflammation by TH5487. TH5487 (30, 15, and 8 mg per kg) or equivalent volume of vehicle (saline containing 5% DMSO and 10% Tween 80) was administered to groups of mice (n=5–7) via intraperitoneal route (i.p.) 3 h and 1 h before lungs were challenged with TNFα (20 ng per lung) or vehicle (saline). Sixteen hours after challenge, the mice were euthanized and lavaged and the number of cells in bronchoalveolar lavage fluids (BALF) was determined after Modified Wright–Giemsa staining in a blinded fashion. At least 1,000 cells were counted per mouse. n = 9 (vehicle), n = 12 (TNFα and 30 mg/kg), n = 10 (TNFα and 15 mg/kg), n = 9 (TNFα and 8 mg/kg), n = 9 (TH5487 alone, 30 mg/kg), n = 12 (TNFα and vehicle). Panel C indicates the neutrophil count in the respective samples. Data are average ± SD, from two independent experiments. **(E)** Inhibition of LPS-induced airway inflammation by TH5487. TH5487 (30 mg/kg) or vehicle (saline containing 5% DMSO and 10% Tween 80) was administered to groups of mice (n = 6, 50% ♂ and 50% ♀) via intraperitoneal route (i.p.) 3 h and 1 h before challenge of lungs with LPS (20 ng per lung) or vehicle (saline). Sixteen hours after challenge, the mice were euthanized, lavaged and the number cells in bronchoalveolar lavage fluids determined. Differential cell counts were performed after Modified Wright–Giemsa staining, as in the legend to S16B-D. Data are average ± SD, representative of six experimental animals from one experimental run. **(F)** Visual depiction of cell composition of BALF derived from mouse lungs. Mice were TH5487-treated and challenged with LPS as in legend to E. Ten to sixteen randomly selected fields of view per cytospin slide were photographed using a WHN10×/22 eyepiece and 20× objective (field of view is 1.1 mm, and camera correction is 0.63) on an OLYMPUS Microscope System BX53P. **(G)** Representative histology of LPS-induced lung inflammation. After bronchoalveolar lavage, the lungs were fixed with 4% paraformaldehyde, embedded in paraffin, sectioned to 5 μm and stained with hematoxylin and eosin (Research Histopathology Core, UTMB). Perivascular and peribronchial inflammation were evaluated by a pathologist in a blinded fashion. The view in G is representative of four sections per lung (n=6) and were photographed using an OLYMPUS Microscope System BX53P an in the legend to F.

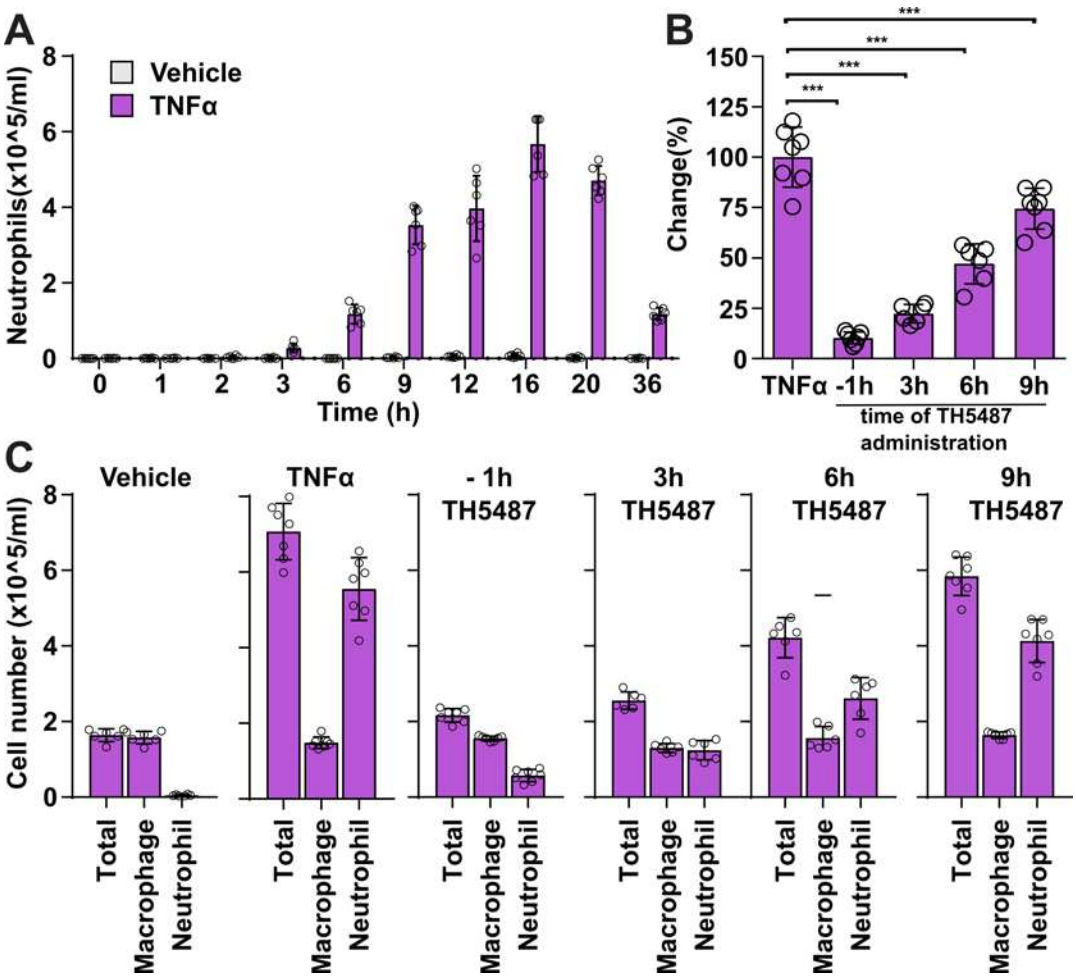

Supplementary Fig. S17: TH5487 interrupts ongoing TNFα-induced lung inflammation

(A) Recruitment kinetics of neutrophil into lungs after TNFα challenge. Parallel groups of mice (n =6) were intranasally challenged with TNFα (20 ng per lung). Mice were euthanized at the indicated times after challenge, lavaged and the number of cells in bronchoalveolar lavage fluids (BALF) was determined. Differential cell counts were performed after Modified Wright–Giemsa staining on coded slides by two independent investigators in blinded fashion. Data are average ± SD from six individual animals per condition from one experimental run. (**B** and **C**) TH5487 interrupts ongoing inflammatory processes induced by TNFα. Randomly selected groups of mice (n = 6, 50% ♂ and 50% ♀) were challenged via nasal route with 40 µl vehicle or TNFα (20 ng per lung) in 40 µl of vehicle. TH5487 (30 mg/kg) in saline containing 5% DMSO and 10% Tween 80 was administered i.p. 1 h before or 3 h, 6 h or 9 h after TNFα challenge. Sixteen hours after TNFα challenge, groups of mice were euthanized, and lavaged. The number of cells in BALF was determined as in legend to A. All values indicate average ± SD, from six individual animals per condition from one experimental run. *** signifies $p < 0.001$, using unpaired two-sided t-test.

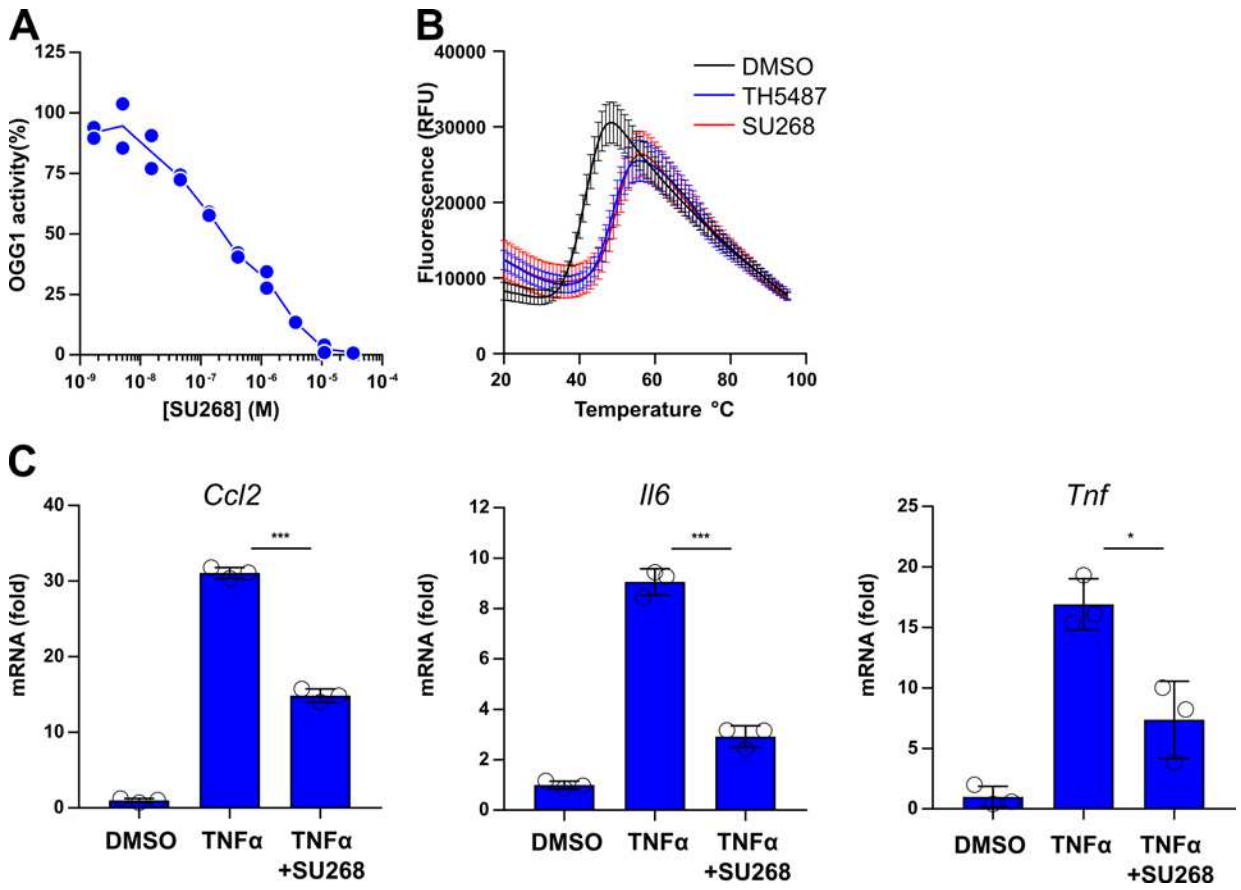

Supplementary Fig. S18: Effect of SU268 on OGG1 activity, OGG1 thermal stability and pro-inflammatory gene expression. (A) Inhibition curve for SU268. Under these conditions, the compound inhibits OGG1 with an IC50-value of 340 nM. The line represents the average of two technical replicates (n=1). **(B)** OGG1 melting curve in the presence of the indicated OGG1 inhibitors. 100 µM of the indicated compounds were incubated with 4 µM OGG1 in the presence of SYPRO Orange. Thermal protein denaturation causes an increase in fluorescence, that is shifted by ~7°C by TH5487 and SU268 compared to DMSO (p<0.001, using unpaired, two-sided t-test). Data are presented as average ± SD of 12 technical replicates, representative of two independent experiments. **(C)** SU268 inhibits pro-inflammatory gene expression. MLE 12 cells were pre-incubated with DMSO or 5 µM SU268 for 1 h and stimulated with 20 ng/ml TNFα for 30 minutes. Expression levels of *Ccl2*, *Il6* and *Tnf* were quantified with qRT-PCR. Data are displayed as average ± SD of three technical replicates and are representative of two independent experiments. * signifies p<0.05, and *** p<0.001, using unpaired, two-sided t-test.

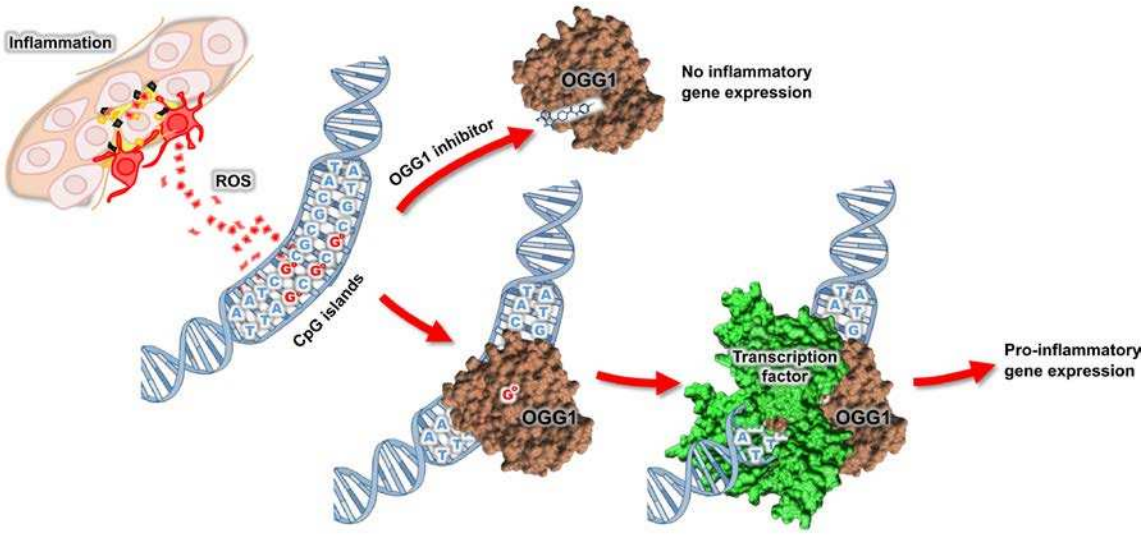

Supplementary Fig. S19: Model of TH5487-mediated inhibition of pro-inflammatory gene expression. The onset and ongoing inflammation is associated with generation of reactive oxygen species, causing damage to DNA in particular at guanine-rich promoters. OGG1 binding to oxidized guanines at promoter regions facilitate recruitment of downstream transcription factors that drive pro-inflammatory gene expression, and a cellular inflammatory response. In the presence of TH5487, OGG1 can no longer interact with DNA substrates in promoters, so pro-inflammatory gene expression is inhibited, and the cellular inflammatory response is prevented.

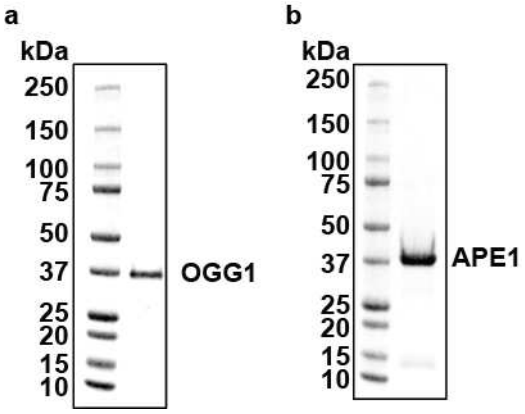

Supplementary Fig. S20: Purity of recombinant human OGG1 and APE1 enzymes. **(A)** Purified OGG1 was stained with Coomassie brilliant blue after separation by SDS-PAGE. **(B)** Purified APE1 was stained with Coomassie brilliant blue after separation by SDS-PAGE.

Supplementary Tables

Supplementary Table S1: Small-molecule screening data.

Category	Parameter	Description
Assay	Type of assay	Fluorescence Intensity
	Target	Human recombinant OGG1 (O15527)
	Primary measurement	Measure increase in fluorescence following cleavage of a duplex oligonucleotide containing fluorophore, quencher and an OGG1 substrate. An excessive amount of APE1 is present to cleave the backbone of the strand containing the substrate base, leading to a dissociation of the fluorophore from the quencher and an increase in signal.
	Key reagents	OGG1 and APE1 recombinant enzymes, duplex oligonucleotide with modified base.
	Assay protocol	Please refer to the materials and methods section.
	Additional comments	
Library	Library size	17,940 compounds
	Library composition	A diversity set originating from Enamine as well as a donation from Biovitrum AB. All compounds are stored as 10 mM DMSO solutions in Labcyte 384 LDV plates until dispensed directly to the assay plates.
	Source	Chemical Biology Consortium Sweden
	Additional comments	
Screen	Format	384-well plates.
	Concentration(s) tested	10 µM compound/0.1% DMSO
	Plate controls	Positive control was a solution where OGG1 enzyme was excluded (n = 16 per plate), negative control was 0.1% DMSO (n = 16 per plate)
	Reagent/compound dispensing system	Labcyte Echo 550 for compounds, PerkinElmer FlexDrop for enzymes and substrate
	Detection instrument and software	PerkinElmer Envision
	Assay validation/QC	Average Z′ score 0.56, negative/positive control ratio 3.4.
Correction factors	Normalization	All data were normalized based on the controls in columns 23 and 24 to yield inhibition values. The data were also corrected for unequal enzyme dispensing by the Flexdrop depending on well position. This was done by calculating a correction factor based on the median position of each well over the 52 screening plates.
	Additional comments	
Post-HTS analysis	Hit criteria	Enzyme inhibition > 25% prompted hit confirmation in several steps. First, primary hits were tested at three concentrations. Those resulting in a concentration-dependent inhibition were then tested in full concentration-response curves at 11 concentrations in duplicate.
	Hit rate	1.2×10^{-4}
	Additional assay(s)	Counterscreen for APE1 inhibition and DNA intercalation.
	Confirmation of hit purity and structure	LC–MS
	Additional comments	

Supplementary Table S2: Selectivity of TH5487 on base excision repair enzymes. A dilution series of TH5487 was incubated with the indicated enzymes and substrates, and the IC50-value was determined.

Enzyme	**Uniprot ID**	**Substrate**	**IC_{50} (µM)**	**Inhibition at 100 µM (%)**
Human OGG1	O15527	10 nM 8-oxoA:C	0.342	97
Mouse OGG1	O08760	10 nM 8-oxoA:C	0.687	97
Fpg	P05523	10 nM Tg:A	> 100	− 1.5
UNG2	P13051	500 nM U:A	> 100	9
SMUG1	Q53HV7	375 nM U:G	> 100	16.5
TDG	Q13569	10 nM U:G	> 100	14.0
APE1	P27695	20 nM AP-site:C	> 100	18.3
MPG	P29372	10 nM I:T	> 100	2.7
SMUG1	Q53HV7	375 nM U:G	> 100	16.5
NEIL1	Q96FI4	20 nM Tg:A	> 100	− 2

Supplementary Table S3: Inhibitory activity of TH5487 with NUDIX hydrolases and diphosphatases. Activities of the indicated enzymes were measured at a single, 100 µM dose of TH5487.

Enzyme	Uniprot ID	% Inhibition at 100 µM	Enzyme concentration	Coupled enzyme	Substrate
dCTPase	Q9H773	3	35 nM	PPase 0.2 U/ml	dCTP; 35 µM
dUTPase	P33316	9	1 nM	PPase 0.2 U/ml	dUTP; 12.5 µM
ITPase	Q9BY32	42	0.2 nM	PPase 0.2 U/ml	ITP; 25 µM
MTH1	P36639	26.5	4.75 nM	PPase 0.2 U/ml	dGTP; 100 µM
NUDT12	Q9BQG2	3	20 nM	BIP 10 U/ml	NADH; 50 µM
NUDT14	O95848	− 4	2 nM	BIP 10 U/ml	ADPR; 50 µM
NUDT15	Q9NV35	13	8 nM	PPase 0.2 U/ml	dGTP; 100 µM
NUDT18	Q6ZVK8	24	200 nM	PPase 0.2 U/ml	8-oxodGTP; 50 µM
NUDT2	P50583	− 8	8 nM	BIP 10 U/ml	AP4A; 16 µM
NUDT5	Q9UKK9	8	2 nM	BIP 10 U/ml	ADPR; 50 µM
NUDT9	Q9BW91	2	20 nM	BIP 10 U/ml	ADPR; 50 µM
SAMHD1	Q9Y3Z3	6.4	350 nM	PPase 12.5 U/ml	dGTP; 25 µM

Supplementary Table S4: Effect of OGG1 inhibitors under different assay conditions. 8-oxoA:C substrate (10 nM) was incubated with the indicated enzymes and a dilution series of TH5487 or O8.

Substrate	**Enzymes**	**IC_{50} (nM) TH5487**	**IC_{50} (nM) OGG1 inhibitor O8**
8-oxoA:C	1 nM OGG1; 2 nM APE1	332	5030
8-oxoA:C	20 nM OGG1	495	1290

Supplementary Table S5: Peptides presenting lower deuteration kinetics upon TH5487 binding ($p<0.005$). The peptide start and end sequences are derived from the nuclear isoform of human OGG1 (Uniprot O15527-1).

Start	End	Peptide sequence	Color in Fig. 1G
34	44	RLDLVLPSGQS	Black
34	45	RLDLVLPSGQSF	Black
36	45	DLVLPSGQSF	Black
36	59	DLVLPSGQSFRWREQSPAHWSGVL	Black
107	120	AQLYHHWGSVDSHF	Orange
110	120	YHHWGSVDSHF	Orange
121	129	QEVAQKFQG	Yellow
121	132	QEVAQKFQGVRL	Yellow
133	141	LRQDPIECL	Yellow
143	158	SFICSSNNNIARITGM	(Dark) Cyan
145	158	ICSSNNNIARITGM	(Dark) Cyan
159	170	VERLCQAFGPRL	(Dark) Cyan
241	252	CILPGVGTKVAD	Light blue
241	253	CILPGVGTKVADC	Light blue
257	271	MALDKPQAVPVDVHM	Dark blue
257	278	MALDKPQAVPVDVHMWHIAQRD	Dark blue
258	271	ALDKPQAVPVDVHM	Dark blue
259	271	LDKPQAVPVDVHM	Dark blue
272	278	WHIAQRD	Purple
279	302	YSWHPTTSQAKGPSPQTNKELGNF	Pink
303	313	FRSLWGPYAGW	Brown
303	314	FRSLWGPYAGWA	Brown
303	315	FRSLWGPYAGWAQ	Brown
303	318	FRSLWGPYAGWAQAVL	Brown

Supplementary table S6: X-ray crystallography-data collection and refinement statistics
[a] Values in parentheses are for highest-resolution shell. [b] Values for each molecule of the asymmetric unit

	mOGG1	**mOGG1:TH5675**
Data collection		
PDB code	6G3X	6G3Y
Beamline	DLS-I04	DLS-I24
Space group	$P2_12_12_1$	$P2_12_12_1$
Cell dimensions□ □		
a, *b*, *c* (Å)	80.8, 81.2, 167.5	80.8, 81.4, 169.2
α, β, γ (°)	90, 90, 90	90, 90, 90
Resolution (Å)	2.06-83.8 (2.06-2.09)[a]	2.51-84.6 (2.51-2.56)[a]
No. total / unique reflections	863,263 / 68,950	270,221 / 38,585
R_{merge}	0.089 (0.88)[a]	0.116 (0.85)[a]
R_{pim}	0.026 (0.30)[a]	0.047 (0.34)[a]
$CC_{1/2}$	0.999 (0.33)[a]	0.976 (0.14)[a]
I / sI	16.9 (2.0)[a]	9.3 (1.8)[a]
Completeness (%)	99.9 (95.7)[a]	99.6 (89.8)[a]
Redundancy	12.5 (9.6)[a]	7.0 (7.1)[a]
Wilson B factor	34.4	54.4
Refinement		
No. reflections used	61,280	36,660
R_{work} / R_{free} (%)	22.4 / 27.4	23.6 / 28.2
B-factors		
Protein (all atoms)[b]	40/46/49	60/77/90
Ligand[b]	N/A	60.5/66.1/84.9
Water	44	54
R.m.s. deviations		
Bond lengths (Å)	0.006	0.007
Bond angles (°)	1.06	1.16
Ramachandran statistics		
Favored (%)	96.4	96.7
Outliers (%)	0.11	0.21

Supplementary Table S7: Absorption, Distribution, Metabolism, and Excretion (ADME) properties for TH5487. MLM: mouse liver microsome; HLM: human liver microsome; PPB: plasma protein binding: fu, free fraction.

Parameter	Value
Kinetic solubility (µmol/l)	3
MLM CL_{int} (µl/min/mg)	29.7
HLM CL_{int} (µl/min/mg)	6.1
PPB (Human), fu (%)	0.06
CaCo2 permeability A-B (cm/s)	4×10^{-6}
CaCo2 permeability B-A (cm/s)	8.3×10^{-7}
Efflux ratio	0.2

Supplementary Table S8: Pharmacokinetic (PK) properties for TH5487 after intravenous (IV) and oral (PO) treatment with 10 and 30 mg/kg doses, respectively. IV and PO pharmacokinetics were performed independently but using the same mouse strain and gender. Plasma samples were collected at eight time points during 24 h after treatment. Cmax: maximal plasma concentration; Tmax: time for maximal plasma concentration; AUC: area under curve; λ_z range: time points used for calculation of t½; t½: half-life in plasma; Vd: volume of distribution; Vss: volume of distribution at steady state; CL: clearance; F%: bioavailability (or fraction absorbed).

Parameter	**IV**	**PO**
Dose (mg/kg)	10	30
C_{max} (µM)	97.4*	68.4
T_{max} (h)	0.08	4
AUC $_{0\text{-}24}$ (µM*h)	546	1012
AUC $_{0\text{-}inf}$ (µM*h)	562	1015
λ_z range (h)	6-24	12-48
t½z (h)	4.79	5.36
V_d (l/kg)	0.18	-
V_{ss} (l)	0.16	-
CL (l/h/kg)	0.03	-
F%	-	60

*First sampling time point.

Supplementary Table S9: Hematological parameters following intraperitoneal administration of TH5487. Mice were administered daily intraperitoneal injections of vehicle or 30 mg/kg TH5487 for 5 days. Data are shown as average ± SD. No significant differences ($p < 0.01$) between treatments for either sex were observed. RBC: red blood cells; HCT: haematocrit; MCV: mean cell volume; RDW: red blood cell distribution width; HGB: haemoglobin; MCH: mean cell haemoglobin; MCHC: mean cell haemoglobin concentration; PTL: platelets; MPV: mean platelet volume; WBC: white blood cells; LYM: lymphocytes; GRANL: granulocytes; MONO: monocytes.

Parameter	Unit	Vehicle		TH5487 30 mg/kg	
		Male (n = 3)	**Female (n = 3)**	**Male (n = 3)**	**Female (n = 3)**
RBC	10^{12}/l	9.1 ± 0.3	9.0 ± 0.2	8.2 ± 0.3	8.7 ± 0.1
HCT	%	40.7 ± 1.0	40.9 ± 1.1	38 ± 1.3	40.1 ± 0.6
MCV	Fl	44.8 ± 0.6	45.4 ± 0.1	46.3 ± 1.1	45.8 ± 0.1
RDW	%	22.2 ± 0.2	22.4 ± 0.7	22.1 ± 0.1	22.4 ± 0.7
HGB	g/dl	14.5 ± 0.5	14.5 ± 0.3	13.1 ± 0.4	13.9 ± 0.3
MCH	pg	16.0 ± 0.04	16.1 ± 0.2	16.0 ± 0.1	15.8 ± 0.1
MCHCH	g/dl	35.8 ± 0.4	35.5 ± 0.4	37.7 ± 0.7	34.63 ± 0.3
PTL	10^{9}/l	329 ± 10	319.6 ± 21.8	287 ± 38	291 ± 12
MPV	Fl	4.96 ± 0.04	5.06 ± 0.1	5.1 ± 0.04	5.0 ± 0.1
WBC	10^{9}/l	2.6 ± 0.7	4.6 ± 0.8	3.2 ± 0.8	3.5 ± 1.0
LYM	%	79.7 ± 4.1	80.6 ± 2.2	75.4 ± 2.7	75.5 ± 2.6
GRANL	%	17.5 ± 3.8	16.2 ± 2.0	21.5 ± 2.5	21.4 ± 2.4
MONO	%	2.7 ± 0.4	3.2 ± 0.3	3.1 ± 0.3	3.1 ± 0.2

Supplementary Table S10: Serum parameters following intraperitoneal administration of TH5487. Mice were treated with daily intraperitoneal injections of vehicle or 30 mg/kg TH5487 for 5 days. Data are shown as average ± SD. Significant differences (** $p < 0.01$) are indicated.

Parameter	Unit	Vehicle		TH5487 30 mg/kg	
		Male (n = 3)	**Female (n = 3)**	**Male (n = 3)**	**Female (n = 3)**
Alkaline Phosphatase	U/l	109 ± 7	126.6 ± 7.7	96 ± 11	97.3 ± 9.8
Alanine aminotransferase	U/l	17.3 ± 5.0	19.6 ± 3.3	21.3 ± 4.1	18.3 ± 3.1
Amylase	U/l	764 ± 33	793.3 ± 12.8	673.6 ± 32.9	769.6 ± 31.3
Total Bilirubin	µmol/l	5.7 ± 0.5	5.6 ± 0.5	6.3 ± 1.2	6 ± 1
Blood urea nitrogen	mmol/l	7.3 ± 0.6	7.23 ± 0.04	5.7 ± 0.1	8.5 ± 0.5
Calcium	mmol/l	2.47 ± 0.02	2.3 ± 0.1	2.45 ± 0.04	2.6 ± 0.1
Phosphorus	mmol/l	2.0 ± 0.2	2.1 ± 0.1	2.0 ± 0.1	2.0 ± 0.3
Creatinine	µmol/l	21.0 ± 4.2	27 ± 10	22.7 ± 4.1	23 ± 5
Glucose	mmol/l	10.6 ± 1.2	10.3 ± 1.5	8.5 ± 1.6	8.2 ± 0.8
Sodium	mmol/l	145 ± 2	145 ± 0.8	143.3 ± 0.5	145.3 ± 1.2
Potassium	mmol/l	5.7 ± 0.2	5.7 ± 0.2	5.8 ± 0.1	5.7 ± 0.1
Total Protein	g/l	49.3 ± 1.0	49.3 ± 0.5	**45 ± 1****	48.6 ± 1.7
Albumin	g/l	39.7 ± 0.5	42.3 ± 1.0	**36.6 ± 0.5****	41.3 ± 1.2
Globulin	g/l	9.7 ± 0.5	7.0 ± 0.8	8.3 ± 0.9	7.7 ± 1.0

Supplementary Table S11: qRT-PCR primers used in this study.

Gene Name	**Catalog no**	**Sequence**
Gapdh	Mm.PT.39a.1	F: 5′-AAT GGT GAA GGT CGG TGT G-3′ R: 5′-GTG GAG TCA TAC TGG AAC ATG TAG-3′
Tnf	Mm.PT.58.12575861	F: 5′-AGA CCC TCA CAC TCA GAT CA-3′ R: 5′-TCT TTG AGA TCC ATG CCG TTG-3′
Cxcl2	Mm.PT.58.10456839	F: 5′-CAG AAG TCA TAG CCA CTC TCA AG-3′ R: 5′-CTT TCC AGG TCA GTT AGC CTT-3′
Il6	Mm.PT.58.10005566	F: 5′-AGC CAG AGT CCT TCA GAG A-3′ R: 5′-TCC TTA GCC ACT CCT TCT GT-3′
Cxcl10	Mm.PT.58.43575827	F: 5′-ATT TTC TGC CTC ATC CTG CT-3′ R: 5′-TGA TTT CAA GCT TCC CTA TGG C-3′
Ccl2	Mm.PT.58.42151692	F: 5′-CAT CCA CGT GTT GGC TCA-3′ R: 5′-AAC TAC AGC TTC TTT GGG ACA-3′
Ccl20	Mm.PT.58.13906306	F: 5′-CCA GCA CTG AGT ACA TCA ACT-3′ R: 5′-GTA TGT ACG AGA GGC AAC AGT C-3′
GAPDH	Hs.PT.39a.22214836	F: 5′-ACA TCG CTC AGA CAC CAT G-3′ R: 5′ -TGT AGT TGA GGT CAA TGA AGG G-3′
TNF	Hs.PT.58.45380900	F: 5′-TGC ACT TTG GAG TGA TCG G-3′ R: 5′-TCA GCT TGA GGG TTT GCT AC-3′
CXCL1	Hs.PT.58.39039397	F: 5′-TCTCTCTTTCCTCTTCTGTTCCTA-3′ R: 5′-CATCCCCCATAGTTAAGAAAATCATC-3′
IL6	Hs.PT.58.40226675	F: 5′ -GCA GAT GAG TAC AAA AGT CCT GA-3′ R: 5′ -TTC TGT GCC TGC AGC TTC-3′
CXCL10	Hs.PT.58.3790956.g	F: 5′-GAC ATA TTC TGA GCC TAC AGC A-3′ R: 5′-CAG TTC TAG AGA GAG GTA CTC CT-3′
CCL20	Hs.PT.58.19600309	F: 5′-CCA TGT GCT GTA CCA AGA GT-3′ R: 5′-TTA GGA TGA AGA ATA CGG TCT GTG-3′
CCL2	Hs.PT.58.45467977	F: 5′-AGC AGC CAC CTT CAT TCC-3′ R: 5′-GCC TCT GCA CTG AGA TCT TC-3′
OGG1	Hs.PT.58.24618622	F: 5′- CAT ATG AGG AGG CCC ACA AG-3′ R: 5′- CAG AAG ATA AGA GGA CGC AGA AG-3′

Supplementary Table S12: Probes used for NF-κB electrophoretic mobility shift assays. G* signifies the inclusion of 8-oxoG. The NF-kB binding motif is underlined.

Probe	**Sequence**
Probe containing 8-oxoG and NF-κB binding motif (derived from *TNF* promoter)	Sense: 5′-TGGG**G***AGTGTGA**GGGGTATCC**GATGCTTG-3′ Anti-sense: 5′-ACCCCTCACACTCCCATAGGCTACGAAC-biotin-3′
Undamaged probe containing NF-κB binding motif	Sense: 5′-TGGGGAGTGTGA**GGGGTATCC**GATGCTTG-3′ Anti-sense: 5′- ACCCCTCACACTCCCATAGGCTACGAAC-biotin-3′
Cold probe containing 8-oxoG and NF-κB binding motif	Sense: 5′-TGGG**G***AGTGTGA**GGGGTATCC**GATGCTTG-3′ Anti-sense: 5′-ACCCCTCACACTCCCATAGGCTACGAAC-3′
Probe containing 8-oxoG and NF-κB binding motif (derived from *Cxcl2* promoter)	Sense: 5′ -TTCCCTGGTCCCC**GGGCTTTTCC**AGACATCG-3′ Anti-sense: 5′-biotin-CGATGTCTGGAAAAGCCCGGGGACCA**G***GGAA-3′
Undamaged probe containing NF-κB binding motif	Sense: 5′ -TTCCCTGGTCCCC**GGGCTTTTCC**AGACATCG-3′′ Anti-sense: 5′-biotin-CGATGTCTGGAAAAGCCCGGGGACCAGGGAA-3’
Cold probe containing 8-oxoG and NF-κB binding motif	Sense: 5′ -TTCCCTGGTCCCC**GGGCTTTTCC**AGACATCG-3′ Anti-sense: 5′-CGATGTCTGGAAAAGCCCGGGGACCA**G***GGAA-3′

Supplementary Table S13: Primers used for ChIP-qPCR

Gene name	Base pairs	Location	Sequence
Tnf	−252 – −55	Promoter	F: 5′-GCCCCAGATTGCCACAGAAT 3′ R: 5′-GCTCTCATTCAACCCTCGGA 3′
Cxcl2	−242 – +62	Promoter/exon	F: 5′-AGCGCAGACATCACTTCCTT 3′ R: 5′-TGAAGTGTGGCTGGAGTCTG 3′
Il6	−106 – +65	Promoter/exon	F: 5′-CCCCACCCTCCAACAAAGATT 3′ R: 5′-CAGAGAGGAACTTCATAGCGGT-3′

Caption for Movie S1: Ligand-induced conformational change in OGG1. Conformational change upon ligand binding. Extrapolation (morph) between the native mouse OGG1 structure and its complex with TH5675, which illustrates the conformational change of the catalytic pocket upon ligand binding. Movie produced with Chimera (*58*).

Supplementary References (30-58)

30. N. Scaramozzino *et al.*, Characterisation of the substrate specificity of homogeneous vaccinia virus uracil-DNA glycosylase. *Nucleic Acids Res.* **31**, 4950–4957 (2003).
31. B. Kavli *et al.*, hUNG2 is the major repair enzyme for removal of uracil from U:A matches, U:G mismatches, and U in single-stranded DNA, with hSMUG1 as a broad specificity backup. *J Biol Chem.* **277**, 39926–36 (2002).
32. J. Carreras-Puigvert *et al.*, A comprehensive structural, biochemical and biological profiling of the human NUDIX hydrolase family. *Nat. Commun.* **8**, 1 (2017).
33. W. C. Tse, D. L. Boger, A Fluorescent Intercalator Displacement Assay for Establishing DNA Binding Selectivity and Affinity. *Acc. Chem. Res.* **37**, 61–69 (2004).
34. A. A. Baykov, V. N. Kasho, S. M. Avaeva, Inorganic pyrophosphatase as a label in heterogeneous enzyme immunoassay. *Anal. Biochem.* **171**, 271–276 (1988).
35. N. Herold *et al.*, Targeting SAMHD1 with the Vpx protein to improve cytarabine therapy for hematological malignancies. *Nat. Med.* **23**, 256–263 (2017).
36. K. D. Jacob *et al.*, Alzheimer's Disease Associated Polymorphisms in Human OGG1 Alter Catalytic Activity and Sensitize Cells to DNA Damage. *Free Radic. Biol. Med.* **63**, 115–125 (2013).
37. D. M. Molina *et al.*, Monitoring Drug Target Engagement in Cells and Tissues Using the Cellular Thermal Shift Assay. *Science*. **341**, 84–87 (2013).
38. F. Gorrec, The MORPHEUS protein crystallization screen. *J. Appl. Crystallogr.* **42**, 1035–1042 (2009).
39. G. Winter, xia2: an expert system for macromolecular crystallography data reduction. *J. Appl. Crystallogr.* **43**, 186–190 (2010).
40. J. M. Parkhurst *et al.*, Robust background modelling in DIALS. *J. Appl. Crystallogr.* **49**, 1912–1921 (2016).
41. P. Evans, Scaling and assessment of data quality. *Acta Crystallogr. D Biol. Crystallogr.* **62**, 72–82 (2006).
42. C. C. Project, Number 4, The CCP4 suite: programs for protein crystallography. *Acta Crystallogr. D Biol. Crystallogr.* **50**, 760–763 (1994).
43. A. J. McCoy *et al.*, Phaser crystallographic software. *J. Appl. Crystallogr.* **40**, 658–674 (2007).
44. G. N. Murshudov *et al.*, REFMAC5 for the refinement of macromolecular crystal structures. *Acta Crystallogr. D Biol. Crystallogr.* **67**, 355–367 (2011).
45. P. Emsley, B. Lohkamp, W. G. Scott, K. Cowtan, Features and development of Coot. *Acta Crystallogr. D Biol. Crystallogr.* **66**, 486–501 (2010).
46. V. B. Chen *et al.*, MolProbity: all-atom structure validation for macromolecular crystallography. *Acta Crystallogr. D Biol. Crystallogr.* **66**, 12–21 (2010).
47. D. Mangal *et al.*, Analysis of 7,8-Dihydro-8-oxo-2′-deoxyguanosine in Cellular DNA during Oxidative Stress. *Chem. Res. Toxicol.* **22**, 788–797 (2009).
48. Q. Malik, K. E. Herbert, Oxidative and non-oxidative DNA damage and cardiovascular disease. *Free Radic. Res.* **46**, 554–564 (2012).

49. M. Dizdaroglu, Facts about the artifacts in the measurement of oxidative DNA base damage by gas chromatography-mass spectrometry. *Free Radic. Res.* **29**, 551–563 (1998).
50. K. K. Bhakat, S. K. Mokkapati, I. Boldogh, T. K. Hazra, S. Mitra, Acetylation of Human 8-Oxoguanine-DNA Glycosylase by p300 and Its Role in 8-Oxoguanine Repair In Vivo. *Mol. Cell. Biol.* **26**, 1654–1665 (2006).
51. F. A. Ran *et al.*, Genome engineering using the CRISPR-Cas9 system. *Nat. Protoc.* **8**, 2281–2308 (2013).
52. E. K. Brinkman, T. Chen, M. Amendola, B. van Steensel, Easy quantitative assessment of genome editing by sequence trace decomposition. *Nucleic Acids Res.* **42**, e168–e168 (2014).
53. R. D. Ramirez *et al.*, Immortalization of Human Bronchial Epithelial Cells in the Absence of Viral Oncoproteins. *Cancer Res.* **64**, 9027–9034 (2004).
54. I. Boldogh *et al.*, ROS generated by pollen NADPH oxidase provide a signal that augments antigen-induced allergic airway inflammation. *J. Clin. Invest.* **115**, 2169–2179 (2005).
55. K. J. Livak, T. D. Schmittgen, Analysis of Relative Gene Expression Data Using Real-Time Quantitative PCR and the $2^{-\Delta\Delta CT}$ Method. *Methods*. **25**, 402–408 (2001).
56. Z. Chen, S. S. Viboolsittiseri, B. P. O'Connor, J. H. Wang, Target DNA Sequence Directly Regulates the Frequency of Activation-Induced Deaminase-Dependent Mutations. *J. Immunol.* **189**, 3970–3982 (2012).
57. K. Brown, S. Gerstberger, L. Carlson, G. Franzoso, U. Siebenlist, Control of I kappa B-alpha proteolysis by site-specific, signal-induced phosphorylation. *Science*. **267**, 1485–1488 (1995).
58. E. F. Pettersen *et al.*, UCSF Chimera--a visualization system for exploratory research and analysis. *J. Comput. Chem.* **25**, 1605–1612 (2004).